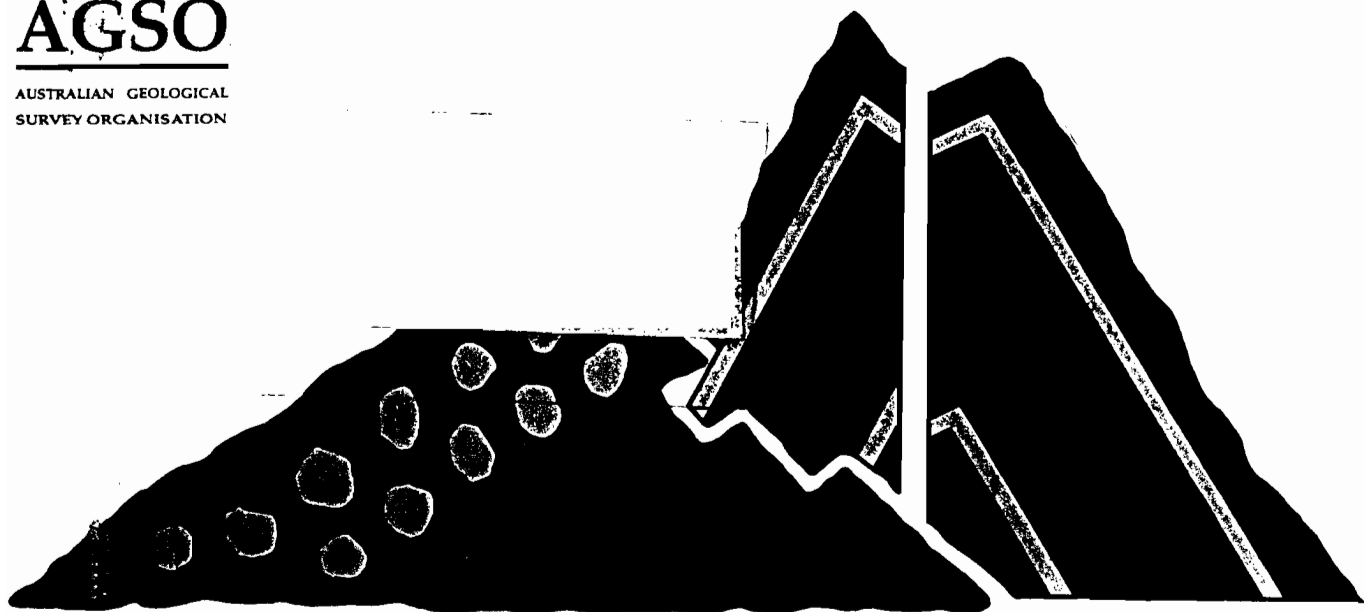


AGSO

AUSTRALIAN GEOLOGICAL
SURVEY ORGANISATION



I A V C E I CANBERRA 1993

EXCURSION GUIDE

THE GEOLOGY, VOLCANOLOGY, PETROLOGY-
GEOCHEMISTRY, AND TECTONIC EVOLUTION OF THE NEW
HEBRIDES ISLAND ARC, VANUATU

Claude Robin, Michel Monzier, Anthony J. Crawford and Stephen M. Eggins

GENERAL ASSEMBLY
SEPTEMBER 1993 - CANBERRA AUSTRALIA

**ANCIENT VOLCANISM
& MODERN ANALOGUES**

DEPARTMENT OF PRIMARY INDUSTRIES AND ENERGY

Minister for Resources: Hon. Michael Lee

Secretary: Greg Taylor

AUSTRALIAN GEOLOGICAL SURVEY ORGANISATION

Executive Director: Harvey Jacka

© Commonwealth of Australia

ISSN: 1039-0073

ISBN: 0 642 19660 5

This work is copyright. Apart from any fair dealings for the purposes of study, research, criticism or review, as permitted under the Copyright Act, no part may be reproduced by any process without written permission. Copyright is the responsibility of the Executive Director, Australian Geological Survey Organisation. Inquiries should be directed to the **Principal Information Officer, Australian Geological Survey Organisation, GPO Box 378, Canberra City, ACT, 2601.**

FIELD-GUIDE

IAVCEI 1993 PRE-CONFERENCE EXCURSION A5

THE GEOLOGY, VOLCANOLOGY, PETROLOGY- GEOCHEMISTRY, AND TECTONIC EVOLUTION OF THE NEW HEBRIDES ISLAND ARC, VANUATU

**Claude Robin¹, Michel Monzier¹,
Anthony J. Crawford², Stephen M. Eggins³**

- 1: Centre ORSTROM de Port Vila, BP 76, Port Vila, VANUATU
- 2; Dept. of Geology, University of Tasmania, GPO Box 252C, Hobart,
Tasmania, AUSTRALIA 7001
- 3: Research School of Earth Sciences, Australian National University,
GPO Box 4, Canberra, ACT, AUSTRALIA 2600

Table of Contents

PART 1

THE GEOLOGY, PETROLOGY-GEOCHEMISTRY AND TECTONIC EVOLUTION OF THE NEW HEBRIDES ISLAND ARC

Anthony J. Crawford and Stephen M. Eggins

	PAGE
Introduction and Acknowledgements.....	1
Previous Work.....	2
Regional Seismotectonic Setting.....	3
Tectonic Development of the New Hebrides Island Arc.....	9
Geology of the Islands.....	13
The Western Belt.....	13
The Eastern Belt.....	19
The Central Chain.....	23
Petrogenesis in the New Hebrides Island Arc.....	27
Primitive Magma Compositions and Differentiation.....	27
Estimating Primary Magma Bulk Compositions.....	29
Trace Element Geochemistry.....	33
Radiogenic Isotope Geochemistry.....	36

PART 2

VOLCANOLOGICAL ASPECTS OF THE NEW HEBRIDES ISLAND ARC - A FIELD GUIDE

Claude Robin and Michel Monzier

Lopevi.....	39
Ambrym.....	39
Volcanology and Structure of the Edifice.....	39
Petrological-Geochemical Summary.....	47

	PAGE
Santa Maria (Gaua).....	47
Structure of the Volcano.....	47
The Santa Maria Pyroclastic Series and the Problem of Caldera Formation.....	50
Mount Garet Volcanic Activity.....	51
Petrological-Geochemical Summary.....	51
VanuaLava.....	51
Suretamatai Volcano.....	51
A Remarkable Volcanic Formation: The Irsa Lion Formation.....	52
Aoba.....	54
Crystallization and Differentiation of Aoba Magmas.....	56
Kuwae Caldera.....	59
Background and Previous Studies.....	59
Morphology of the Caldera.....	59
Age.....	60
Products of the Terminal Maar Phase of the Caldera.....	60
Petrology of the Tuffs.....	63
Discussion.....	64
Tanna.....	68
Structure of the Tanna Volcanic Complex.....	68
Field Characteristics of the Ignimbrites.....	70
Petrological Summary.....	72
Yasur Volcano.....	77
Structure and Volcanic Products.....	77
References.....	79
Appendix A: Wholerock Analyses of New Hebrides Arc Lavas.....	83

PART I

THE GEOLOGY, PETROLOGY-GEOCHEMISTRY AND TECTONIC EVOLUTION OF THE NEW HEBRIDES ISLAND ARC

Anthony J. CRAWFORD¹ and Stephen M. EGGINS²

INTRODUCTION

The New Hebrides Island Arc (Fig. 1), of which the Republic of Vanuatu and the Santa Cruz Islands (Eastern Outer Solomon Islands) are the subaerial expression, is part of a narrow chain of Tertiary to Recent volcanic island arcs extending from Papua New Guinea and the Solomon Islands, through Fiji, Tonga, and the Kermadec Islands, to New Zealand. The Vanuatu segment, which extends from the Torres Islands in the north to the islands of Matthew and Hunter in the south, is a 700 km-long, partly emergent ridge with an average width of 200 km, overlying a steeply eastward-dipping subducted slab.

Major physiographic features of the New Hebrides Arc (Fig. 2) include (1) a trench to the west; (2) an arc platform complex that consists of emergent bedrock ridges (Western Belt and Eastern Belt), submarine grabens (Jean Charcot and Coriolis Troughs), an active volcanic chain (Central Chain) within a central sedimentary basin, and (3) a backarc zone continuous with the North Fiji Basin (Greene et al. 1988).

The island geology of Vanuatu has been described as consisting of three volcanic provinces (Mitchell & Warden 1971; Mallick 1973): the calc-alkalic volcanics of the Western Belt (late Oligocene to middle Miocene); the tholeiitic volcanics of the Eastern Belt (late Miocene to early Pliocene); and the active Central Chain (late Miocene or Pliocene to Holocene).

In this Guide, we provide a summary of the tectonic and geological evolution of the New Hebrides Island Arc based on published and unpublished information, followed by a detailed field guide for the proposed IAVCEI Fieldtrip. The section detailing the geological evolution of the arc

was assembled by AJC, drawing heavily on Macfarlane, Carney, Crawford and Greene (1988); the tectonic synthesis is based on a compilation by AJC of published works. The petrological summary was largely written by SME, based on published and unpublished studies. The bulk of the actual field guide, including all the volcanological aspects of the proposed fieldtrip, descriptions of locations to be visited, and pertinent background, was prepared by CR and MM.

ACKNOWLEDGMENTS

The authors acknowledge the cooperation of the Government of Vanuatu in the planning and support of this trip, in particular Stanley Temakon, Director of the Department of Geology, Mines and Water Resources in Port Vila, and his predecessor Cedric Mortimer of BGS. We thank ORSTOM (France) for providing the R/V Alis for this trip, and the captain and crew of the Alis for their expertise. AJC wishes to thank Gary Greene (USGS), Sandy Macfarlane (BGS) and Neville Exon (AGSO) for encouraging his involvement in the geology of the western Pacific (and particularly Vanuatu), the Australian Research Council for financial support for this work, and especially Claude Robin and Michel Monzier for their efforts in the organization and planning of this fieldtrip.

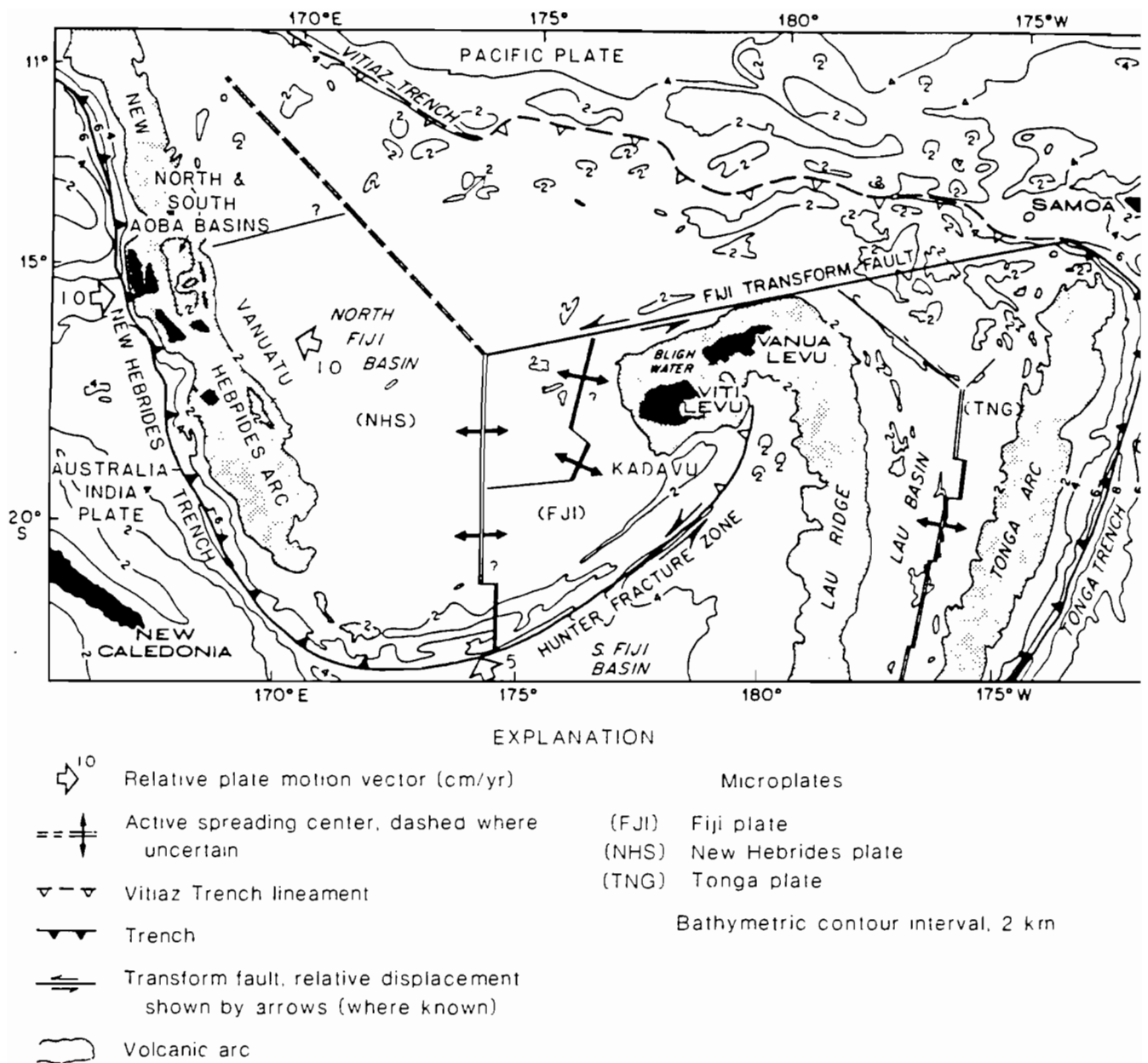


Figure 1: Tectonic setting of the New Hebrides Island Arc and North Fiji Basin. After Falvey & Greene (1988)

PREVIOUS WORK

The earliest known geologic observations in Vanuatu are attributed to the explorer Queiros, in 1606, the first European to visit the islands. He is reported as having seen smoke rising from the now-extinct Merelava volcano in the Banks Islands. Over 150 years later, Captain Cook, on his second voyage of exploration to the Pacific, landed at Port Resolution on Tanna in 1774, where he sampled the hot springs and witnessed an eruption of Yasur volcano. In the next hundred years or so, accounts by the early

Christian missionaries of volcanic activity and descriptions of rock specimens collected during naval visits entered the literature.

The first systematic geologic investigations were made by Douglas Mawson, an Australian geologist who visited most of the islands in 1903. He recognized the essentially volcanic nature of the archipelago and the presence of raised coral platforms in many areas (Mawson 1905). Mineral prospecting in the 1930's, in particular by the French geologist Aubert de la Rue, led to reconnaissance accounts of the general geology and volcanism of

individual islands. However it was not until after World War II that the first geologic maps were produced. These maps largely were based on research instigated by French mining companies (e.g. Obellianne 1961; Lemaire 1965).

As a result of this interest in the mineral potential, the then Joint Administration of the Anglo-French Condominium of the New Hebrides (since 1980 the independent republic of Vanuatu) initiated in 1959 a program of regional reconnaissance geological mapping at a scale of 1:100,000. This survey was completed in 1979, and resulted in the publication of eleven coloured geological maps of individual island groups, and a 1:1,000,000 coloured geological map of the archipelago. With two exceptions (Aoba and Ambrym islands), these maps are accompanied by detailed reports, all of which are referenced below.

Collaboration (USA, New Zealand, Australia, and nations of the SW Pacific) within the SOPAC program began in 1982 with the first Tripartite cruise, which investigated the potential for offshore oil and gas resources in Tonga, Vanuatu and the Solomon Islands. Joint surveys using USGS vessels continued during Tripartite II cruises, and data gathered in the waters of the Republic of Vanuatu are reported in Volume 8 of the Circum-Pacific Council for Energy and Mineral Resources (Eds. Greene & Wong 1988).

The French scientific agency ORSTOM has played a major role in the geophysical and volcanological study of the islands and offshore Vanuatu, and two detailed bathymetric maps have been published covering all of the arc south of about 14°S (Monzier et al. 1984; 1991). Seismometers have been deployed on a number of islands, and detailed volcanological investigations of Ambrym, Tanna, Santa Maria, and the small islands that make up the devastated Kuwae caldera are published or in progress (Robin et al. 1993; Picard et al. in press; Monzier et al. submitted). Maillet et al. (1986) reported a detailed petrological study of Matthew and Hunter Islands at the very southern termination of the arc.

The petrology group at the University of Tasmania has been working in Vanuatu since 1987, and detailed studies of Epi (Crawford et al. 1988; Barsdell & Berry 1990; Merelava (Barsdell 1988; Barsdell & Smith 1989); Aoba (Eggins 1993) are published, and on-going studies of the isotopic composition and petrogenesis of the arc

lavas are nearing completion (Eggins in prep.). Another set of samples from a number of islands, and taken from the collections of the Geological Survey of Vanuatu, are being analyzed for Sr-Nd-Pb isotopes by Dr D Peate (Durham). A paper detailing the setting and petrogenesis of the submarine volcanoes in southern Vanuatu is completed (Monzier et al. in press), and further studies of these lavas are underway at UTas (Crawford, Danyushevsky, Monzier, Eggins). Detailed petrological-geochemical studies of the dredged lavas from the narrow Coriolis and Jean Charcot 'backarc' troughs are also nearing completion (Crawford, Maillet, Danyushevsky & Eggins, in prep.). Lavas dredged from the submarine Hunter Ridge, including primitive arc tholeiites and boninites, have been described (Sigurdsson et al. 1993) and further work on this suite of rocks is in progress at the University of Tasmania. Finally, a cruise to surveying and sampling the remainder of the Hunter Ridge is scheduled for October, 1993, and will involve French (Maillet, Monzier) and Australian petrologists (Crawford, Eggins, Verbeeten, Danyushevsky).

REGIONAL SEISMOTECTONIC SETTING

The New Hebrides Island Arc is underlain by an east-dipping Benioff zone that is relatively continuous along the length of the arc and marks the site of subduction of the Australia-India plate beneath the Pacific plate (Figs 1, 2 and 3). The New Hebrides Trench, which lies west of, and runs parallel to, the New Hebrides Island Arc over much of its length, is absent opposite Espiritu Santo and Maikakula, due to collision of the twin-spined d'Entrecasteaux Zone with the arc. At the southern end of the arc, east of the islands of Matthew and Hunter, the trench passes eastward into a complex basin-and-ridge feature known as the Hunter Fracture Zone - Hunter Ridge, and the Early Tertiary Loyalty Ridge is in incipient collision with the southern end of the arc.

Immediately west of the New Hebrides Trench, with depths of ~1,000-5,000 m, is the North Loyalty Basin, which is floored by oceanic crust that has been dated at DSDP Site 286 (Andrews, Packham et al. 1975) as middle

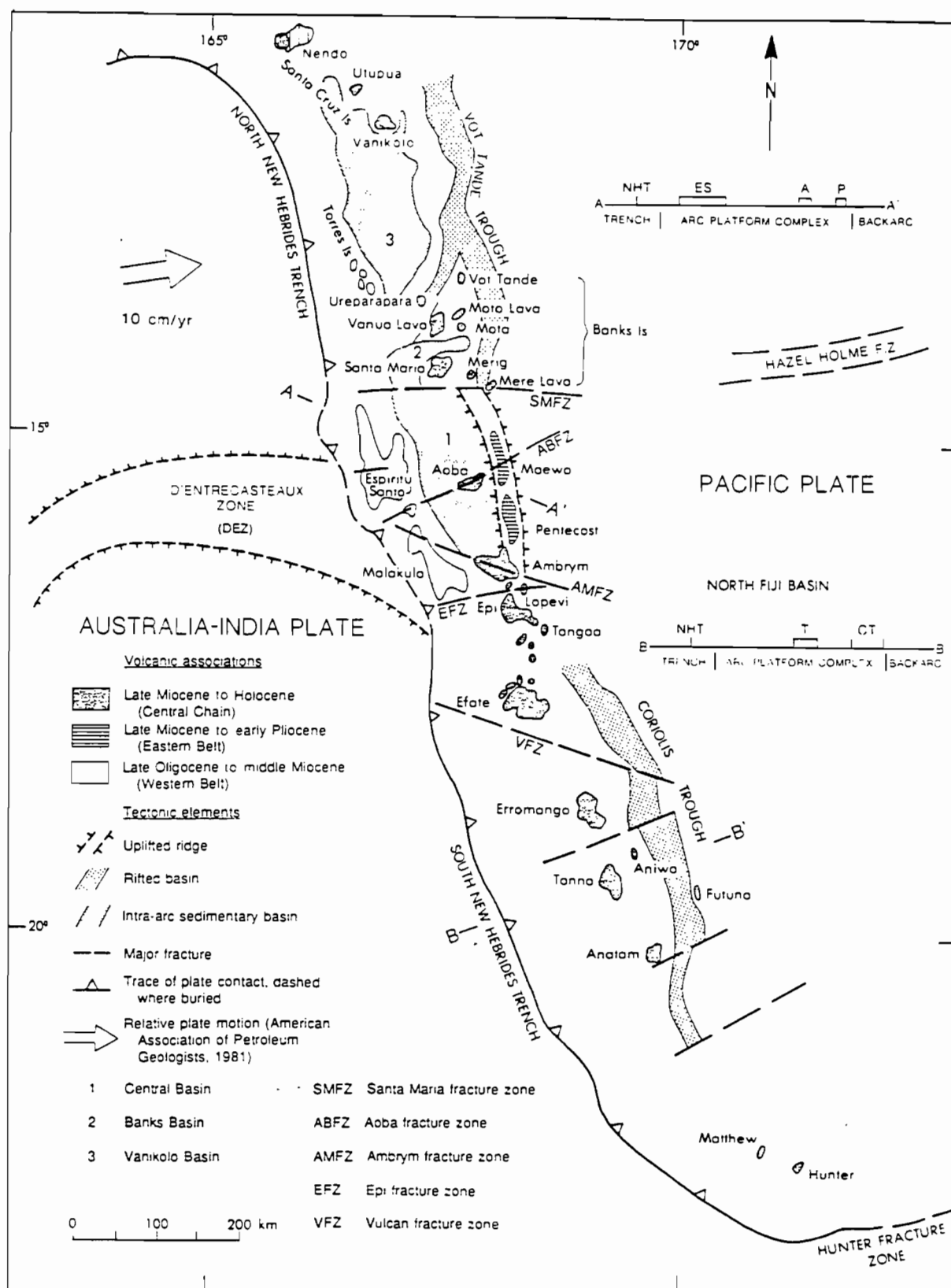


Figure 2: Generalized geological and structural setting of the New Hebrides Island Arc. After Greene et al. (1988)

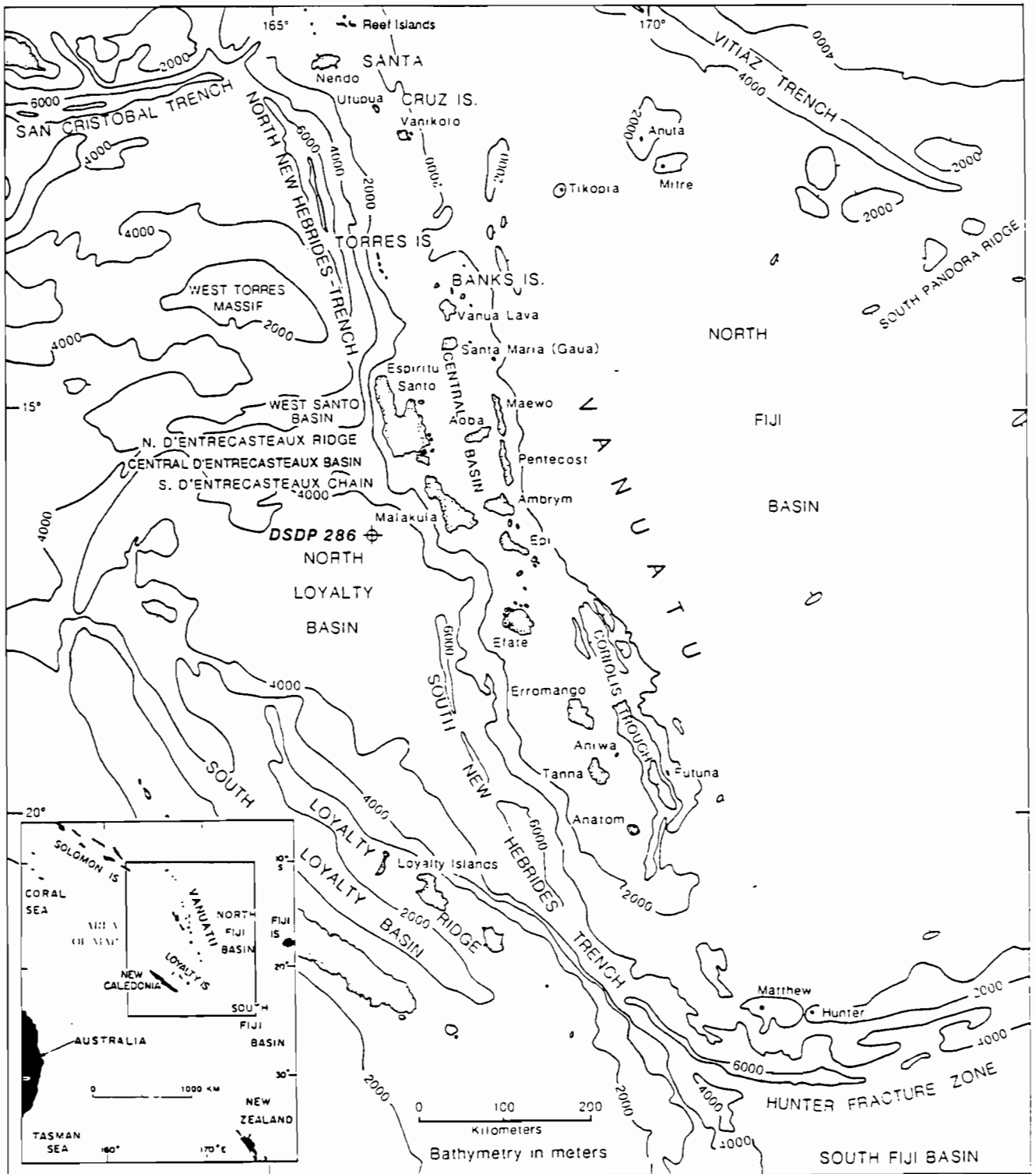


Figure 3: Bathymetric map of the New Hebrides Island Arc - Loyalty Basin region (after Greene et al. 1988)

Eocene (Fig. 3). The Loyalty Ridge, together with the ridge bearing the island of New Caledonia, passes northwestward into the d'Entrecasteaux Zone (DEZ), an arcuate horst-and-graben structure some 100 km wide. Opposite Espiritu Santo and Malakula, the DEZ is being subducted beneath the Pacific plate. Here, the east-west-trending DEZ is made up of the North d'Entrecasteaux Ridge of oceanic-type crust, the smooth-bottomed Central d'Entrecasteaux Basin (to 4,000 m deep), and a line of seamounts, the South d'Entrecasteaux Chain. The DEZ is considered to be a late Eocene south-dipping subduction zone that was uplifted during Miocene time. This subduction event caused island arc volcanism in the Loyalty Islands and the South d'Entrecasteaux Chain (Maillet et al. 1982; Collot et al. 1985; 1992). North of the DEZ are the West Santo Basin and the West Torres Massif, which, from the few data available, are considered to be, respectively, an old trench-like feature (Collot et al. 1985) and an oceanic plateau with intermediate crust. The West Torres Massif, like the DEZ, is impinging on the arc just north of Espiritu Santo island and is about to be subducted.

East of the New Hebrides Island Arc lies the North Fiji Basin, a marginal sea no older than middle to late Miocene (Malahoff et al. 1982). This basin is separated from the older South Fiji Basin of Oligocene age (Malahoff et al. 1982) by the northeast-trending Hunter Fracture Zone. Complex multi-stage opening of the North Fiji Basin (Auzende et al. 1988a; Lafoy et al. 1990) and backarc extensional troughs (Recy et al. 1990; Monjaret et al. 1991) accompanied rotation of the arc (see below). At the northern margin of the North Fiji Basin are the inactive volcanic islands of Mitre and Anuta (Fig. 3), which were derived from former subduction of the Pacific plate along the "fossil" Vitiaz Trench (Jezek et al. 1977).

Underthrusting and subduction of the Australia-India plate result in intense shallow and intermediate depth seismicity (Fig. 4) that has been extensively studied since 1960. Overall seismic properties have been described by Pascal et al. (1978), Louat et al. (1982), Marthelot & Isacks (1985) and Prevot et al. (1991). More detailed studies, including analysis of local network data from the central and southern part of the arc, have been reported by Isacks et al. (1981), Marthelot et al. (1985) and Hamburger & Isacks (1987).

The direction of relative plate convergence, determined from shallow thrust-type mechanisms occurring between 11°S and 21°S is N75°E, and the present convergence rate varies from 16 cm/yr at 11°S to 12 cm/yr at 20°S (Louat & Pelletier 1989). Significantly, the orientation of the transform faults at the southern (Hunter FZ) and northern ends of the arc parallel this computed plate convergence. A minimum convergence rate occurs where the DEZ is colliding with the central part of the arc (9 cm/yr). Oblique extension generally occurs along the eastern (backarc) flank of the main part of the New Hebrides Island Arc, except at the latitude of the DEZ collision, where backarc compression is active. A well-defined Benioff zone dips steeply to the east (Fig. 5), extending to 350 km downdip along much of the arc, although it is apparently shorter (~220 km or less) south of Anatom Island in the southern part of the arc. Along the main part of the arc, Quaternary-Recent volcanoes of the Central Chain lie at 100-200 km above the subducted slab.

In contrast to subduction zones such as the Alaska-Aleutian or Chile convergent margins, shallow seismicity in the New Hebrides Island Arc cannot be described in terms of precisely bounded segments ruptured regularly by events of large magnitude (e.g. Marthelot & Isacks 1985; Louat et al. 1988). The extreme structural complexity of the subducted plate, as described above, may be responsible for this observation. Ridge-arc and massif arc collisions have played an increasingly important role in the tectonic and magmatic evolution of the arc (Daniel et al. 1986; Collot et al. 1992).

The abrupt change in the width of the arc platform between Tanna and Anatom Islands at the southern end of the arc coincides with the sudden shortening of the subducted slab and Benioff zone (Fig. 6a, b), and has been interpreted by Monzier et al. (1984) and Louat et al. (1988) as a former southern termination of the arc at the latitude of Anatom Island. During rotation of the subduction zone, spreading in the North Fiji Basin led to southward lengthening of the arc-trench system from Anatom, to the present general areas of Hunter Island (Falvey 1978; Daniel 1978; Falvey & Greene 1988; Louat et al. 1988). To account for the southward decreasing dip of the Benioff zone, and sharp changes in seismic and petrological features in the southernmost section of the New Hebrides Island Arc, Monzier et al. (1984) proposed

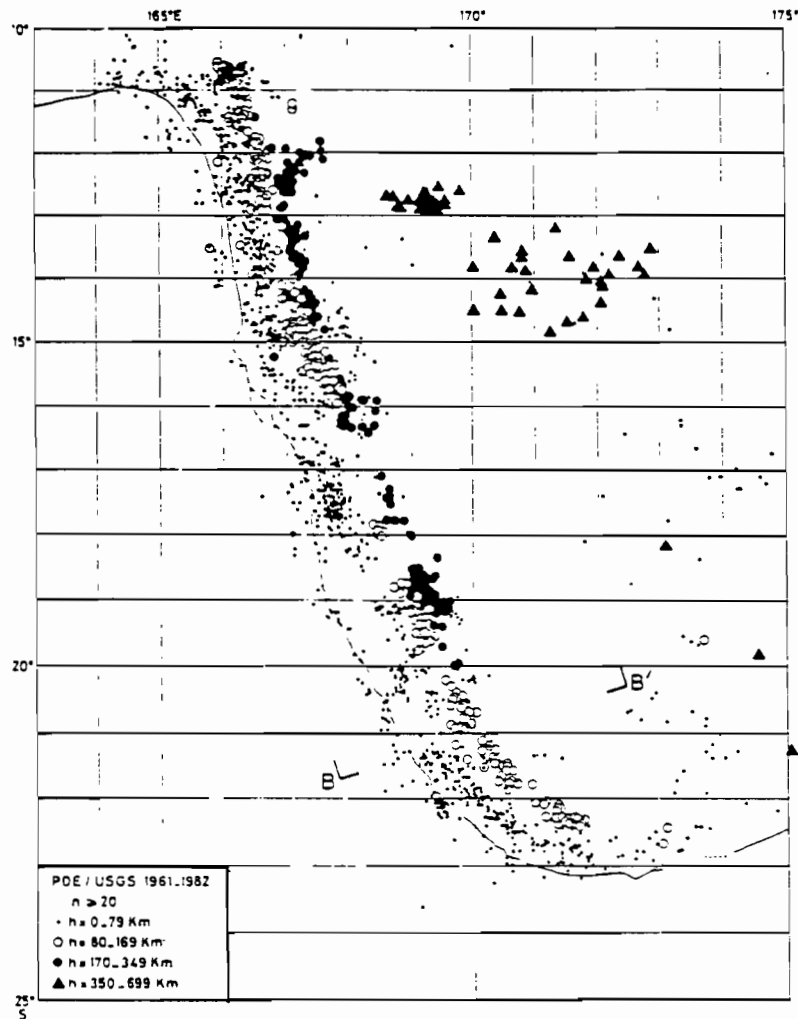


Figure 4: Spatial distribution of earthquakes along the New Hebrides Island Arc plate margin (1961-1983). B-B' marks line of section shown in Figure 5 below (from Louat et al. 1988.)

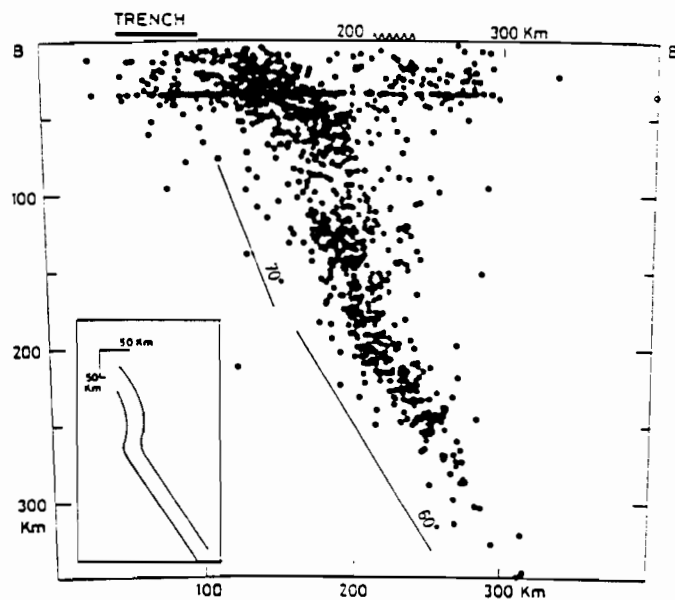


Figure 5: Transverse section across the New Hebrides Island Arc at B-B' (see Figure 4 above). Triangles show locations of Quaternary volcanoes.

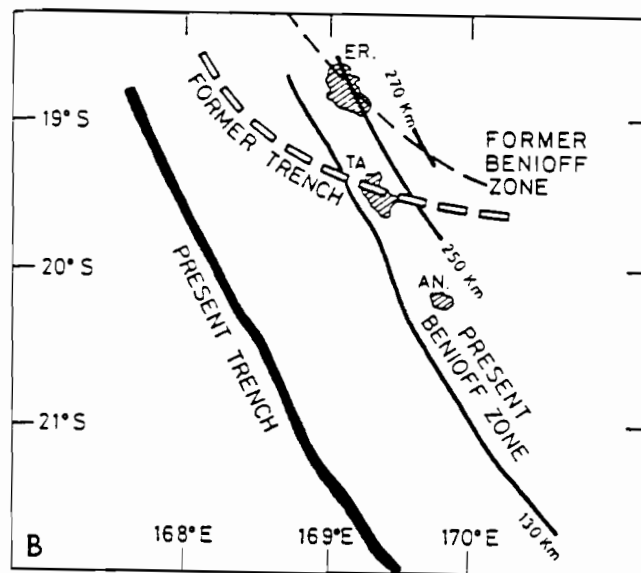
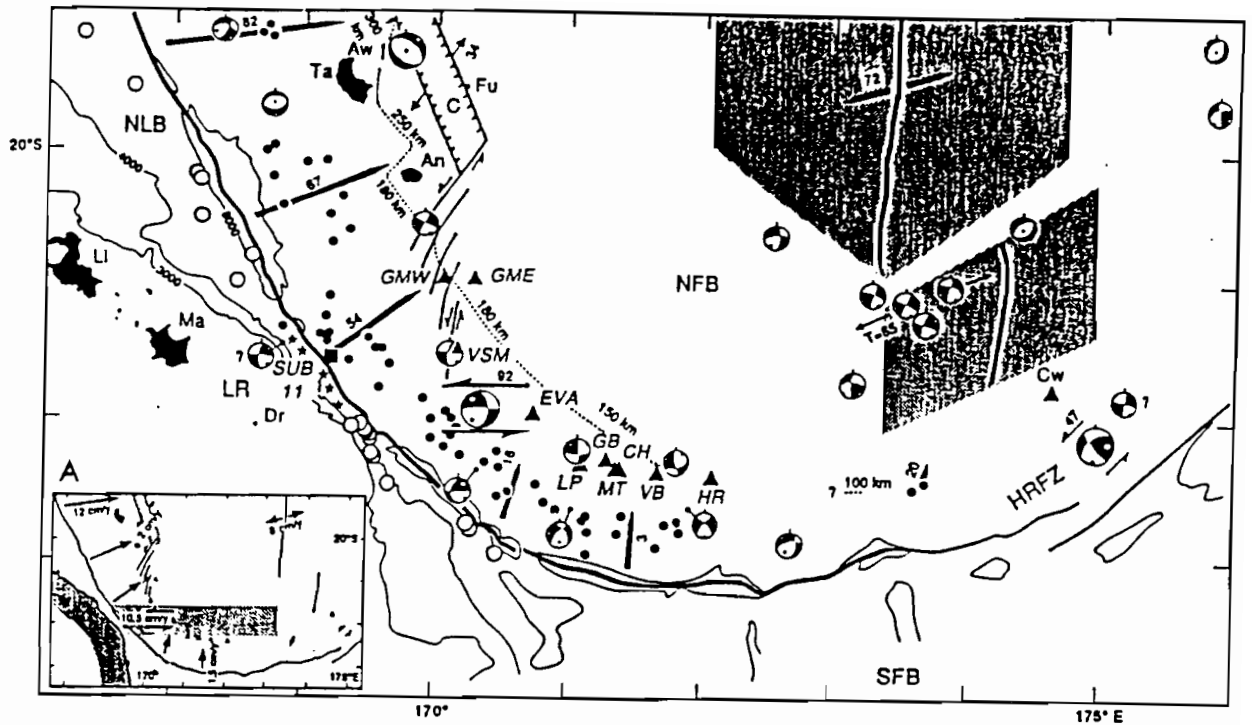


Figure 6: (a) Seismotectonics and present day plate motions in the southern part of the New Hebrides Island Arc. Triangles represent (mainly submarine) volcanoes; shaded areas represent oceanic crust < 2 Ma in the North Fiji Basin. Black dots are thrust fault mechanisms, open circles normal fault mechanisms. C = Coriolis Trough, Li = Lifou Is, Ma = Mare Is, Ta = Tanna Is, An = Anatom Is: Submarine volcanoes include GME and GMW = Mons Gemini, VSM = Volsmar, EVA = Eva, LP = Laperouse, GB = Gilbert, VB = Vauban. HR = Hunter Is and MT = Matthew Is. Depth to Benioff zone shown by finely dotted line. Arrows show present day relative convergent motion, with azimuth of motion derived from underthrust solutions. After Monzier et al. (in press). (b) Schematic diagram of possible southern termination of the New Hebrides Island Arc around 2 Ma. The former trench position is not marked by any present morphological feature, but is inferred by abrupt bathymetric and geophysical discontinuities just south of Anatom island, including a shallowing from 300 km to 200 km in the maximum depth of the Benioff zone; former Benioff zone is schematic, and intended to show the orientation and possible configuration of the former subduction zone (After Louat et al. 1988).

that the subducted slab was torn by two hinge zones, parallel to the plate convergence vector (Fig. 6a). One such hinge is an active E-W sinistral transform that may extend as far east as the offset of the southernmost spreading centre in the North Fiji Basin. North of this transform, near-orthogonal convergence is driven by active subduction of the oceanic lithosphere of the North Loyalty Basin. South of this boundary, oblique convergence has stopped, and only a small amount of orthogonal (northward) convergence occurs at the trench, with the Matthew-Hunter microplate being strongly coupled to the Indian - Australian plate. The volcanic islands of Matthew and Hunter lie only 85 km above the Benioff zone. Clearly, the southern end of the New Hebrides Island Arc is a tectonically unstable and transient region, with considerable tectonic and petrological complexity (Maillet et al. 1989; Sigurdsson et al. 1993).

TECTONIC DEVELOPMENT OF THE NEW HEBRIDES ISLAND ARC

The early history of the New Hebrides Island Arc is generally considered to have occurred behind the late Eocene Vitiaz trench, above the southwest-dipping, subducting Pacific plate (Falvey 1978; Carney & Macfarlane 1977a, 1978; Hamburger & Isacks 1987; Auzende et al. 1988; Falvey & Greene 1988; Musgrave & Firth in prep.). The composite Vitiaz-New Hebrides arc system formed part of the Outer Melanesian Arc System, and was continuous along strike from the Tongan and Solomon Islands arcs. Choking of this long subduction zone due to arrival at the trench of the immense submarine Ontong Java plateau in the Solomon Islands sector is believed to have forced a reversal of subduction polarity. The timing of subduction polarity reversal is poorly constrained, but is generally believed to have been around 10 Ma. Shortly before (Carney & Macfarlane 1977b; 1978) or shortly after subduction reversal (Falvey 1978), backarc spreading in the North Fiji Basin began. A tectonic reconstruction of the Vitiaz arc (Falvey 1978) and a rifting model for the evolution of the New Hebrides Island Arc (Greene et al. 1988a) are given in Figure 7.

Magnetic anomaly 4 has been identified over the oldest crust in the North Fiji Basin, indicating that

spreading between the New Hebrides arc and the remnant Vitiaz arc was underway by at least 8 Ma (Malahoff et al. 1982). The opening of the North Fiji Basin and resultant rotation of the New Hebrides and Fijian island arcs has been in the manner of opening double doors, with the northern 'door' bearing the New Hebrides arc swinging clockwise as the basin opened, and the southern 'door' carrying the Fijian arc swinging anti-clockwise (Figs. 7 & 8). Musgrave & Firth (in prep.) suggest that the entire New Hebrides Island Arc has been rotated clockwise by $50 \pm 13^\circ$ since the late Miocene (beginning no later than 8 Ma), and that subduction may have continued beneath the Vitiaz arc until as recently as 3 Ma, implying simultaneous subduction, to the east along the New Hebrides Trench and to the west along the older Vitiaz Trench. The northern end of the Vitiaz Trench may have been subparallel to the late Miocene Pacific - Australia plate convergence direction in this region, thus acting as a transform boundary, with little associated subduction-related magmatism.

Pacific plate motion changed significantly around 3 Ma (Pollitz 1986), and Musgrave & Firth (in prep.) suggest that this resulted in increased subduction along the New Hebrides Trench. As described later, significant events in the New Hebrides Island Arc at around 3 Ma include uplift of the Western Belt islands of Pentecost and Maewo and cessation of active arc volcanism on these islands, and emplacement of horsts of Basement Complex ophiolites probably along the entire ridge now delineated by the Western Belt (Macfarlane et al. 1988).

A restoration of the Outer Melanesian Arc System relative to a fixed Australian plate for the Middle Miocene is shown in Figure 8, after Musgrave & Firth (in prep.). The Tongan arc has been restored to its pre-Lau Basin opening position and the Fiji Platform and northern Lau Arc have been rotated clockwise to close them against the Tongan Arc and bathymetric highs of the Vitiaz Arc. This reconstruction reconnects the New Hebrides Island Arc and the Fiji Platform as a continuous, roughly collinear feature, rather than placing the Fiji Platform north of the New Hebrides Island Arc, as required by the Falvey (1978) model (Fig. 7). In this model, the Fiji Platform is rotated 25° , and subduction along the northern Hunter Fracture Zone (Kadavu Trench) also began as the fracture zone rotated eastwards as part of the rotation of Fiji.

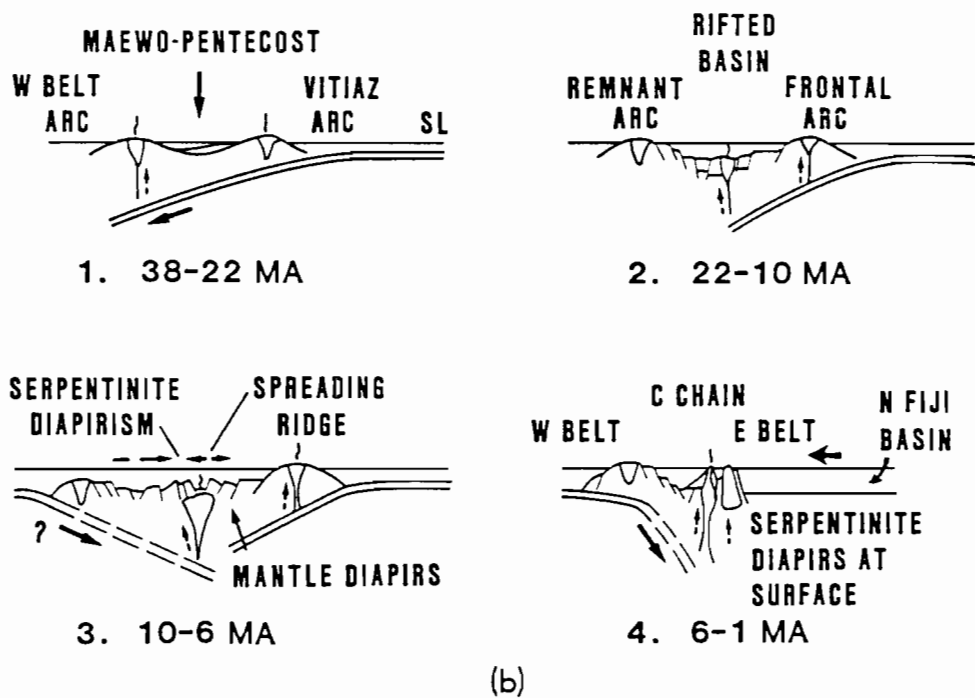
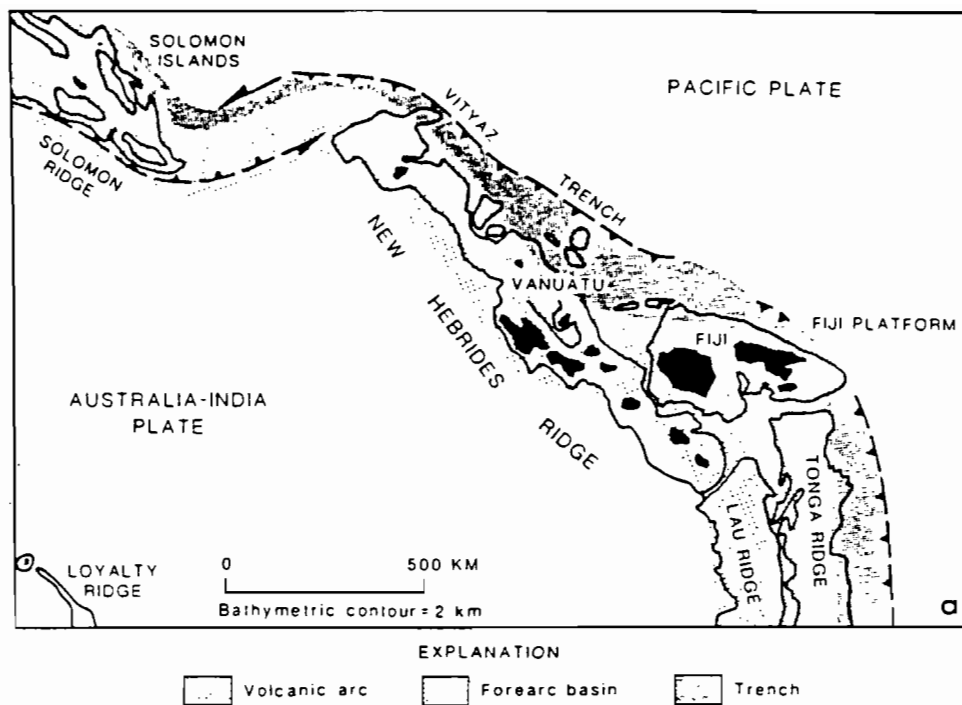


Figure 7: (a) Middle Miocene reconstruction of the Viti Levu arc by Falvey (1978), and (b) tectonic model for evolution of the New Hebrides Island Arc (Greene et al. 1988)

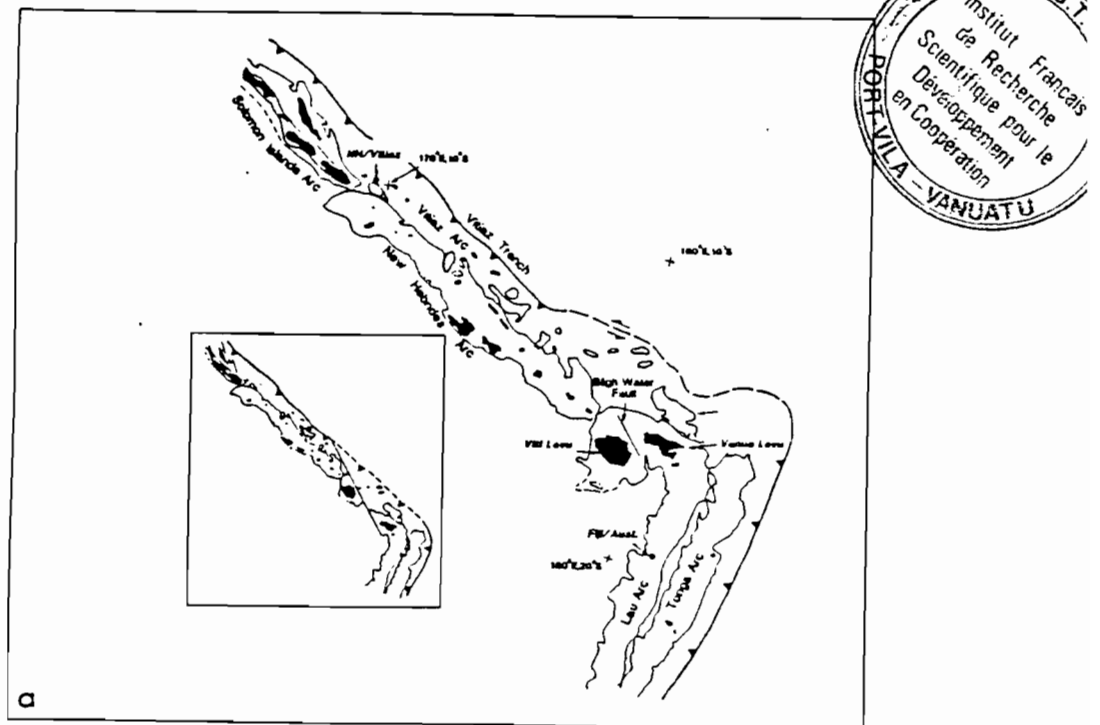


Figure 8: (a) Middle Miocene reconstruction of the Outer Melanesian Arc relative to a fixed Australian Plate. Inset shows a more speculative Middle Miocene reconstruction. After Musgrave & Firth (in prep).

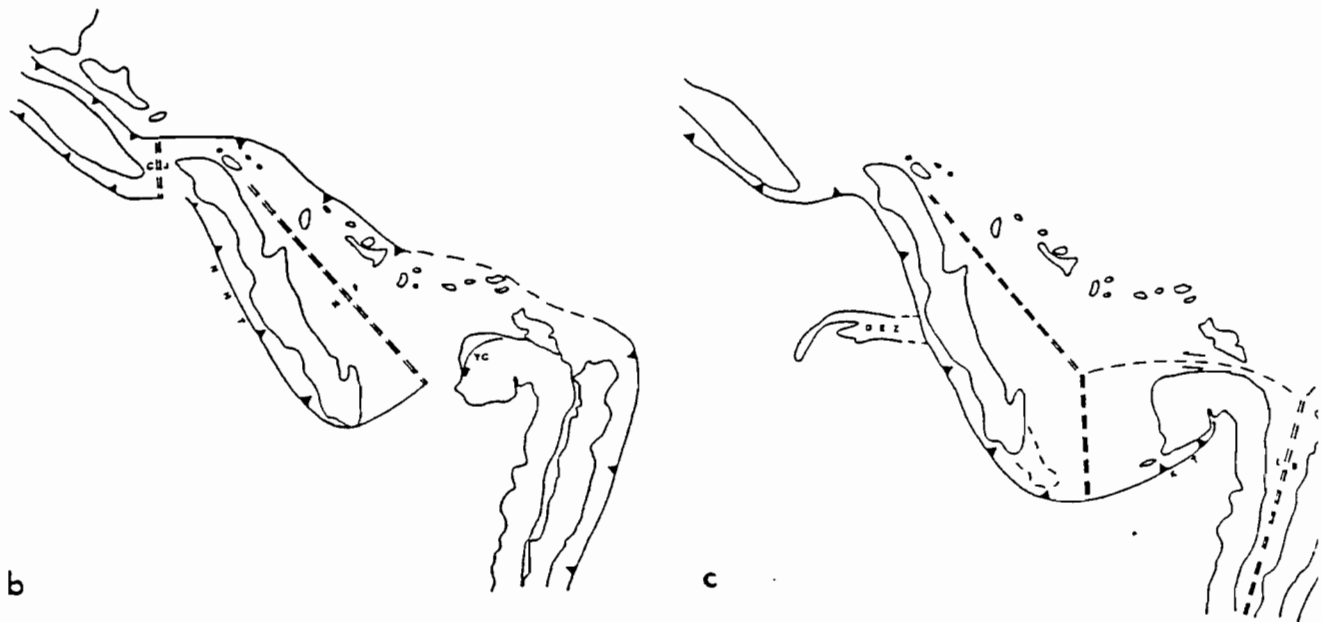


Figure 8: (b) About 5 Ma: Oblique subduction continues below the Solomons on both the North Solomons Trench and South Solomons Trench; subduction is active along the New Hebrides Trench (NHT), and subduction of Pacific Plate continues along the Vitiaz Trench. Subduction along the NHT is negligible in the north and increases southward. The North Fiji Basin is opening in response. (c) About 3 Ma: In response to a change in Pacific Plate motion, oblique subduction along the North Solomons Trench and Vitiaz Trench halts, and subduction rate along the South Solomons Trench increases to take up 100% of the Australia - Pacific convergence. Subduction rate also increases along the NHT. Solomon Islands and Vitiaz arc both transferred to the Pacific Plate. Rotation of the Fiji Platform causes subduction along the Kandavu Trench (Hunter Fracture Zone). As the New Hebrides Island Arc swings southwestward, it intercepts the d'Entrecasteaux Zone; the NHT grows southward, and new volcanic edifices extend the arc (After Musgrave & Firth, in prep.)

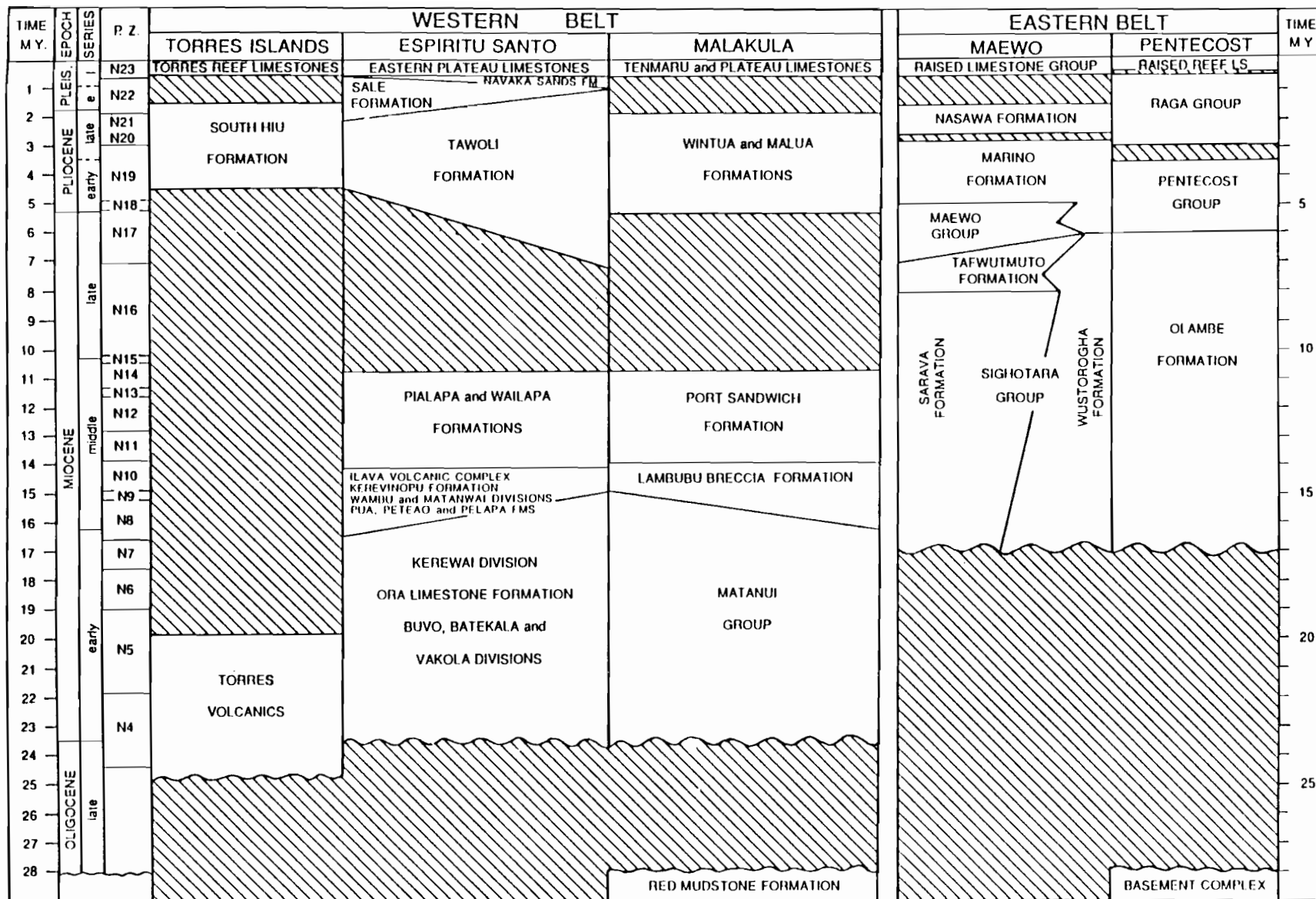


Figure 9: Principal stratigraphic units in the Western and Eastern Belts. After Macfarlane et al. (1988)

GEOLOGY OF THE ISLANDS

The Western Belt

The Western Belt (Fig. 2) consists of a crustal wedge of rocks up to 26 km thick along the western edge of the central arc platform complex in Vanuatu and is exposed on the islands of the Torres group, Espiritu Santo, and Malakula.

The Torres Islands (Greenbaum et al. 1975) form the most northerly landmass in Vanuatu and consist of a cluster of small, mainly coral islands with a total land area of no more than 120 km² and a maximum elevation of 366 m.

Espiritu Santo (Robinson 1969; Mallick & Greenbaum 1977; Carney & Macfarlane 1985), some 120 km farther to the south, is the largest island in Vanuatu and covers about 4,150 km². Physiographically it can be divided into a deeply dissected western mountain range of volcanics and volcanoclastics, including in the southwest Mt. Tabwemasana at 1,879 m (the highest point in Vanuatu), and an eastern reef limestone plateau series tilted eastward. In the Big Bay area, between these two blocks, is an extensive, low-lying alluvial plain.

Malakula (Mitchell 1966, 1971) is immediately southeast of, and comparable in size to, Espiritu Santo but has a much more subdued topography. The central volcanic area is deeply dissected and rises to only 879 m on Mt. Penot in the south. It is surrounded by an elevated coral limestone plateau and, at the coast, by narrow "ribbons" of alluvium bordering the major rivers that drain the interior.

Stratigraphic columns for the Western Belt islands are given in Figures 9 and 10.

Oligocene

Pelagic sediments of presumed Oligocene age accumulated in water depths of 4,000-6,000 m and are the oldest rocks known from the Western Belt (Fig. 10). They are exposed only in northwest Malakula, where they are assigned to the Red Mudstone Formation (Mitchell 1971). The sediments are well-indurated dark-red and chocolate-brown mudstones containing altered volcanic fragments and plagioclase crystals, which alternate with graded

sandstone and minor limestone laminae. The maximum thickness exposed is no more than 200 m. No diagnostic organic remains have been recognized. Because of their zeolite-facies metamorphic grade, these sediments are considered to be ocean floor deposits older than the dominantly volcanic Matanui Group to the east, with which they are in high-angle fault contact (Mitchell 1971). However, they could equally well be the uplifted deepwater-facies correlate of these volcanics (Carney et al. 1985).

Red claystone cobbles of probable deepwater origin, and similar to the Red Mudstone Formation pelagites, are present in a Quaternary limestone conglomerate on Efate to the southeast. They may have been derived from a southern extension of the Western Belt that was once in an elevated position near Efate (Carney 1982).

Late Oligocene to Early Miocene

The earliest event common to all the Western Belt islands was extensive submarine volcanic activity (Fig. 10) that locally built up small landmasses linked by fringing reefs. Basinal sediments were deposited between volcanic highs.

Torres Islands: The oldest rocks belong to the Torres Volcanics (Fig. 10; Greenbaum et al. 1975). Outcrops of the formation are confined largely to coastal sections. Rock types include autobrecciated and massive lavas interbedded with reworked pyroclastic and epiclastic breccias and tuffs.

The earliest volcanism was confined to the two northernmost islands in the group, and representative lavas include calc-alkaline hornblende andesites. Eruptive centers subsequently migrated southward, producing basaltic andesite and olivine basalt lavas. Deposition was largely submarine and the lavas are locally pillowed, of low vesicularity and not generally oxidized. However, minor subaerial flow units at the top of the succession indicate eventual emergence of the islands. Shallow water conditions, which supported reefal growth are also evident from limestone clasts in polymictic breccias from the southernmost island.

K/Ar determinations on porphyritic andesites from the northernmost island have yielded ages of 39 Ma and 37 Ma and place the Torres Volcanics at the late Eocene/

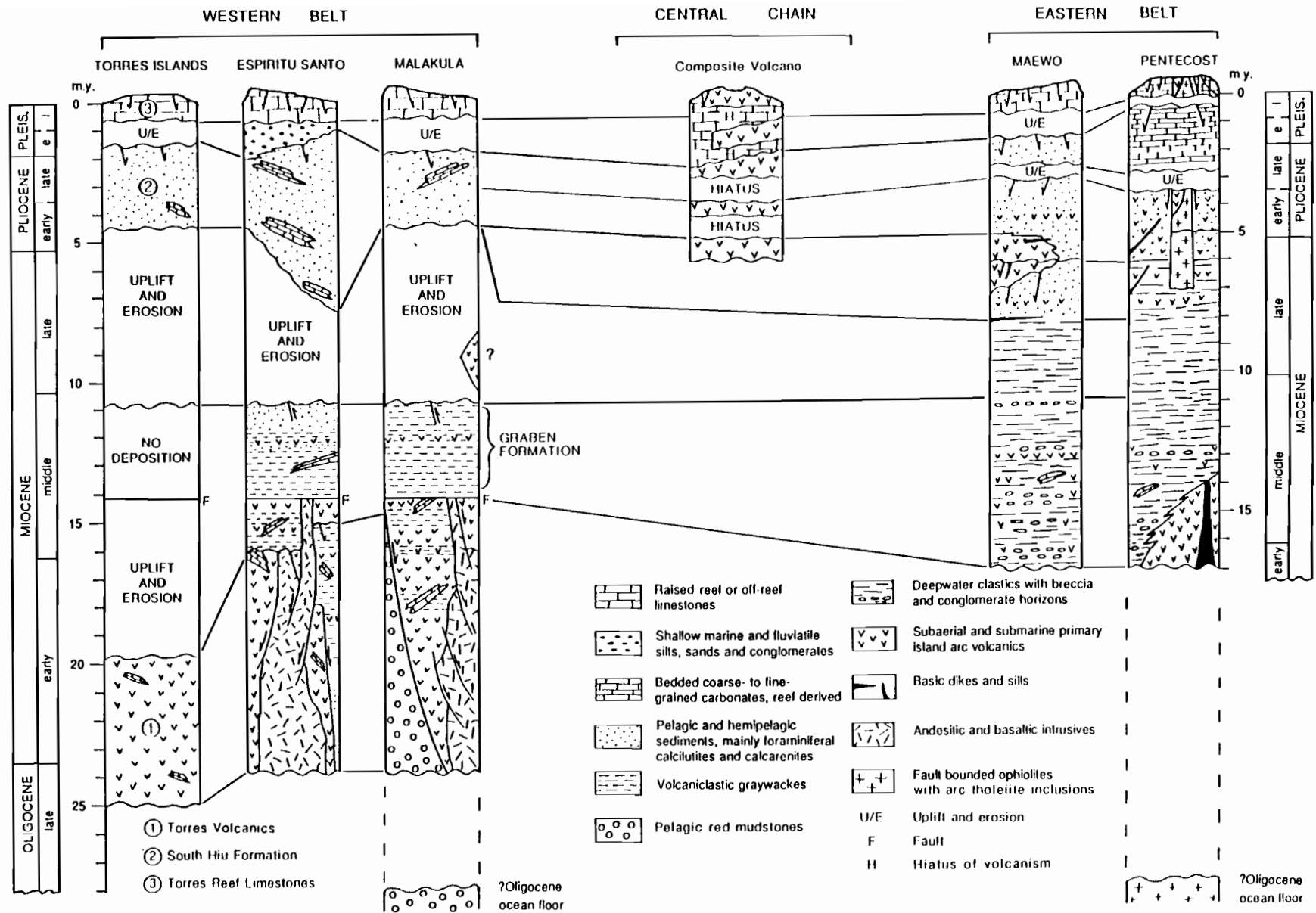


Figure 10: Correlation of principal stratigraphic units and geological events in the Western and Eastern Belts.
After Macfarlane et al. (1988)

early Oligocene boundary. However, foraminifers from limestone clasts indicate a late Oligocene to early Miocene age of no more than 20-25 Ma. Therefore, either a great time range exists within the Torres Volcanics or else, as preferred by Greenbaum et al. (1975) and Macfarlane et al. (1988), the radiometric ages are anomalously high. Kroenke (1984), on the other hand, argues for the validity of the K/Ar dates and an early Oligocene age for the Torres Volcanics. The problem remains unsolved.

Espiritu Santo: The oldest rocks (Fig. 10) occur in the southwest and are mainly coarse, massive submarine volcanic breccias derived by fragmentation of basaltic and andesitic lavas (Mallick & Greenbaum 1977). Accumulation was by mass transport close to the source vents that lay to the west, southwest, and east. Included within the breccias are graded units of fine breccias and sandstones together with local calcirudite bands and minor limestone horizons. No base to the breccias is exposed and minimum thicknesses are estimated at 3,000 m in the north and 1,000-2,000 m in the east.

Massive and discontinuous lenses of algal-nodule limestones with characteristic latest Oligocene to early Miocene microfossils, both overlie and are intercalated with the volcanic breccias. They indicate shallow-water deposition and the presence of fringing reefs around volcanic highs.

Malakula: Volcanics, volcanoclastics, and carbonates, equivalent in age to those of southwest Espiritu Santo, dominate the central regions of Malakula and are collectively assigned to the latest Oligocene to early Miocene Matanui Group (Mitchell 1966, 1971). They are the products of submarine volcanoes, which from time to time emerged as small islands surrounded by fringing reefs. Estimated thicknesses range from 7,000 m in the north to 3,000 m in the south, although nowhere is the base of the succession exposed.

Volcanic breccias and unsorted and unstratified submarine and subaerial autobreccias are the characteristic rock types. These grade with increasing proportions of matrix into volcanic paraconglomerates interbedded with greywackes and limestones. Andesite and basaltic andesite are the main clast types; mudstone, carbonized wood fragments and limestone are less common. Thin pyritized

sandstone and carbonaceous siltstone with wood and plant remains form thin bands and laminae in the finer sediments and are often associated with discontinuous beds and lenses of fragmental limestone; the latter may occur also as large exotic blocks up to 300 m in size. Dacitic pumiceous agglomerates and tuffs interlayered with the sediments are evidence of minor explosive volcanic activity and with the limestones form distinctive marker horizons.

K/Ar dates of 20-14 Ma from seven hornblende-bearing dikes cutting the volcanics (Mitchell 1971; Gorton 1974) support the latest Oligocene to early Miocene age for the Matanui Group.

Early to Middle Miocene

Thick basinal sequences accumulated in fault-bounded lows on Espiritu Santo and Malakula during early to middle Miocene time. Extensive submarine eruptions then followed, which largely buried the older sediments. No equivalent events are recognized in the Torres Islands at this time (Fig. 10).

Espiritu Santo: In early to middle Miocene time, sediments of the Pua, Peteao, and Pelapa Greywacke Formations were deposited in a large basin that extended between the volcanic highs of southwest Espiritu Santo and a landmass that once lay to the north or northwest of the Cumberland Peninsula on Santo (Carney & Macfarlane 1985).

Submarine accumulations of coarse volcanic breccias in south and southwest Espiritu Santo are derived from nearby source vents to the east and lie with unconformable, discordant, and fault-bounded contact on the older Miocene sequences. Primary pyroclastic material predominates as pyroxene and hornblende andesites and olivine basalts. Paraconglomerates, volcanoclastic sandstones and calcareous interbeds are minor. The age of the rocks is probably late early to early middle Miocene, although there is no supportive faunal evidence.

Along the Cumberland Peninsula, submarine deep-water accumulations of the Ilava Volcanic Complex (Carney & Macfarlane 1985) consist of coarse epiclastic paraconglomerates, predominantly basaltic breccias, and calcirudites. Eastward, primary basaltic pillow lavas, pillow breccias, and palagonitic tuffs predominate and

indicate deposition in shallower water close to former eruptive centers in the Big Bay area. Contact with the older Peteao Greywacke and Pelapa Greywacke Formations in the west is conformable and intergradational; thicknesses in this area approximate 500-600 m, and increase northward and eastward to a minimum of 2,500 m. Foraminifers indicate an early middle Miocene age (ca. 15 Ma) for the Ilava Volcanic Complex (Fig. 9). A K/Ar date of 21 Ma from an andesite breccia clast in the Ilava volcanics is thought to reflect derivation from an older, early Miocene source (Carney & Macfarlane 1985).

Malakula: Possible age equivalents of the early to middle Miocene Espiritu Santo volcanics are the coarse flow breccias of the 500 m thick Lambubu Breccia Formation (Mitchell 1971), which lie in isolation on the narrow neck joining northern and central Malakula. Other age equivalents (Figs. 9 & 10) may be the upper Matanui Group sediments of northern Malakula, where finely laminated volcanogenic siltstones and mudstones, 1,500 m thick, are equated with the early middle Miocene Pelapa Greywacke Formation of northern Espiritu Santo. The sediments are overlain by volcanic breccias, some of which are identical in composition and degree of alteration to those of the Lambubu outcrop (Carney 1985).

The exact relationship of the Lambubu Breccia Formation to the Matanui Group is not known, but it could be part of an upper subdivision within the older volcanics, not recognized or differentiated by Mitchell (1971) elsewhere on Malakula. The youngest K/Ar age of 14 Ma (Mitchell 1971) obtained from an intrusion cutting the volcanics would certainly accommodate such a subdivision.

An isolated outcrop of glassy basaltic andesite flow breccias located by Gorton (1974) on the southeast coast is from an uncertain provenance. His K/Ar ages of 10.7-7.5 Ma on three samples have been equated (Carney et al. 1985) with the 12.7-Ma date for the volcanics of Mitre Island (Jezek et al. 1977), which in the middle Miocene lay close to the Western Belt (e.g. Carney & Macfarlane 1978). Kroenke (1984), however, considers these ages as the first evidence of volcanism associated with east-facing subduction in the New Hebrides Island Arc.

Early to Middle Miocene Intrusions

Emplacement of early to middle Miocene late-stage intrusions is associated with the volcanism on Espiritu Santo and Malakula. No equivalent intrusive phase related to the Torres Islands volcanism has been identified, however.

Espiritu Santo: Composite intrusions of basalt, basaltic breccia, andesite, microdiorite, and minor gabbro, cut by later basalt and andesite dikes, are generally elongate in shape and parallel to the north and northeast-trending faults that controlled emplacement. Propylitic alteration and associated pyritization are common, phyllic and argillic alteration less so.

Three intrusive episodes are apparent. (1) A middle early Miocene episode is associated with the final phase of Oligocene to early Miocene volcanism in southwest Espiritu Santo. The N-S elongated intrusion in the extreme southwest of the island belongs to this episode (Mallick & Greenbaum 1977). (2) Intrusions of west-central Espiritu Santo and the Cumberland Peninsula are associated with the final phase of early to middle Miocene volcanism (Mallick & Greenbaum 1977; Carney & Macfarlane 1985).

Malakula: Late-stage intrusions are distributed throughout the Matanui Group (Mitchell 1966; 1971) but are known in detail only from northern and central Malakula (Carney 1985). In these latter localities, they are composite intrusions of basalt, andesite, microdiorite, and quartz diorite emplaced along NNE- and NNW-trending faults. Propylitic alteration with pyrite and minor chalcopyrite mineralization is pervasive.

K/Ar determinations on several of the intrusions give an age range of 2-14 Ma (Mitchell 1971; Gorton 1974). This age range is compatible with the early to middle Miocene timespan of the Espiritu Santo intrusions, although three separate episodes have not been demonstrated on Malakula.

Middle Miocene

In middle Miocene time, volcanogenic sediments and reefal carbonates derived from uplifted volcanic landmasses accumulated in fault-bounded, subsiding basins along the eastern margins of western Espiritu Santo and Malakula, and possibly off northern Efate. No

comparable sediments are found on the Torres Islands (Figs. 9 & 10).

Late Miocene to Early Pliocene

Uplift and erosion at the end of the middle Miocene was followed by progressive subsidence and marine transgression across all the Western Belt islands.

Torres Islands: The volcanic basement of the Torres Islands is overlain with gradational contact by the Pliocene-Pleistocene South Hiu Formation (Greenbaum et al. 1975), a thin and discontinuous horizon <10 m thick.

Espiritu Santo: Hemipelagites of the extensive Tawoli Formation on Santo lie with marked unconformity on early and middle Miocene rocks. The basal beds are diachronous, extending in age from late Miocene to earliest Pliocene, and were deposited after a marine transgression over highly dissected topography, in at least 700m water depth.

Malakula: Pliocene marine transgression across Malakula deposited sediments of the Wintua and Malua Formations on a marked angular unconformity on the Matanui Group. These mainly shallow marine and lagoonal sediments are never thicker than 200m and include calcareous sandstones and mudstones and occasional conglomerates.

Late Pliocene to Holocene

Shallow, regressive sequences of late Pliocene to Pleistocene age formed during uplift of Espiritu Santo, but occur nowhere else in the Western Belt. Reef limestones cap the older rocks of the Western Belt, and are the dominant rocktype in the Torres Group, over eastern Santo, and large parts of Malakula where they form a wide, nearly continuous platform around the island.

Geological History of the Western Belt

The oldest tectonic event in the Western Belt took place in late early Miocene time (ca. 16 Ma). It involved considerable east-west extension and intrusion into the southwest Espiritu Santo volcanic axis. It was followed by uplift and erosion and sediment accumulation in the

east-west fault-bounded Peteao-Pelapa-Pua Basin. Ages of 20-16 Ma on some of the Malakula intrusions may indicate that extension took place there also, but no comparable events are known from the Torres Islands.

In early middle Miocene time (15-14 Ma) NNE-SSW dextral wrenching and NW-SE reverse faulting, accompanied by uplift and erosion, were the sites of major intrusions on Espiritu Santo. A change in stress regime to one of tensional faulting followed, and grabens developed along the eastern margin of the main volcanic axes on both islands; structures of this age either truncated or reactivated the former wrench lines. The Torres Islands were submerged during this period.

Major uplift and erosion began in early late Miocene time (11-8 Ma) and was associated with E-W sinistral wrenching on Espiritu Santo. Equivalent events on Malakula were NW-SE reverse faulting and synclinal development. The Torres Islands emerged at this time.

In the middle late Miocene (8-7 Ma) subsidence began along the Western Belt, with deposition of the Tawoli Formation. Total submergence had occurred by the early Pliocene, at which time subsidence had also begun on Malakula and the Torres Islands, leading to the deposition of the Malua and Wintua Formations, and the South Hiu Formation, respectively.

The general subsidence of the Western Belt was interrupted by brief intervals of uplift and erosion in the Pliocene (5-3 Ma) (Taylor 1977). At this time considerable terrigenous material, including reef-derived calcarenite and calcirudite, was added to the sedimentary column.

Final vertical uplift of the Western Belt along normal faults parallel to its general NW-SE axis in latest Pliocene to Holocene time (2-0 Ma), was rapid, and influenced by the subduction of the d'Entrecasteaux Zone. It brought about elevation of the Quaternary limestones on all three islands. Subduction of this bathymetric high caused tilting of southern Espiritu Santo to the east, and of northern Malakula to the northeast. Inferred rates of uplift for Espiritu Santo are 1-7 mm/yr increasing from east to west, and for Malakula 0.4-5 mm/yr increasing from northeast to southwest (Jouannic et al. 1980; Taylor et al. 1980). Limestone plateaux in the Torres group, in contrast, are generally horizontal.

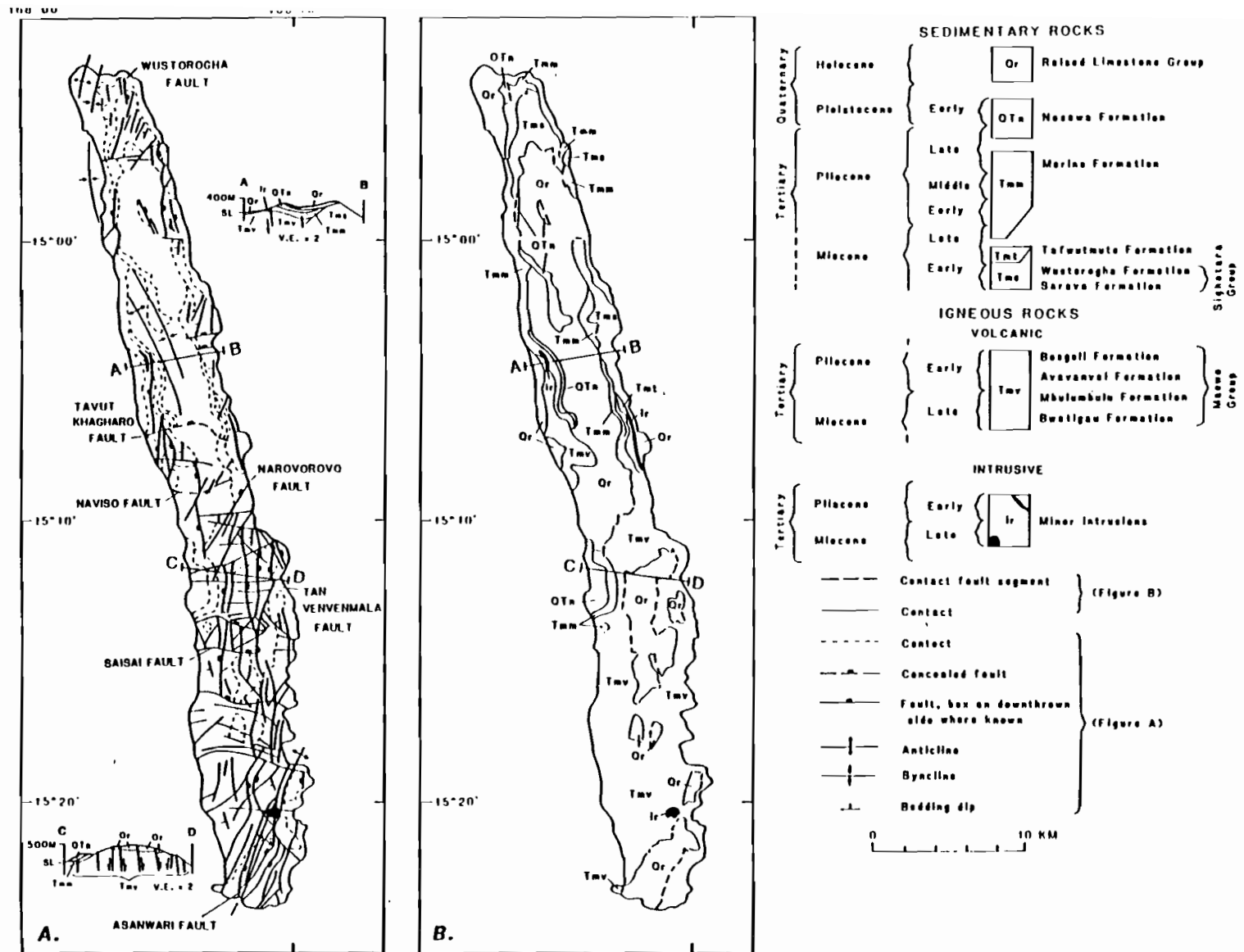


Figure 11: Main structural (a) and geological (b) divisions of Maewo. After Macfarlane et al. (1988).

The Eastern Belt

The islands of Maewo (Carney 1988) and Pentecost (Mallick & Neef 1974) are the subaerial expression of the Eastern Belt (Fig. 2), a narrow, uplifted horst more than 120 km long and 4-11 km wide on the eastern edge of the arc platform complex (Greene et al. 1988). Structural and geological maps of Maewo and Pentecost are given in Figures 11 and 12 respectively. Morphologically, both islands have much in common. They are linear in outline, of similar areal extent and elevation (just over 800 m maximum), and bounded by steep coastal scarps. The southern half of each island consists of deeply dissected volcanics, volcanoclastics and, in the case of Pentecost, ophiolites. The less dissected northern parts, however, are dominated by reefal limestone plateaux.

Oligocene

The oldest known rocks from the Eastern Belt (Figs. 9 & 10) belong to the Basement Complex, an ophiolite suite emplaced into younger sequences, both as horst blocks and as narrow irregular masses in east-west fractures, along the southern spine of Pentecost (Mallick & Neef 1974). These ophiolites have oceanic affinities and may be derivatives of Oligocene seafloor upon which the Eastern Belt island arc volcanics originally accumulated. Alternatively, they may represent the earliest manifestations of North Fiji Basin magmatism, erupted around 15-12 Ma, which have been thrust back westward over the arc, perhaps associated with collision of the d'Entrecasteaux Zone.

Principal components of the Basement Complex are (1) an ultramafic group of harzburgite, serpentinite, dunite, and banded feldspathic peridotite, all carrying blocks and rafts of schistose epidote amphibolite and cut by gabbroic stocks and dikes, and (2) a thick pile of submarine pillow basaltic lavas (the Baumar Metalavas of Mallick & Neef 1974), which are thermally and metasomatically altered by gabbroic intrusions, themselves partly metamorphosed. They are believed to be the same age as the ultramafic rocks although the relationship between the two is not clear.

Two K-Ar dates of 35 ± 2 Ma and 28 ± 6 Ma suggest an early Oligocene age for the amphibolite metamorphism, and a late Oligocene or early Miocene age for the

ultramafics and metalavas intruded by the gabbro (Mallick & Neef 1974). Other determinations of 13.6 Ma and 5.7 Ma (Gorton 1974), have been attributed to later retrograde modifications such as re-equilibration during later volcanism and tectonism (Macfarlane et al. 1988). The 13.6 Ma age on a gabbro dike (Gorton 1974) matches the age of interpreted earliest North Fiji Basin opening (Monjaret et al. 1991). It also accords with known tholeiitic eruptions in the Vitiaz arc at about this time, as shown by the 12.7 Ma volcanics on Mitre Island (Jezek et al. 1977). Although the oceanic affinity of the Basement Complex is not in dispute, certain of the metalavas and gabbroic intrusions are compositionally more typical of arc tholeiitic magmas, and further petrological - geochemical - geochronological (T. Crawford) and palaeomagnetic (R. Musgrave) studies are in progress to determine the age and tectonic affinities of this suite.

Intrusion as horst blocks is thought to have occurred first in latest Miocene to earliest Pliocene time and continued into the middle Pliocene, when the complex was unroofed by erosion. Further vertical uplift occurred in Quaternary time.

No equivalent of the Basement Complex is found on Maewo. However, a large Bouguer anomaly over the island, similar to one over Pentecost, suggests ophiolite masses at shallow depths.

Early to Late Miocene

Mainly during the middle Miocene, clastic sediment transported by mass flow accumulated on both Maewo and Pentecost. By late Miocene time, quiet-water deposition prevailed (on Maewo) and submarine eruptions, the precursors of later Eastern Belt volcanism, began (Figs. 9 & 10).

Maewo: The oldest rocks on Maewo belong to the Sigihotara Group (Carney 1988) which is exposed along the northeast coast of the island as a 600-m-thick succession of predominantly medium- to fine-grained and well-bedded epiclastic sediments; the base of the sequence is nowhere exposed (Fig. 11). The lowermost beds are very coarse grained and consist of cobble conglomerates, intraformational breccias, and minor calcarenites. Rounded cobbles of metabasalt, dacitic welded tuff, microdiorite, sediment, and reef limestone

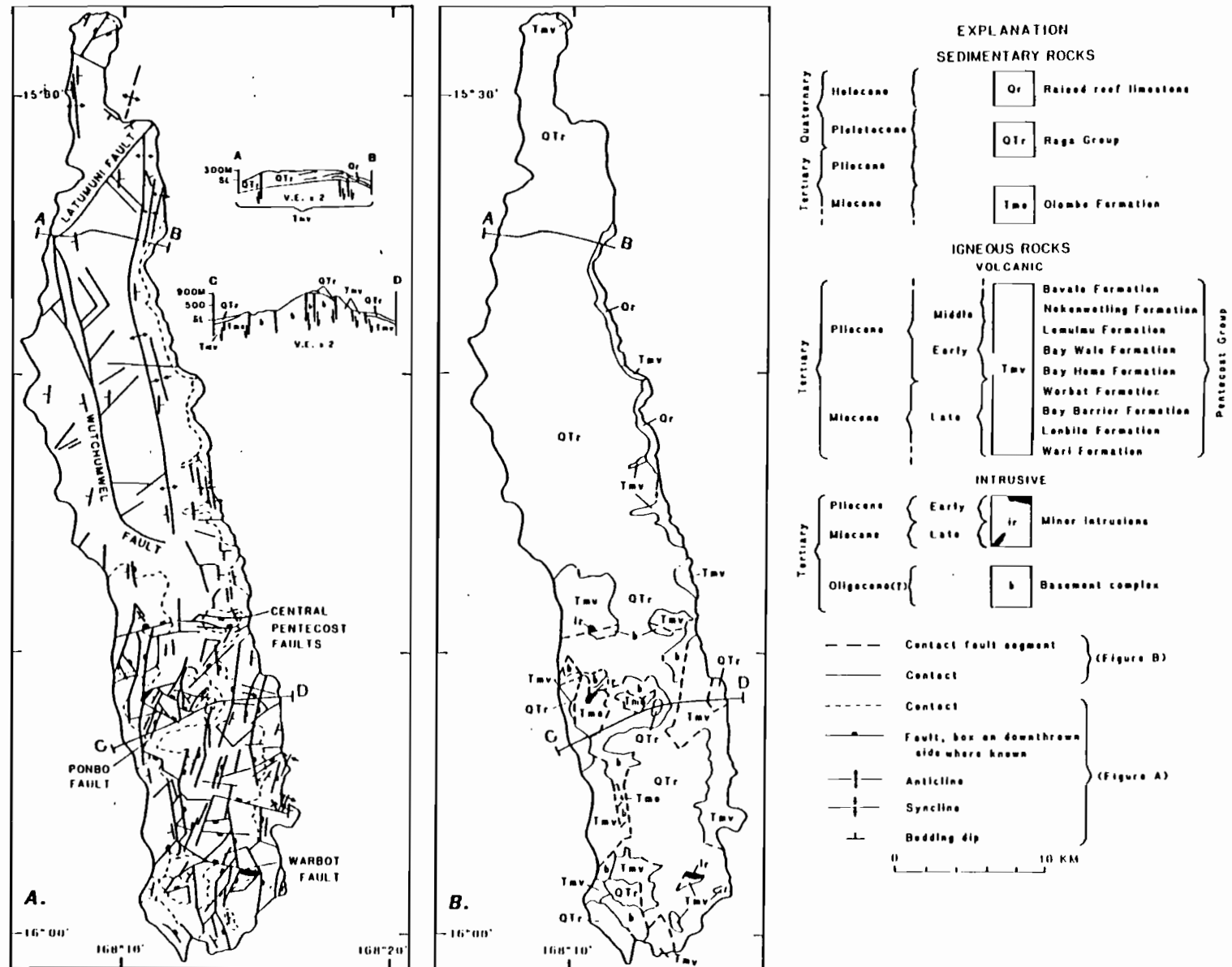


Figure 12: Main structural (a) and geological (b) divisions of Pentecost. After Macfarlane et al. (1988)

with benthonic foraminifers are the most common clast types. These beds are succeeded by tuffaceous siltstones and fine sandstones which make up the bulk of the sequence. The sediments are turbidites with repeated graded bedding, cross-lamination, convolute lamination, and load casts; occasional globigerinid foraminifers are present. Well-preserved glass shards within them indicate pyroclastic activity contemporaneous with deposition.

The lower part of the Sighetara Group is at least early middle Miocene in age (ca. 15 Ma) and probably as old as the late early Miocene (Carney 1988). The uppermost mudstones range somewhere between Zones N16 to N18 (10-5 Ma) in the late Miocene (Fig. 9). In contrast, calcareous clasts from the basal conglomerates have been dated as late Eocene and early Miocene, and their microfaunal content and lithology match rocks of similar ages in Fiji (Coleman 1969; Carney & Macfarlane 1978). The source of the igneous clasts can also be matched petrologically and geochemically with Eocene to middle Miocene arc tholeiitic suites from Fiji, whereas they bear no similarity to the calcalkaline early to middle Miocene volcanics of the Western Belt (Carney & Macfarlane 1978; Carney 1988).

Conformable on the uppermost unit in the Sighetara Group but confined to its southern outcrop is the Tafwutmuto Formation. This formation consists of 60-120 m of massively bedded foraminiferal mudstones with minor micritic limestone and some horizons of pumiceous tuff. On the basis of microfossils, the formation is placed in the late Miocene, no older than 8.6-6.0 Ma. Deposition of the Tafwutmuto Formation took place adjacent to a shallow slope, in quiet water at depths of 2,000-3,000 m. The tuff horizons are the first indication of the main Eastern Belt volcanism that followed.

Pentecost. Rocks of mainly middle Miocene age on Pentecost belong to the Olambe Formation (Mallick & Neef 1974), a 300-m-thick sequence of massive polymictic breccia conglomerates overlain by fine-bedded volcanoclastic sandstones that pass upward into siltstones and fine sandstones (Fig. 12).

The breccia conglomerates contain rounded basaltic and andesitic lava pebbles, angular clasts of coral limestone with large benthonic foraminifers, and epiclastic siltstone; in some beds angular pyroclastic fragments of acid andesite

and latite pumice are present. The volcanoclastic sandstones and siltstones, the dominant lithologies, are free of terrigenous material. They do, however, have occasional horizons rich in planktonic foraminifers, heavy mineral layers, and repeated graded units indicative of deposition by turbidity currents. Also several horizons of pillowed basalt lavas near the top of the formation are cut by dolerite dikes.

Two K/Ar dates of 12 ± 5 Ma (Mallick & Neef 1974) and 6 Ma (Gorton 1974) on a dolerite dike in pillowed basalt indicate a minimum age of middle to latest Miocene for the Olambe Formation. A faunal age of late early Miocene to early middle Miocene is given (Mallick & Neef 1974) by an assemblage of larger foraminifers from the breccias.

Initial accumulation of the Olambe Formation breccia conglomerates was in shallow water. Graded sandstones mark a change to deeper water conditions, although the association with heavy-mineral layers suggests mass transport of shallow-water sediment into a deeper water environment. The intercalated primary volcanic material, as in the Tafwutmuto Formation on Maewo, probably derives from precursors of the main Eastern Belt volcanism that followed.

Late Miocene to Late Pliocene

From middle late Miocene to middle Pliocene time, copious volcanism took place in the Eastern Belt, beginning first on Maewo then spreading south to Pentecost. By the early Pliocene, however, volcanism had ceased on Maewo and had given way to quiet-water sedimentation. By the beginning of the Pliocene, the Basement Complex on Pentecost had moved to a high structural level beneath the volcanic pile.

Maewo: The late Miocene to late Pliocene succession on Maewo is represented by the Maewo Group and the Marino Formation (Carney 1988). The Maewo Group is a diverse series of submarine volcanic and volcanoclastic rocks deposited unconformably on a block-faulted and west-tilted "basement" of older Miocene sediments. Exposures are confined to the southern half of the island, where the sequence reaches a maximum thickness in the west of 700-800 m. However, the succession pinches out rapidly toward the north and east where it abuts the

Sighotara Group.

The major part of the Maewo Group (Bwatigau Formation) is a thick (as much as 800 m) sequence of pillow lavas and associated intrusions ranging in composition from basal ankaramites, picrites, and mafic-enriched porphyritic basalts to an upper series of feldsparphyric basalts and basaltic andesites. These rocks erupted from large-volume submarine fissures and were deposited as shield or plateau-like accumulations in a pelagic environment at depths of 2,000-3,000m.

Subsequent block faulting of the lavas was followed by more explosive volcanism in shallow water over the source vents. These events led to deposition on an irregular topography of a restricted 40 m-thick sequence of reworked fine tuffs and fossil *Globigerina* ooze in the southwest (Mbulumbulu Formation), and in the west and south of 80-100 m of medium- to coarse-grained palagonitized tuffs and coarse breccias (Avavanvai Formation). Clasts in the breccias include pillow basalt, basaltic andesite and reefal limestone. Contemporaneous with the explosive volcanism was quiet-water sedimentation in the north, giving rise to an 80-100 m-thick sequence of fine-grained, reworked, and well-sorted tuffs and intercalated mudstones (Bosgoli Formation), which grades vertically and laterally southward into the Avavanvai Formation.

Foraminiferal assemblages indicate an age of middle late Miocene to earliest Pliocene (7-5 Ma) for the Maewo Group. This age is substantiated by a K/Ar date of 7 Ma on a pillow lava from the Bwatigau Formation.

Deposition of the overlying Marino Formation during the Pliocene (Fig. 9) was in quiet, fairly deep water without significant terrestrial or volcanic influxes other than the tuffaceous sediments of the Maewo Group which interfinger at the base. Contemporaneous magmatism is implied by angular glassy fragments in the sediments and by basaltic stocks and sills associated with late-stage activity in the Maewo Group.

Pentecost: The Miocene to Pliocene volcanic pile on Pentecost belongs to the Pentecost Group (Mallick & Neef 1974). Outcrops are discontinuous and, except for one exposure on the extreme northern tip of the island, are concentrated in the south. On the west coast it lies conformably on the Olambe Formation, but as there is

little petrological difference between the two units there, the exact position of the contact is uncertain.

The Pentecost Group comprises lava piles and thick accumulations of poorly sorted angular pyroclastic rocks that were deposited largely in deep water close to the source vents. Two eruptive cycles are recognized. The first of these gave rise to 250-350 m of pillow basalt lavas on the southeast coast (Wari Formation) and on the west-central coast (Lemulmu Formation). This was followed by 200-600 m of massive basaltic and andesitic breccias in the east (Lonbila and Nokonwetling Formations) and south (lower Warbot Formation). Interbedded with these formations are thick volcanoclastic sequences of graded sandstones and thinly bedded turbiditic sandstones and siltstones, grading into finer foraminifer-rich calcilutites. Large-scale slump folding occurs on the east coast. Thin horizons of basalt and andesite lavas, and rare beds of pelagic limestones of fossil *Globigerina* oozes are also present.

The second eruptive cycle produced a 120-800 m sequence of pillow lava masses and rubble breccias of avalanche type in the east (Bay Barrier Formation), north (Bevala Formation), west (Bay Homo Formation), and south (upper Warbot Formation). The Bay Homo lavas at one locality contain ultramafic xenoliths of partly serpentinized lherzolite. The eruptions were basaltic, with ankaramitic affinities, and on the east coast lie unconformably on the rocks of the first cycle. On the west coast, amygdaloidal lavas and a thin horizon of limestone clastic indicate shallow-water deposition. The youngest beds (Bay Wale Formation) on the west coast are predominantly well-bedded sandstones and fine breccias, 800-1,000 m thick, with a few blocky or brecciated horizons. The sandstones grade into foraminifer-rich mudstones.

Faunal assemblages in the foraminifer-rich beds fall within Zone N18-N19 (Fig. 9) and possibly extend back into the upper part of Zone N17, indicating a late Miocene to middle Pliocene age (6-3 Ma) for the Pentecost Group (Mallick & Neef 1974). This age is supported by K/Ar dates of 6 to 3 Ma on ten lava and breccia samples (Gorton 1974).

Late Pliocene to Holocene

Uplift and erosion of the Eastern Belt occurred in earliest late Pliocene time. During this same interval on Pentecost, the Basement Complex was emplaced and its unroofing began. Subsidence and shallow-water deposition followed on both Maewo and Pentecost. During late Pleistocene to Holocene time, the Eastern Belt emerged and reef limestones accumulated on the peneplained older rock units. On Pentecost, uplift since late Pleistocene time is indicated by the presence of five reef-capped wave-cut platforms (max. elevation 340m) of which the oldest is estimated to be 105,000 B.P., and the average uplift rate is calculated at 2.7mm/yr.

The Central Chain

The active volcanic chain (Central Chain) of the arc platform complex has a maximum width of 160 km. It forms a line of islands, of different ages and erosional states, between Vot Tande in the north and Anatom in the south (Fig. 13), although the submarine Mons Gemini volcanoes south of Anatom are clearly part of the Central Chain (Monzier et al. in press). The eruptive history dates from late Miocene time and thus overlaps with that of the Eastern Belt.

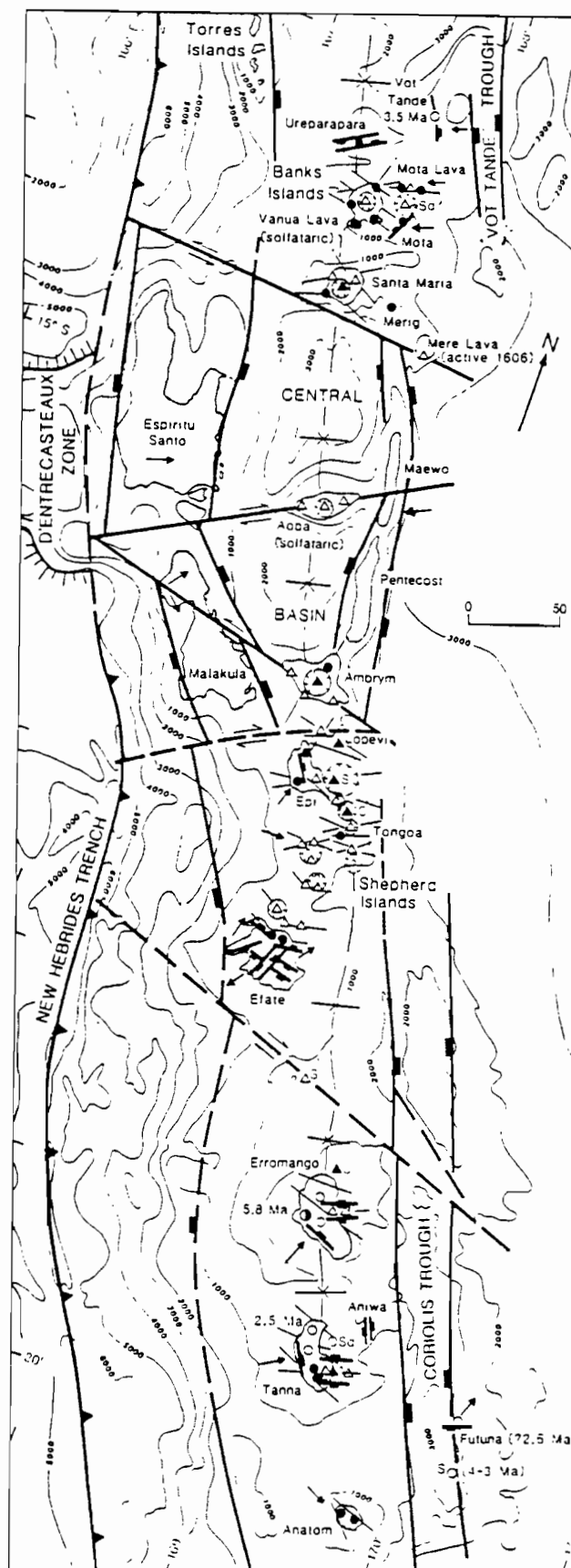
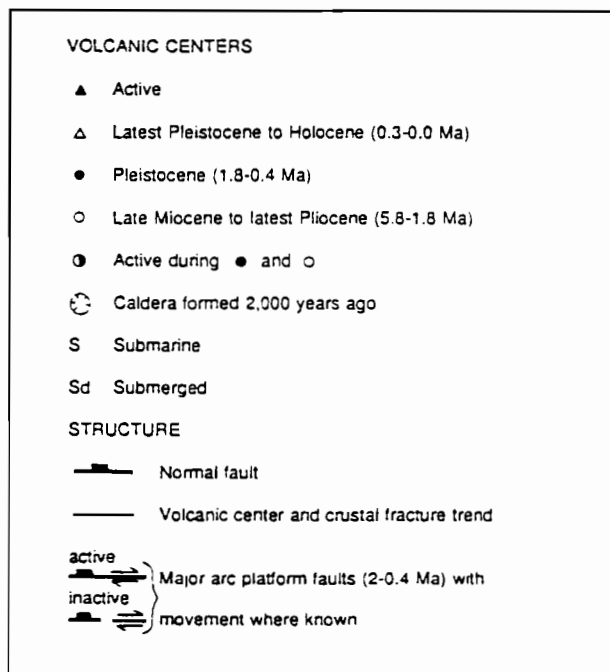


Figure 13: Principal volcanic centres and structural trends in the Central Chain. After Macfarlane et al. (1988).

Based on present evidence, Central Chain volcanism from the late Miocene (at least as old as 5.8 Ma) to the latest Pliocene was confined to Erromango, Tanna, Anatom and the most easterly islands of Futuna and Vot Tande (Fig. 14). From Pleistocene to the present, however, volcanism (mainly subaerial) developed extensively along the length of the active arc, which narrowed at this time to its present width of ~75 km.

One striking feature of the Central Chain (Fig. 13) is the remarkably even spacing between the six southernmost volcanoes of the arc, from Mons Gemini northward to Efate (including the submarine Vulcan Seamount between Erromango and Efate). With an average spacing of 85 km (range 83-91 km), this distribution is far more regular than noted for any other island arc volcanic chain, and presumably reflects Raleigh-Taylor gravitational instability of the source peridotite of these volcanoes above the Benioff zone. Where the arc is complicated by the d'Entrecasteaux Zone collision north of Efate, and in the region of transient tectonics south of Anatom due to recent elongation of the trench and arc, this regular inter-volcano spacing breaks down

History of Volcanism

Late Miocene volcanism (5.8 - 5.3 Ma.) on Erromango is the oldest known from the Central Chain (Colley & Ash 1971; Bellon et al. 1984). Two volcanic centers in the west and central parts of the island were submarine and largely explosive, erupting basaltic and andesitic pyroclastics and rare pillow lava flows.

During early to middle Pliocene time (4.1 - 3.4 Ma), voluminous subaerial extrusions of ankaramitic basalt to basaltic andesite lavas on Erromango came from three centers in the west and north (Colley & Ash 1971; Bellon et al. 1984). Submarine volcanism of this age (4-3 Ma) is also inferred from dredged samples of basalt lava and foraminiferal tuff taken from the scarps and floor of the Coriolis Trough (Dugas et al. 1977). Vot Tande (3.5 Ma), the northernmost island of Vanuatu, was active at this time (Ash et al. 1980).

The late Pliocene was a time of major activity in the southern islands (Fig. 14). On Erromango (2.6 - 2.3 Ma), there were voluminous eruptions of andesitic lavas and pyroclastics from four subaerial centers. Caldera collapse occurred in the north (Colley & Ash 1971; Bellon et al.

1984). Subaerial volcanism commenced on Tanna. (2.5 - 2.4 Ma) from basaltic cones in the north and middle parts of the island. A third, partly submarine andesitic centre east of the island is now submerged. Faunal ages suggest that Futuna was also active in the late Pliocene, volcanism giving rise to a predominantly submarine basalts and culminating in late stage intrusions at ca. 1.8 Ma. The small, lowlying and reef limestone-capped island of Aniwa to the northeast of Tanna may also overlie a late Pliocene volcano.

Throughout most of the Pleistocene, volcanism was extensive along the length of the Central Chain (Fig. 14). In the southern islands the first eruptions of this period gave rise to two large subaerial basaltic stratovolcanoes in southern Tanna (1.7 - 0.6 Ma), with contemporaneous explosive eruptions of andesitic pyroclastics forming a distal apron around them. Ash blown to the northeast settled on the Pleistocene limestone cap of Aniwa as superficial tuff deposits. To the south, two large subaerial basaltic stratovolcanoes built up Anatom; emplacement of multiple basaltic and andesitic intrusions into their vents was associated with caldera formation (Carney & Macfarlane 1979; 1982). On Erromango (1.2 - 1.1 Ma) activity was confined to one centre in the west from which there were terminal effusions of basaltic andesite lavas.

On Efate (1.6 - 1.4 Ma), large submarine explosive eruptions, perhaps associated with caldera subsidence, produced a thick sequence of dacitic to rhyolitic pumice breccias and tuffs that now occupy the central part of the island. Volcanism on Efate moved north (and included the small offshore islands) and from 1.5 - 0.9 Ma mainly submarine basaltic volcanism occurred.

Submarine andesitic pyroclastics are the earliest volcanic events on western Epi (0.7-0.4 Ma), and were followed by voluminous eruptions of pillow basalts, which brought the volcano up to sealevel. Similar but somewhat older basalts also occur on southwest Tongoa (Warden 1967).

The large basaltic shield volcanoes of Aoba (0.7 Ma) and Ambrym (ca. 1.8 - 0.5 Ma) have been built up from the floor of the North Aoba Basin (Carney & Macfarlane 1980), where they appear to be aligned along major faults related to the collision of the d'Entrecasteaux Zone. Both volcanoes include large volumes of picritic and

ankaramitic lavas, and the volcanic and petrogenetic details of these volcanoes are discussed elsewhere, including in this field-guide (Carney & Macfarlane 1982; Robin et al. 1993; Eggins 1993; this guide).

Volcanic products of latest Pliocene to late Pleistocene age in the Banks Islands (1.8 - 0.4 Ma) are mainly subaerial. They are represented on the two largest islands of Santa Maria (Gaua) (1.8 - 0.8 Ma) and Vanua Lava (0.5 Ma) by rugged massifs which are the erosional remnants of two former basaltic stratovolcanoes (see below). Ureparapara is a large basalt and basaltic andesite composite cone with a central crater exposed to the sea through its northeastern flank. Both Mota Lava (0.4 Ma) and Mota have been eroded to expose central basaltic spines. All that remains on Merig (1.1 Ma) is a hornblende andesite plug with basaltic - andesitic breccias around its margins (Mallick & Ash 1975; Ash et al. 1980).

During latest Pleistocene to Holocene time, volcanism gradually decreased and the active belt narrowed to its present width. In the southern islands, only Tanna and Erromango were active from centres that had shifted eastward. On Erromango (ca. 0.3 - 0 Ma), eruptions were mainly pyroclastic, but with basaltic to andesitic lavas at the bottom and top. The sequence grew into three well-preserved subaerial cones. Present activity, however, is restricted to a submarine vent off the northeast coast of the island (Colley & Ash 1971; Bellon et al. 1984). On Tanna, predominantly subaerial eruptions of andesitic pyroclastics followed by flood basaltic andesite lavas began at about 0.2 Ma and continued until the end of the Pleistocene. Renewed volcanism 2,000-3,000 yr B.P. produced andesitic lavas from a late-stage caldera. An active andesitic cinder cone, initiated within the last 500 years, lies within the caldera (Carney & Macfarlane 1979). Tanna volcanology is discussed in more detail below. The southernmost islands of Matthew and Hunter are intermittently active Holocene andesitic volcanoes (Maillet et al. 1986), and these are separated from the remainder of the arc to the north by a number of major submarine volcanoes recently described by Monzier et al. (in press).

Near Efate, eruptions from late Pleistocene to Holocene time (0.2 - 0 Ma) were confined to three islands immediately off the northern coast and built up subaerial composite basaltic cones in the well-preserved craters. Caldera collapse occurred in the very recent past (<2,000

yr B.P., but there is no evidence of present day activity.

Explosive andesitic eruptions built up numerous subaerial cones with well-preserved craters on eastern Epi and Tongoa (0.07-0 Ma) and on the small islands of the Shepherd group. The eruptions culminated in a massive eruptions and collapse of Kuwae caldera, between eastern Epi and Tongoa about 500 yr B.P. (Robin et al. 1993; this guide). Active submarine, mainly pyroclastic, cones have since grown within the Epi-Tongoa calderas (Crawford et al. 1988). The subaerial active basalt to basaltic andesite Lopevi volcano northeast of Epi is entirely Holocene in age (Warden 1967; Macfarlane 1976; Carney & Macfarlane 1977; this guide).

Rapid construction of the modern-day composite basaltic volcanoes on Aoba and Ambrym (see below) commenced in latest Pleistocene time (ca. 0.3 Ma). Fissure eruptions and caldera collapse have both taken place within the last 2,000 years and have given rise to the present low-angle shield morphologies of these islands (McCall et al. 1970; Warden 1970).

In the Banks Islands (0.2 - 0 Ma), renewed subaerial growth (see below) took place in the late Pleistocene centre of Santa Maria (Gaua). A basalt to basaltic andesite cone developed first and was then followed by extensive ash emissions that accompanied quiet caldera collapse. New cinder cones, one of which is active, subsequently built up inside the caldera. On Vanua Lava subaerial eruptions of andesite lavas in the latest Pleistocene were succeeded in Holocene time by the andesitic and basaltic andesite lavas and pyroclastics that preceded caldera collapse. This collapse was probably synchronous with the one on Santa Maria about 2,000 yr B.P. Growth of several composite cones took place later across the caldera's eastern sector. The volcano was considered to be in the solfataric stage until eruptions of ash recommenced in 1962, and minor eruptions from Mt Garete have continued intermittently to the present time (see below).

Two subaerial basaltic cones formed on the older centres of Mota Lava. A third centre on the island's south-central flank is now submerged. Mere Lava, the most eastern of the Banks group, is a Holocene, little-dissected, subaerial basaltic cone with a well-preserved summit crater - cinder-cone complex. The last reported eruption was in 1606 (Ash et al. 1980), and lavas are unusual Ca-rich arc tholeiites (Barsdell 1988).

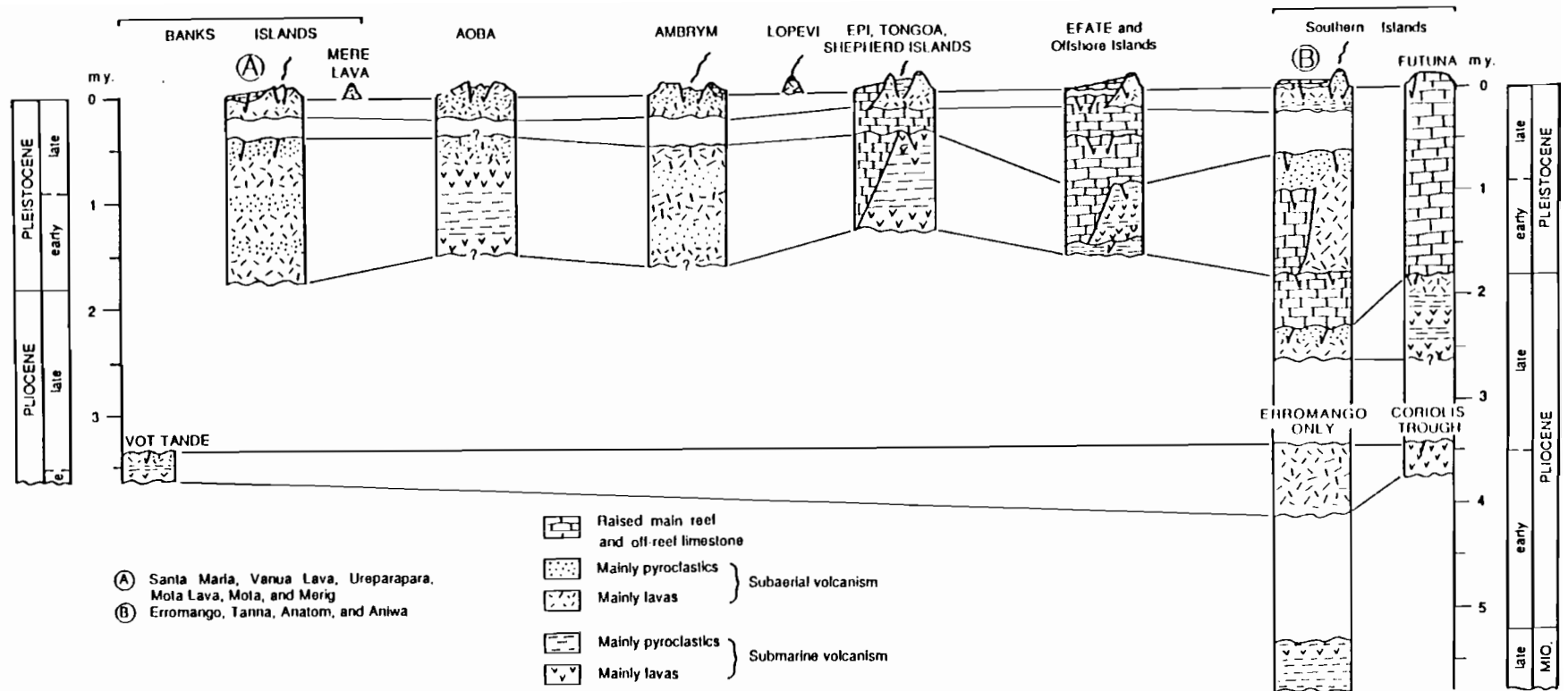


Figure 14: Correlation of volcanism between islands and island groups of the Central Chain. After Macfarlane et al (1988)

PETROGENESIS IN THE NEW HEBRIDES ISLAND ARC

Compared to many island arcs, the New Hebrides Island Arc has received scant attention from igneous petrologists and geochemists. Earliest useful studies of the arc include Colley & Warden (1974) and Gorton (1974, 1977), who pointed out the calc-alkaline affinities of the Miocene Western Belt lavas, and demonstrated the presence in the central part of the active chain of picritic and ankaramitic lavas with high-K compositions. Subsequent work has been largely fragmentary, reporting major and trace element studies of one or two lavas from several of the islands, but lacking any overview of the relationships between magmatic compositions and regional or local tectonics.

The New Hebrides Island Arc is possibly unique among modern subduction zone settings, as it is dominated by basaltic compositions (Fig. 15). Many of these are primitive magnesian basalts, and offer an excellent opportunity to investigate the geochemical character of subduction zone primary magmas.

Magmatic suites in the New Hebrides Island Arc are chemically diverse, and by simply tracing differentiation trends of individual suites, a spectrum of primary magmas ranging from low-K tholeiite to high-K alkaline compositions is shown to exist in the arc (Fig. 16).

Apart from a predominance of relatively high-K primitive compositions where the arc is affected by collision of the d'Entrecasteaux Zone (i.e. Aoba, Santa Maria and Ambrym volcanoes), there exists no clear spatial association of magmatic compositions with tectonic setting within the arc. Elsewhere, separate low-, medium- or high-K suites can occur (e.g. Anatom, Tanna, Epi - also Ambrym), though these suites tend to be temporally distinct. Representative wholerock analyses are given in Appendix A.

Primitive magma compositions and differentiation

Establishing the chemical composition(s) of subduction zone primary magmas provides otherwise difficult to obtain constraints on the processes leading to their formation. Primary melt compositions are direct probes of the conditions (temperature and pressure) of melting,

and also the source mantle's mineralogy and geochemistry. However, this information is usually masked by crustal-level differentiation processes. An example of the fundamental constraints which primary magma compositions may place on subduction zone magma genesis is the long-running debate concerning possible melting of subducting oceanic crust. The voluminous andesites and high-Al basalts erupted in many arcs have led some workers to invoke slab melting. However, careful investigation shows these compositions to be differentiated from more primitive magmas which derive from melting of mantle wedge peridotite (Crawford et al. 1987).

Several volcanoes in the New Hebrides Island Arc are notable for their abundant primitive basalts, in particular Aoba, Merelava, and Western Epi. Accordingly, these volcanoes have attracted detailed petrological and geochemical studies (Barsdell 1988; Barsdell & Berry 1990; Eggins 1993). These studies provide a useful basis for examining and comparing the compositional diversity and the evolution of primary magmas within the arc, given they represent end-member low-K (Merelava and Western Epi) and high-K (Aoba) magma suites.

Despite the striking compositional differences between Merelava and Western Epi lavas (low-K), and those of Aoba (high-K), their crystallisation histories are similar. Phenocrysts in magnesian basalts (>5 wt% MgO) are dominated by cpx, olivine, and accessory Cr-spinel. Plagioclase and Ti-magnetite usually occur only in evolved magmas with <5-6 wt% MgO. Extended differentiation can lead to low-Ca pyroxene crystallisation in the low-K magma suites, but this phase is absent in the high-K suites. Amphibole occurs rarely in evolved magmas.

Wholerock compositional variation is consistent with crystal fractionation occurring in the petrographically determined crystallisation sequence. Compositions span picritic (or ankaramitic), through high-Al basalt (~5wt% MgO), to andesitic and sometimes dacitic compositions. Similar compositional trends occur throughout the arc, with inflections in Al_2O_3 , TiO_2 and FeO concentrations occurring in most suites near 5wt% MgO (Fig. 17). These inflections record the onset of plagioclase and Ti-magnetite fractionation, when magmas reach high-Al basalt compositions. In the case of Aoba, a subtle inflection in CaO concentrations also occurs near 10 wt % MgO, and can be linked to the onset of clinopyroxene crystallisation

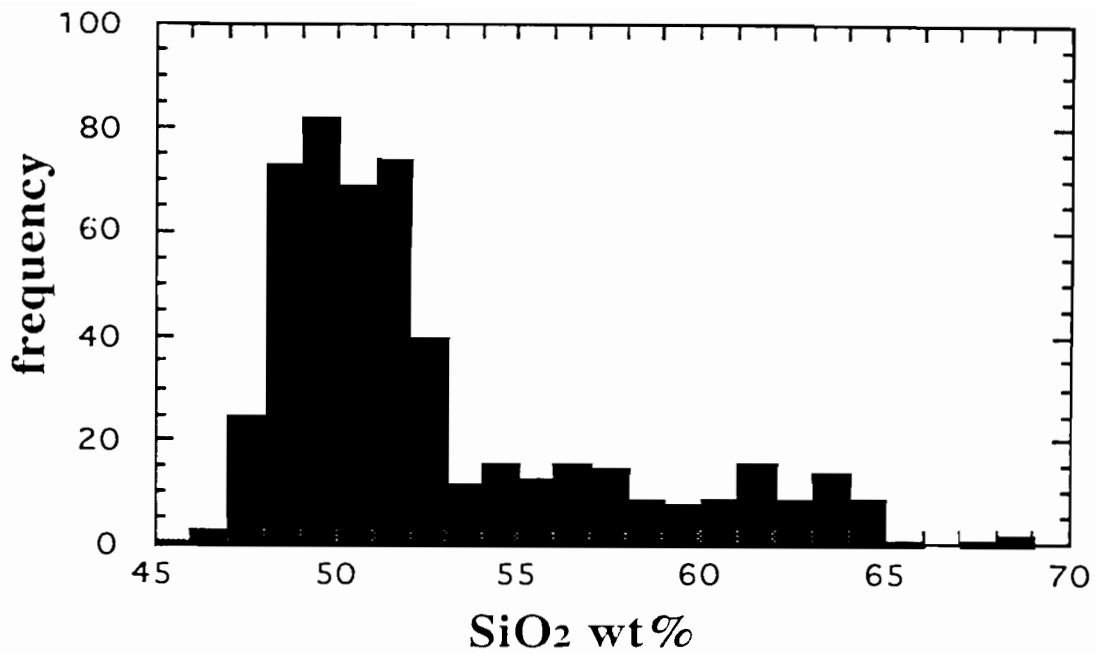


Figure 15. Histogram of SiO₂ concentrations in Vanuatu Arc magmas, which illustrates the abundance of analysed basaltic compositions compared to more evolved andesites and dacites.

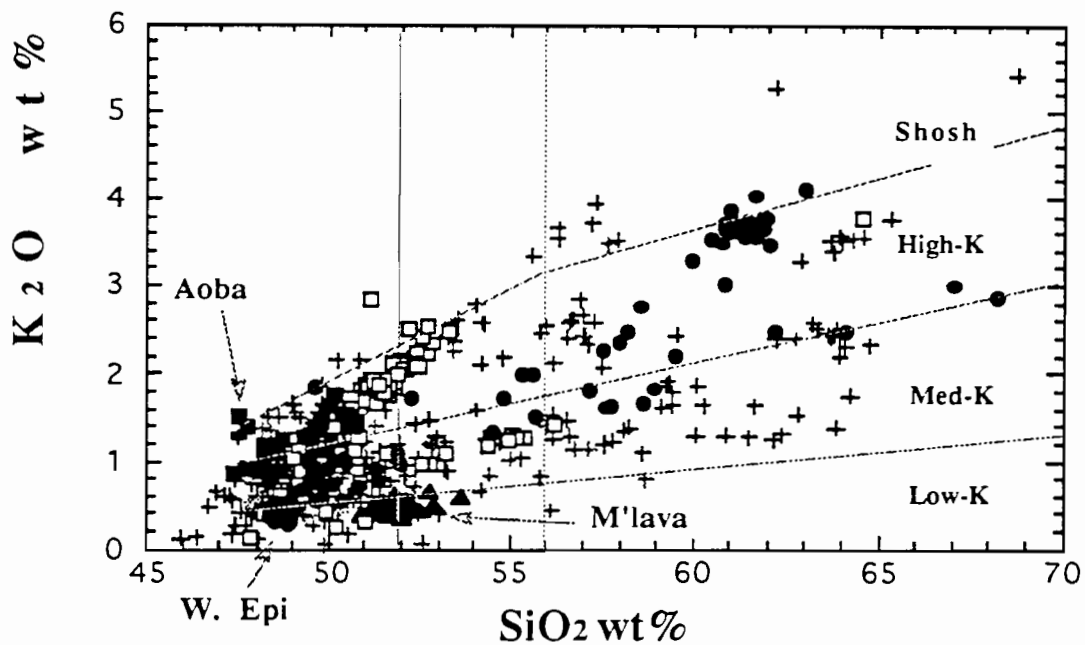


Figure 16. K₂O vs SiO₂ variation for the Vanuatu Arc, illustrating the compositional diversity within the arc, the differentiation trends for several well studied volcanoes/islands, and how these particular magma suites trace back to distinct primitive melt compositions. The K₂O classification fields are after Peccerillo & Taylor (1976). Note how the Western Epi magmas change from Low-K primitive compositions through to medium and High-K compositions during differentiation. Symbols are: filled squares - Aoba, filled circles - Western Epi, filled triangles - Merelava. Compositions for Ambrym are denoted by unfilled squares to illustrate the occurrence of separate High-K and relatively Low-K magma suites on that volcano.

(see Fig. 17). Comparable inflections in CaO concentration are not observed in the low-K magma suites, in which primitive compositions are more calcic and clinopyroxene-rich than the high-K suites.

Detailed electron-microprobe probe studies of phenocryst chemistry reveal subtle but important differences between the crystallisation of the low-K and high-K magma suites. The Aoba (high-K) magmas show a lengthy period of olivine (+Cr-spinel) crystallisation, beginning with extremely magnesian olivine ($\text{Fo}_{93.5}$), prior to clinopyroxene ($\text{Mg\#} \sim 92$) becoming a liquidus phase when crystallising olivine has evolved to $\text{Fo}_{89.4}$. In contrast, an initial period of olivine crystallisation has not been identified for either Merelava or Western Epi, where co-crystallisation of equally primitive phenocrysts of magnesian diopside ($\text{Mg\#} \sim 94$) and olivine (Fo_{91}) takes place. This difference is manifested in the bulk compositional variation difference in these suites at $>10\text{wt\%}$ MgO, with clinopyroxene dominating olivine (4:1) in the case of Merelava and Western Epi, and olivine dominating clinopyroxene (3:1) in the case of Aoba. Plagioclase first appears in all suites as calcic to highly calcic anorthite (An_{85-95}), despite the relatively evolved nature and low $\text{CaO}/\text{Al}_2\text{O}_3$ values of the melts from which it crystallises.

Elsewhere in the arc, magnesian basalts are not always abundant; however, they can be found on virtually every volcano. Like their counterparts on Aoba, Merelava and Western Epi, these lavas have highly magnesian olivine and clinopyroxene phenocrysts and accessory Cr-spinel, and indicate comparable crystallisation sequences and primitive magma compositions to those of Aoba, Merelava and Western Epi.

Compositions of the most primitive olivine and clinopyroxene phenocrysts for each island/volcano are listed in Table 1. These provide a basis for estimating compositions of the primitive melts from which they crystallised. Furthermore, it is emphasized that textural criteria, such as abundant euhedral Cr-spinel inclusions in the olivine phenocrysts, and zoning characteristics of clinopyroxene, indicate crystallisation of these phenocrysts from melts, as opposed to any possible xenocrystic origins. Based on Fe/Mg exchange criteria for olivine-liquid and clinopyroxene-liquid (e.g. Roeder and Emslie 1970) it can be shown that these phenocrysts demand extremely

primitive melt compositions with $100\text{Mg}/(\text{Mg}+\text{Fe}^{2+})$ (herein Mg\#) in the range 75-82. Evidence for similar magnesian primary melt compositions has been reported occasionally from other arcs; however, the New Hebrides Island Arc is unrivalled in that the evolution of most magma suites can be traced to these extremely primitive melt compositions.

Estimating Primary Melt Bulk Compositions

Oxygen fugacity ($f\text{O}_2$) is an important parameter in the reconstruction of primary/primitive melt compositions. It plays a major role in the determination of ferric/ferrous Fe speciation in any crystallising melt, and thus is needed to establish the correct melt Fe^{3+}/Mg values when applying Fe/Mg exchange equilibria between melt and ferromagnesian phases. Magmatic $f\text{O}_2$ values are readily derived from co-existing olivine and Cr-spinel inclusions using recent oxygen barometers (e.g. Ballhaus et al. 1991), which can account for the Cr-rich nature of the New Hebrides Island Arc spinels. Melt $\text{Fe}^{3+}/\text{Fe}^{2+}$ values can then be evaluated by taking into account additional temperature and bulk composition controls on Fe speciation (e.g. Kress & Carmichael 1992). Using this approach, calculated $f\text{O}_2$ values for olivine-spinel pairs in the various volcanic suites cluster between FMQ+1 and FMQ+2 log units, with the low-K tholeiite magmas tending to be slightly less oxidising than the high-K magmas (Fig. 18). These $f\text{O}_2$ values are significantly more oxidising than those of ocean island basalts ($f\text{O}_2 \sim \text{FMQ}$) and of mid-ocean-ridge basalts (FMQ - FMQ-1), as noted previously by Ballhaus et al. (1991).

Primary melt compositions can be constrained using the above $f\text{O}_2$ estimates, and the observed extreme phenocryst compositions. Calculated compositions range between ~ 13 and $\sim 16\text{ wt\%}$ MgO, the exact compositions being moderately sensitive to the $f\text{O}_2$ value applied (see examples in Table 2). These highly magnesian melts clearly require partial melting of mantle wedge peridotite. They are comparable in composition to the primary melts of OIB and are more magnesian than most estimates for MORB primary magmas. They do not constitute evidence for anomalously high mantle temperatures, however, as the presence of reasonable quantities of dissolved volatiles (i.e. 1-2 wt% H_2O) reduces calculated liquidus temperatures

Table 1.

Extreme olivine and clinopyroxene phenocryst compositions in the Vanuatu Arc

Volcano	Olivine (Mg#)	Cpx (Mg#)	Melt (Mg#)
Gaua	93.3	90.7	81
Merelava	91.7	94.0	78
Ambae (Low-Ti suite)	93.4	92.4	81
Ambae (High-Ti suite)	90.9	91.5	75
Ambrym	93.7	93.5	82
Western Epi	92.1	94.4	79
Erromango	88.4	89.7	70
Tanna	92.5	94.8	81
Anatom	93.4	93.6	81
Mathew&Hunter	92.7	88.2	79

Data from Barsdell (1988), Barsdell and Berry (1990), Maillet et al. (1986), Marcelot et al. (1983), Eggins (1993), and Barsdell and Eggins (unpublished data).

Table 2.

Primary melt estimates for Ambae, Merelava, and Western Epi Volcanoes

	Ambae	Ambae	Merelava	Western Epi
Log fO ₂	FMQ+1	FMQ+2.2	FMQ+1	FMQ+1
wt%				
SiO ₂	47.57	48.25	49.07	50.20
TiO ₂	0.52	0.58	0.38	0.46
Al ₂ O ₃	10.57	11.74	11.00	10.30
FeO ₂ O ₃	2.10	3.82	2.43	2.30
FeO	7.86	6.39	6.53	6.02
MnO	0.18	0.18	0.15	0.17
MgO	18.78	15.27	14.53	13.71
CaO	9.68	10.76	14.78	13.69
Na ₂ O	1.75	1.95	1.02	1.60
K ₂ O	0.80	0.89	0.29	0.38
P ₂ O ₅	0.14	0.16	0.07	0.06

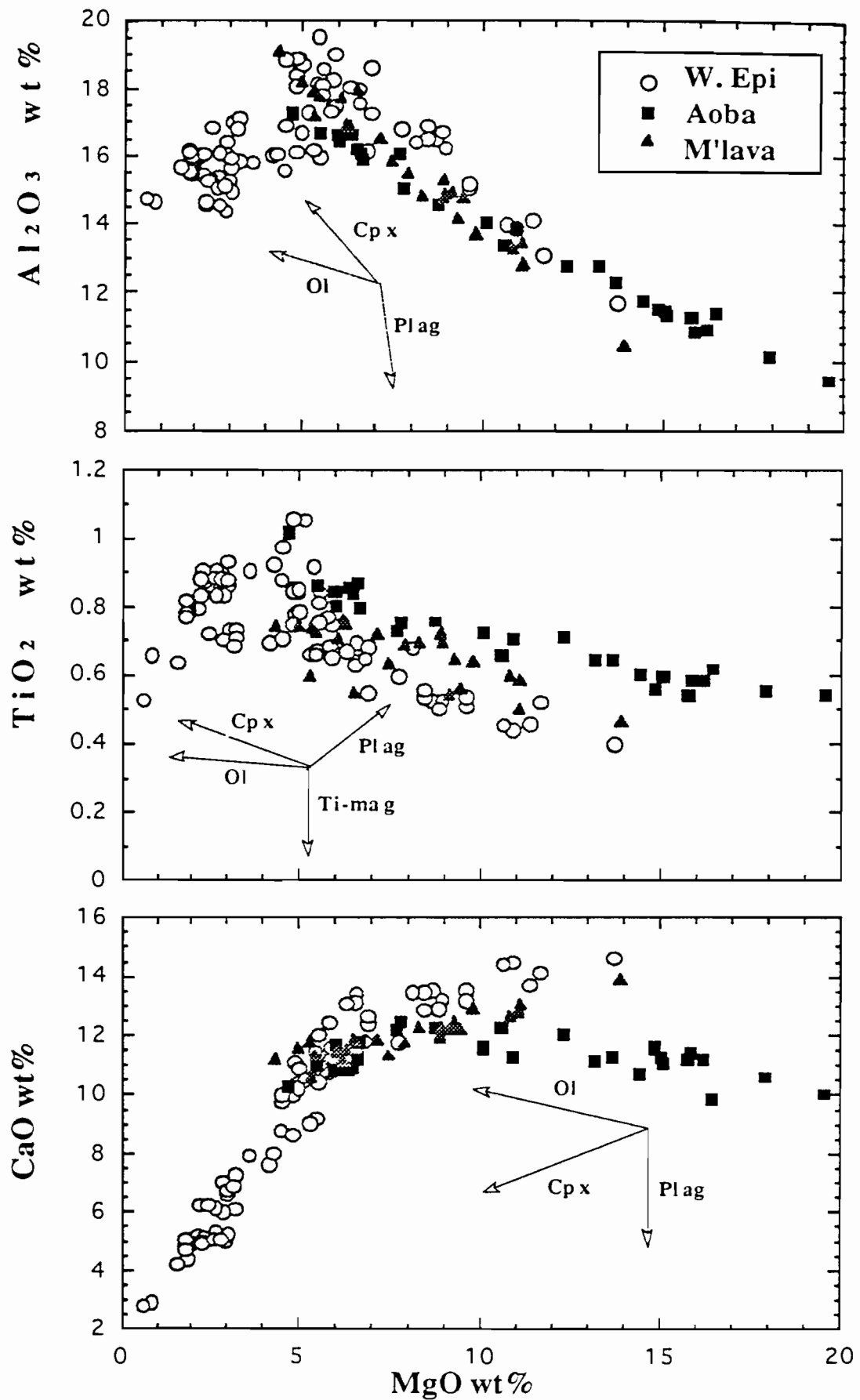


Figure 17: Selected major element oxide variation diagrams for Aoba, Western Epi, and Merelava. These illustrate how fractionation of the major crystallising phenocryst phases controls geochemical differentiation in these magma suites.

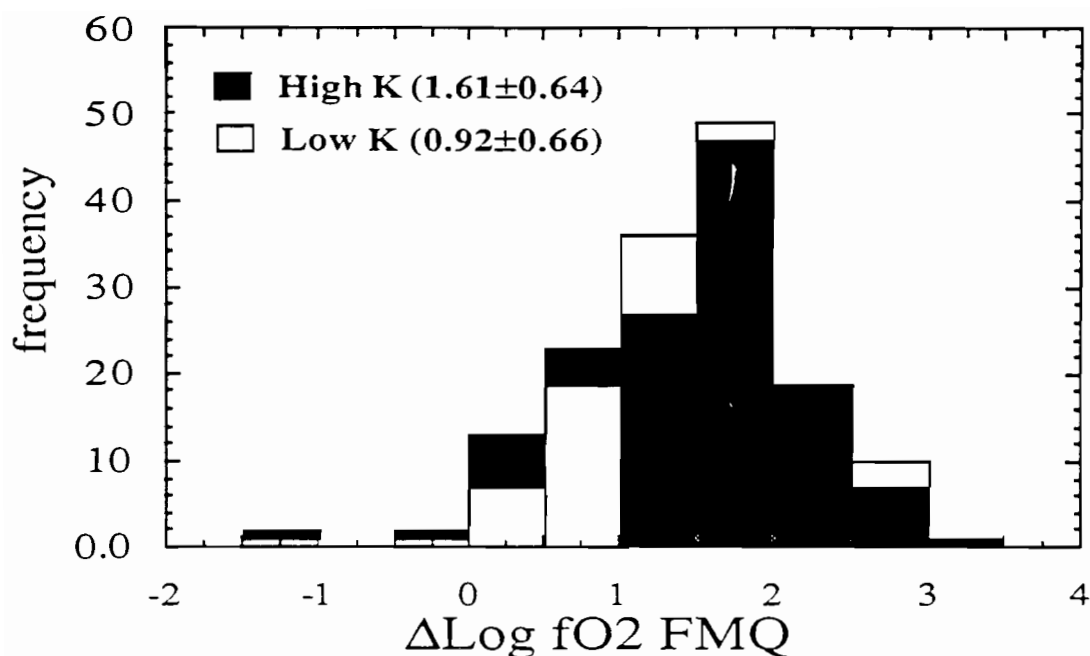


Figure 18: Histogram of oxygen fugacity values for olivine - Cr-spinel pairs in Low-K and High-K New Hebrides Island Arc basalts. FMQ refers to the Fayalite-Magnetite-Quartz oxygen buffer, and ΔLog value to the number of log units above or below FMQ. For details of the calculation procedure see text and Ballhaus et al. (1991).

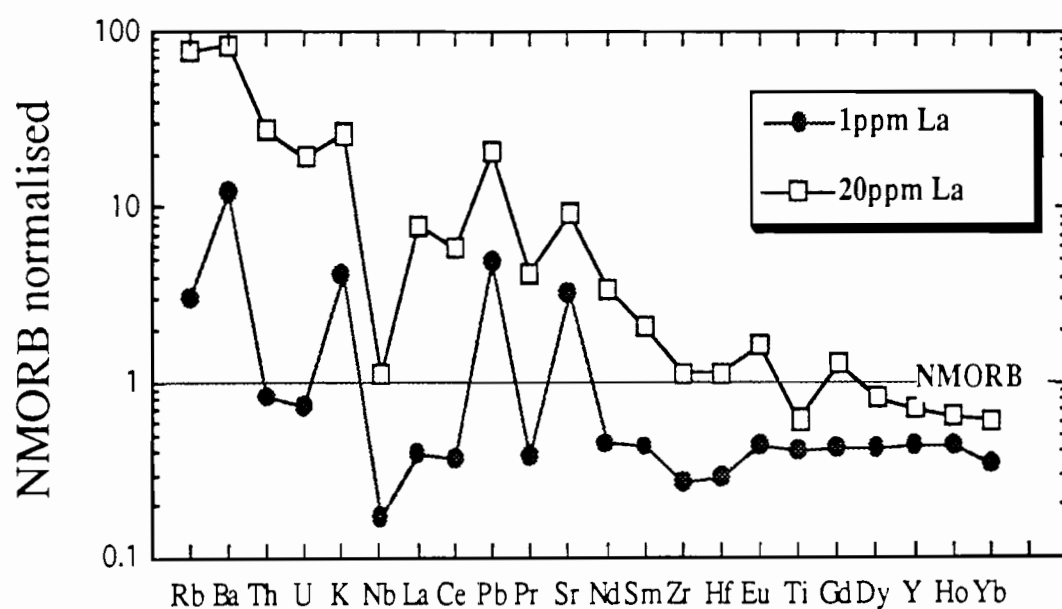


Figure 19: Calculated end-member basalt compositions for the New Hebrides Island Arc. Compositions are based on regression analysis of a database comprising basalts with $> 5\text{wt}\%$ MgO for REE and other incompatible trace elements are available. The 1ppm La composition corresponds to the primitive Low-K island arc tholeiite end-member and the 20ppm La composition to the primitive High-K alkaline end-member.

to values consistent with or slightly below those appropriate for melting of the convecting upper mantle in the deep (~2.0-3.0 GPa) mantle wedge (i.e. ~1300°C potential temperature).

In addition to constraining primary melt compositions, the high fO_2 estimates obtained from olivine-spinel pairs may also explain several significant features of the Vanuatu magmas, including;

1) the occurrence of primitive phenocrysts, which are more magnesian than counterparts in other tectonic settings (i.e. MORB and OIB) due to higher Fe^{3+}/Fe^{2+} values during crystallisation at shallow-levels, and

2) the absence of sulfide phases during differentiation, due to stabilisation of dissolved sulphate (SO_4^{2-}) in the melt.

Trace Element Geochemistry

Only limited detailed trace element geochemical studies have been undertaken on various volcanoes/islands within the arc (Gorton 1974, 1977; Barsdell et al. 1982; Dupuy et al. 1982; Marcelot et al. 1983a, b; Briquieu et al. 1984; Maillet et al. 1986; Crawford et al. 1988; Barsdell 1988; Barsdell & Berry 1990; Eggins 1993; Crawford & Eggins, unpubl. data). Approximately 80 samples having $5 > \text{wt\% MgO}$ have been analysed for a range of trace elements including REE. These samples have essentially primary geochemistry, affected by only relatively minor olivine, clinopyroxene and accessory Cr-spinel fractionation. The measured abundances of the incompatible elements in these samples may vary by up to a factor of ~2 as a consequence of this differentiation, but relative concentrations of these elements should preserve primary ratios. Importantly, these samples do not suffer from the effects of plagioclase and/or Ti-magnetite fractionation, which will disturb key petrogenetic elements such as Eu, Sr, and Ti. A fractionation correction scheme could be employed to 'normalise' the data to primary compositions; however, combined uncertainties arising from modelling cotectic crystallisation of olivine and clinopyroxene, the partition coefficients for these phases, and the primary melt compositions to correct for each suite, make this task unprofitable at present.

The New Hebrides Island Arc basalt data display

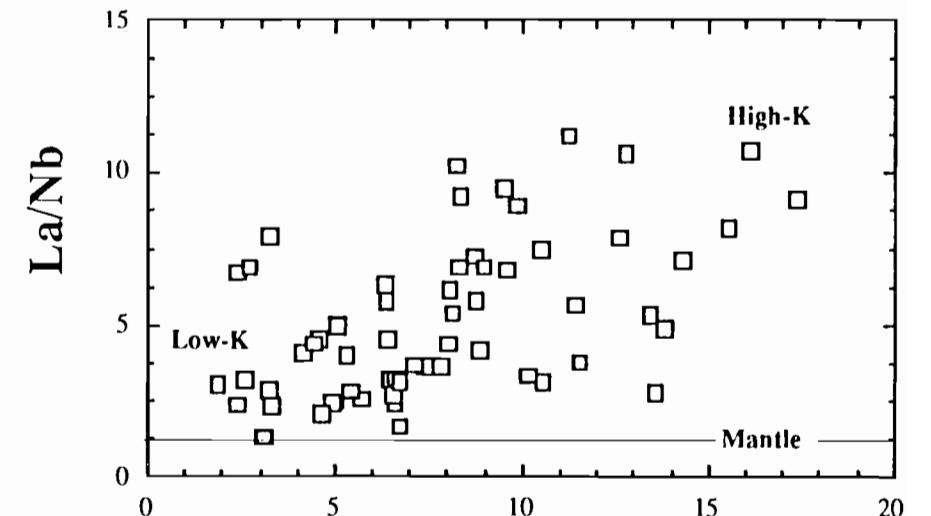
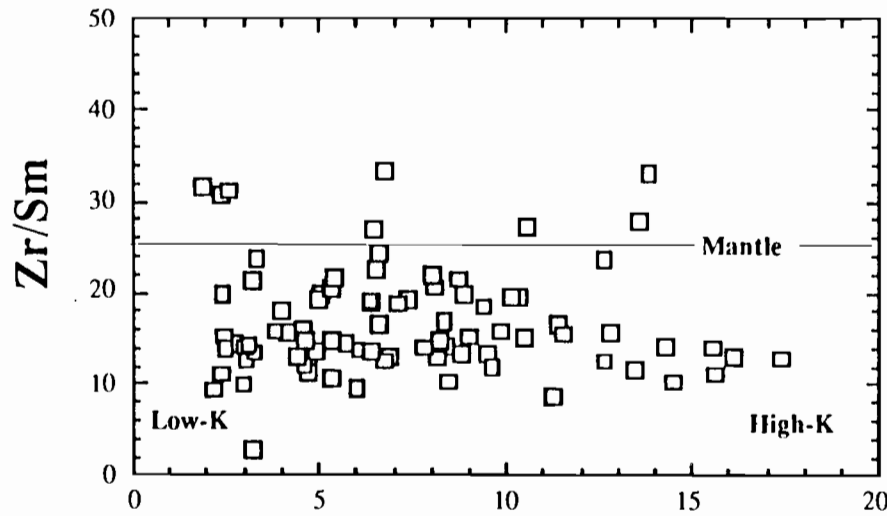
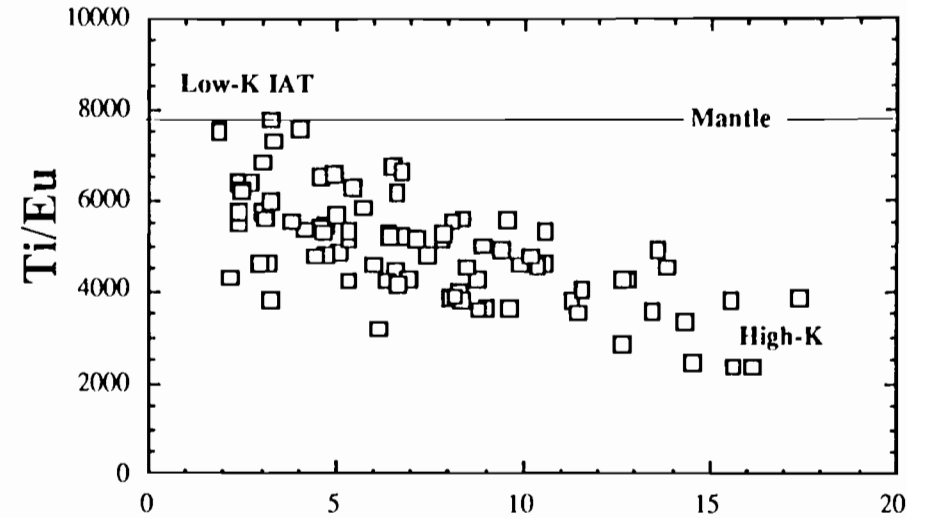
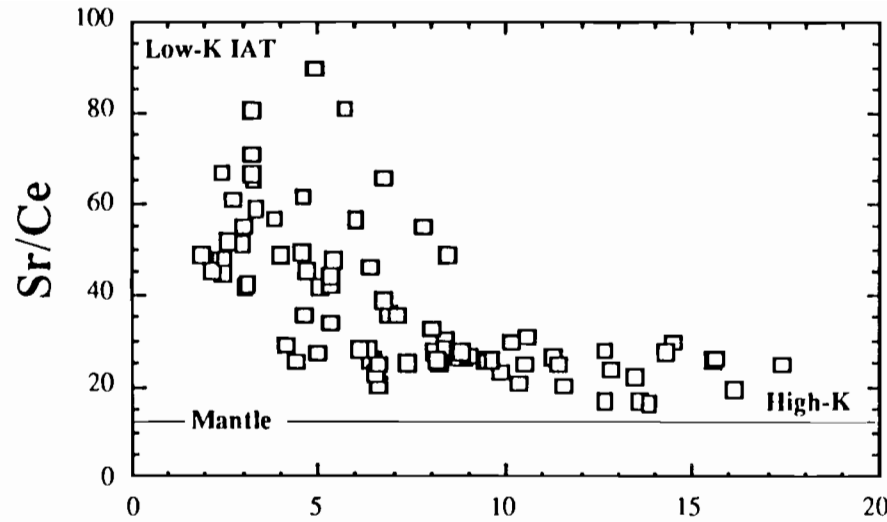
large and systematic trace element variations (Appendix A), which can be attributed to the primary process(es) operating during magma genesis. Simple geochemical plots suggest, and principal component analysis of the data demonstrates, that the compositional variation can be described by a linear combination of two end-member compositions/components. These end-members correspond to low-K (LREE-poor) island arc tholeiite and high-K (LREE-rich) alkaline compositions respectively. Regression analysis has been used to determine the "average" end-member compositions, which have the following characteristics (see Fig. 19):

The Low-K tholeiitic end-member has large LILE (Cs, Rb, Ba, K, Sr) and Pb over-abundances relative to the REE and the HFSE (Nb, Zr, Hf, Ti). Both the latter element groups are notable for being highly depleted relative to abundances in N-MORB. Small depletions of Zr and Hf occur relative to Sm, and also of Nb relative to La, but no depletion of Ti is evident relative to Eu or Gd. This unique chemistry matches that of island arc tholeiites elsewhere (e.g. Tonga, South Sandwich Islands, Kuriles etc.), and reflects a commonality of process during their formation on a global scale.

The High-K alkaline end-member is strongly enriched in LILE, Pb, Th, U, Zr, Hf and LREE, but depleted in Nb, Ti and the HREE. The relative enrichment of LILE and Pb over the LREE is greatly diminished in this end-member, whereas depletion of Ti, and probably also Nb, relative to La and Eu or Gd respectively, are well developed. Zr and Hf also are depleted with respect to Sm, but the extent of this depletion is equivalent to that in the low-K end-member.

These trace element characteristics, and the systematic variation of relative depletions and enrichments of elements between the end-members (Fig. 20) provide fundamental insights into the processes responsible for their development.

The extremely low concentrations of REE and HFSE relative to N-MORB in the low-K end-member require melting of a more depleted source than that of N-MORB, as it is unlikely these low concentrations can be explained either by extremely large degrees of melting (up to 50% or more) of an N-MORB source, or by the presence of residual phases in the mantle wedge which have high partition coefficients for REE and HFSE.



La ppm

La ppm

Figure 20: Variation of selected trace element ratios as a function of La concentration in New Hebrides Island Arc basalts with >5 wt% MgO, illustrating the systematic behaviour of various LILE/HFSE and REE/HFSE ratios across the compositional spectrum from Low-K to High-K primitive melts. Element ratios are compared to those of the primitive mantle (Sun & McDonough 1989) to illustrate the sense of LILE enrichments and HFSE depletions as a function of varying La concentration composition.

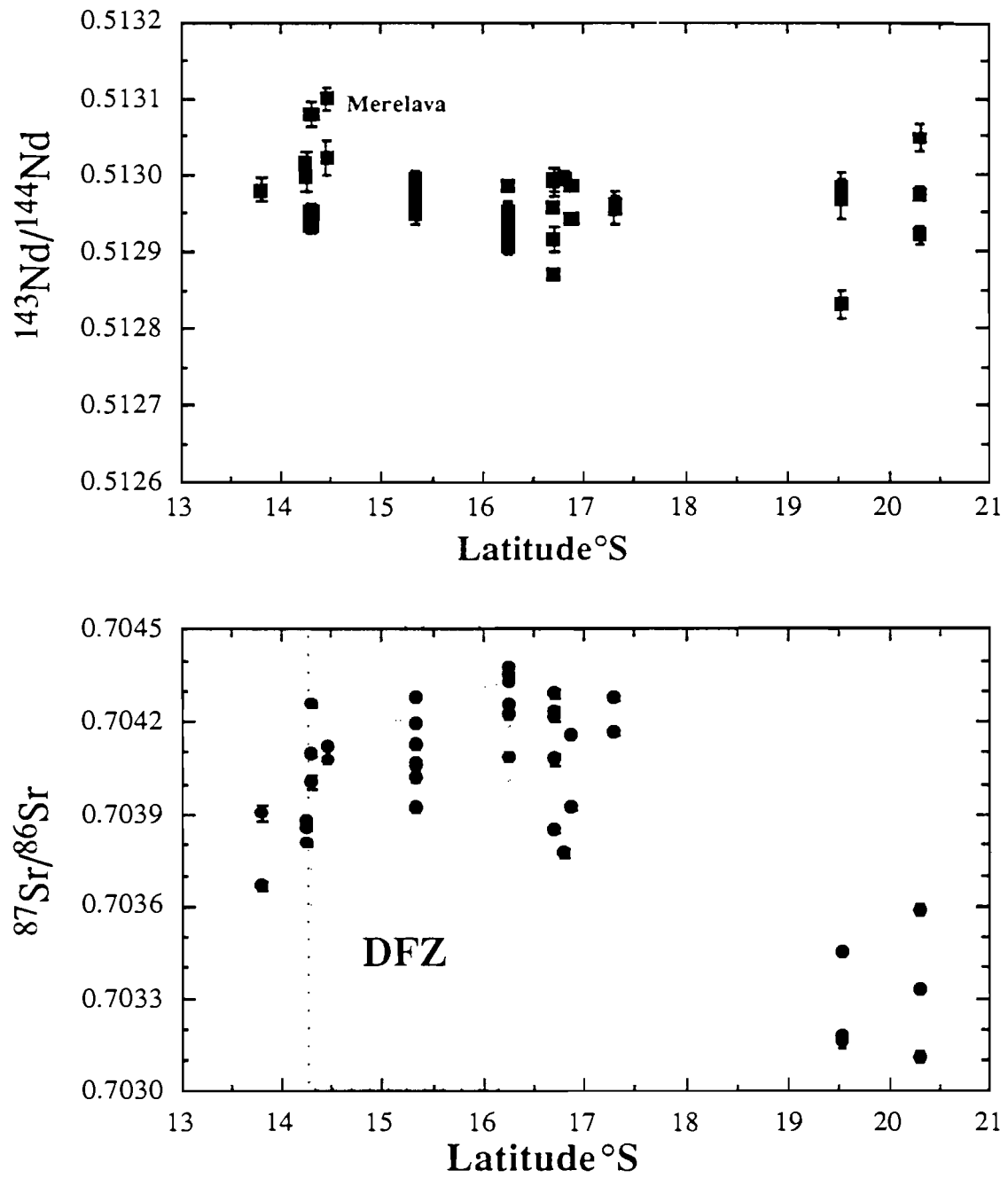


Figure 21: Variation of Nd and Sr isotopes with Latitude in the New Hebrides Island Arc. The region of d'Entrecasteaux Zone collision is indicated by the stippled region and marked DFZ. Error bars indicate 2 sigma values, or else symbol size exceeds this error level.

The strong enrichment of LILE and Pb in the low-K end-member is indicative of their addition to the mantle wedge source. The low charge/large ionic radius ratios of these elements makes attractive those models which invoke these elements being preferentially transported into the mantle wedge via supercritical fluids released from the dehydrating subducting ocean crust (or overlying hydrous, cold peridotite).

The high-K, LREE-rich end-member has characteristics consistent with relatively small degree silicate melts. The strong depletion of Ti and Nb in these compositions suggests a link with partial melting of the subducting ocean crust, in which a titanate phase may be stable (i.e. melting of rutile bearing eclogite?). If correct, these melts may be called upon to flux melting of the mantle wedge to produce the high-K magmas. Alternative scenarios may include:

- 1) small degree mantle wedge melts formed in the presence of phases with relatively high partition coefficients for Nb and Ti (possibly amphibole?) ,

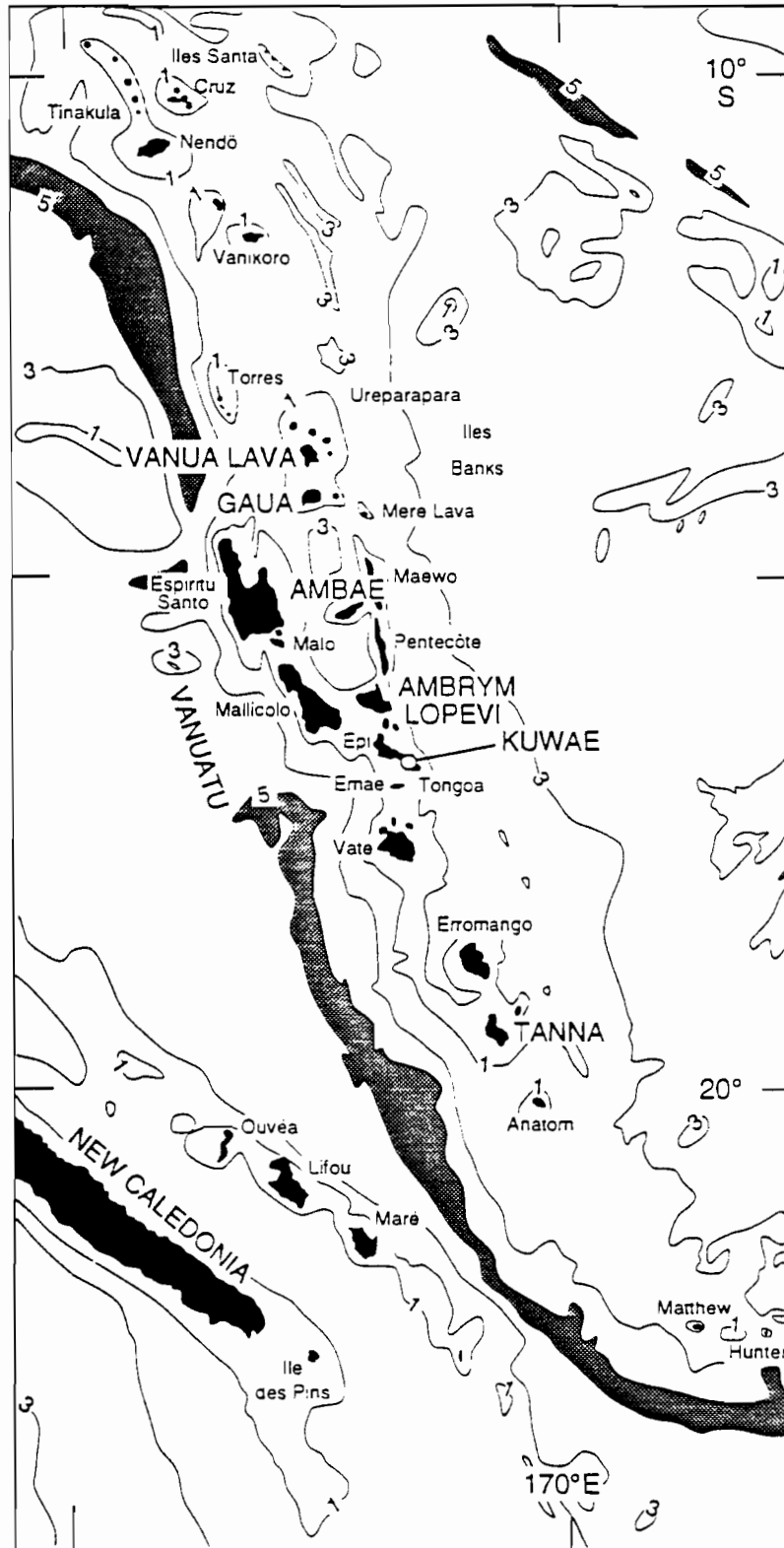
- 2) melting of subducted LREE-rich sediments with Nb and Ti depletions, and,

- 3) mantle-melt interaction processes during ascent of melt (e.g. Kelemen et al. 1991)

Radiogenic Isotope Geochemistry

Nd isotope geochemistry exhibits no significant temporal or spatial variations within the arc (Fig. 21), nor correlation with trace and major element chemical variation. $^{143}\text{Nd}/^{144}\text{Nd}$ values of the Central Chain volcanoes have a restricted range, between ~ 0.51285 and 0.5130 , though higher values do occur with magmatism associated with rifting in the immediate back-arc region (e.g. Merelava). In contrast, $^{87}\text{Sr}/^{86}\text{Sr}$ values vary from ~ 0.7030 to ~ 0.7045 , and show significant spatial variation trends, from low values in the southern part of the arc to high values in the north, with the highest values being centred at the southern margin of the zone affected by the d'Entrecasteaux Zone collision. Considerable variation in $^{87}\text{Sr}/^{86}\text{Sr}$ values can occur on individual islands/volcanoes, but the trend of these variations is not systematic throughout the arc (i.e. higher $^{87}\text{Sr}/^{86}\text{Sr}$ can be associated with either more or less K-rich magmas). Pb isotope data display complex and appreciable

compositional variation both spatially and temporally within the arc. They are part of a detailed integrated study investigating the Sr, Nd, and Pb isotope characteristics of the arc, the subducting plate, back-arc rifts (in collaboration with P. Maillet and J.-P. Eissen; ORSTOM), and the North Fiji Basin. It is notable that Pb isotope characteristics of the central arc volcano lavas are consistent with Indian Ocean MORB-like mantle sources.



**IAVCEI 1993 PRE-CONFERENCE FIELD TRIP
LOCATIONS OF VOLCANOES, NEW HEBRIDES ISLAND ARC**

PART II

VOLCANOLOGICAL ASPECTS OF THE NEW HEBRIDES ISLAND ARC A FIELD GUIDE

Claude ROBIN and Michel MONZIER

DAY 1 : Fly from Port Vila airport over the active volcanic islands of Lopevi, Ambrym and Aoba.

LOPEVI

The following section is mainly from AJ Warden (1967) *The Geology of the Central Islands: New Hebrides Geological Survey Annual Rep. 1967, n°5: 108 pp.*, and from JP Eissen, C Blot & R Louat (1991) *Chronologie de l'activité volcanique de l'arc insulaire des Nouvelles Hébrides de 1595 à 1991, Rapports Scientifiques et Techniques ORSTOM Geol.-Geophys. 1991, n°2. pp 69.*

Lopevi volcano (16°30'S; 168°20'E), a near symmetrical youthful cone (7 km in diameter), rises steeply from sea level to 1413 m in altitude.

In 1967, Warden described a small crater in the summit area, developed within a pyroclastic cone rimmed by the remnants of an older crater (Fig. 22) The stratocone consists of lava flows and pyroclastics. Lavas exposed in cliff sections along the coast are mainly "aa" flow units with basalt, or less frequently basaltic andesite compositions, intersected by many dykes. Deposits of agglomerates and ash generally stratified parallel to the slope, and subordinate radial lava tongues form the upper part of the cone. Following Williams & Curtis (1964), some of these deposits are pyroclastic flow deposits.

Lopevi has been intermittently active, with eruptions recorded in 1864, 1874, 1883-84, 1892-93, 1908, 1922, 1939, 1960, 1962-64, and 1967-1980.

On July 10th, 1960, an eruption began along a fissure on the north-west flank with the emission of pyroclastic flows, and over the next few weeks developed through stages characterised by the production of lava spatter, lava flows, and dense ash clouds. In 1962, Lopevi erupted again and remained intermittently active over a period of two years. Commencing at the crater dormant for over 42 years, the centre of activity migrated to the head of the 1960 fissure. In addition, the volcano erupted at 12 other

points, mostly fissures, producing lava flows from both the crater and flank fissures on the northeastern side (Fig. 1) and ash emissions. The 1960 and 1962-64 eruptions, and the presence of older craters and fissures on the lower slopes, suggest that flank eruptions are a common feature of Lopevi activity.

Whereas olivine basalt was produced in 1960, rocks ranging from andesite to olivine basalt in composition were erupted between 1963 and 1965. From 1967 to 1980, ash emissions in many cases reached Paama island, and even sometimes Ambrym, as in 1969 (Blot 1976; Simkin et al. 1981). During this period, explosions, lava flows and ash emissions were reported each year. On March 1st 1967, a 10,000 m high column of ash rose above the volcano. In 1978, lava flows reached the sea. Two major eruptions (ash emissions and lava flows) occurred in March 1979 and July 1980.

In summary, with Ambrym, and Yasur volcano on Tanna, Lopevi is one of the three most active volcanoes in the New Hebrides Island Arc, almost constantly active, and sometimes quite violently so.

AMBRYM

The following descriptions are from Robin C, Eissen JP & Monzier M (1993) *Giant tuff cone and 12-Km-wide associated caldera at Ambrym Volcano (Vanuatu, New Hebrides Arc). J. Volcanol. Geotherm. Res. 55: 225-238.* and from Picard C, Monzier M, Eissen JP & Robin C (1993) *Concomitant evolution of tectonic environment and magma geochemistry, Ambrym volcano (Vanuatu - New Hebrides arc) J. Geol. Soc. London. (in press)*

I - VOLCANOLOGY AND STRUCTURE

Ambrym (168°08' E; 16°15' S) is a 35 x 50 km wide basaltic volcano, rising about 1800 m above the adjacent sea floor (Chase & Seckins 1988). The main cone is crowned by a circular, ~12 km diameter caldera with a continuous scarp a few tens of meters to 450 m high (Fig.

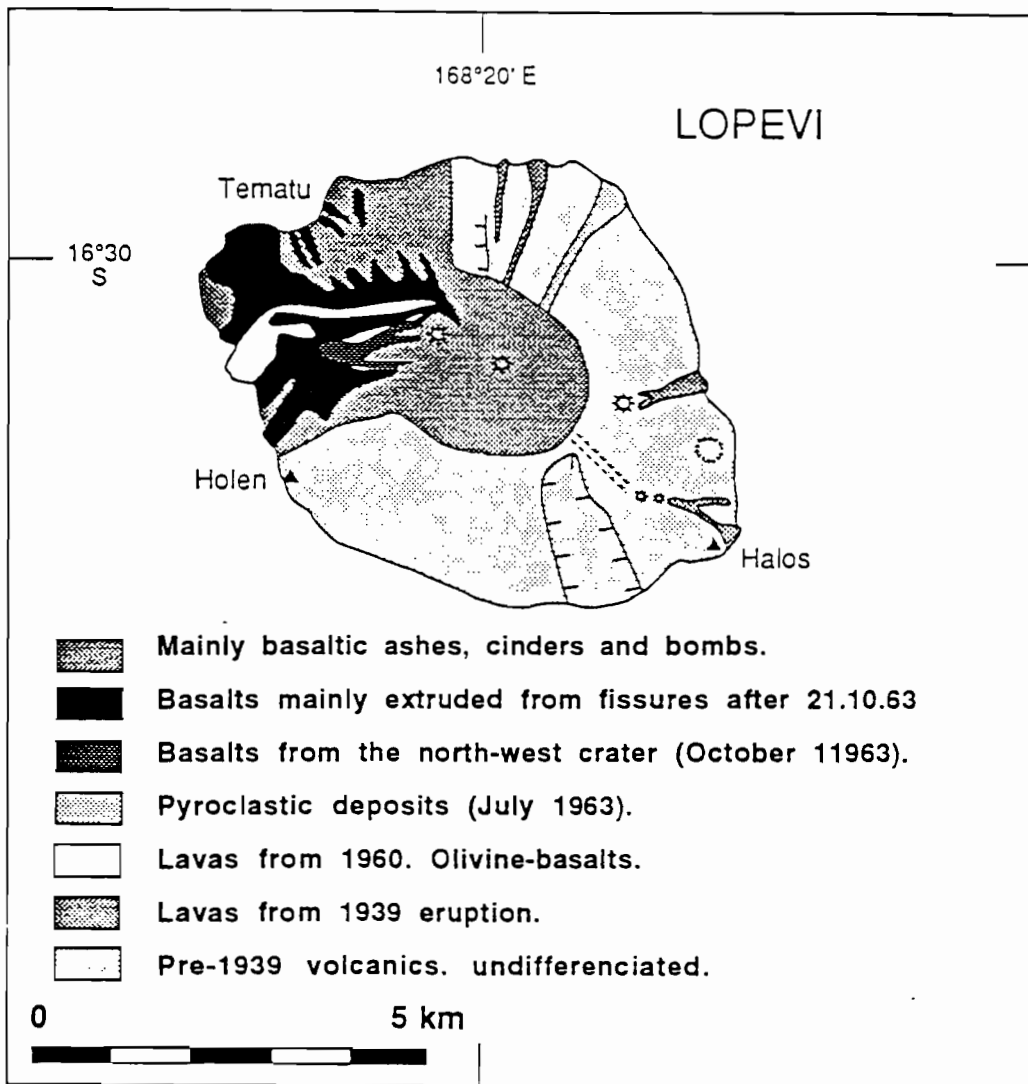


Figure 22: Geological sketch map of Lopevi volcano. After Warden (1972) and Priam (1964).

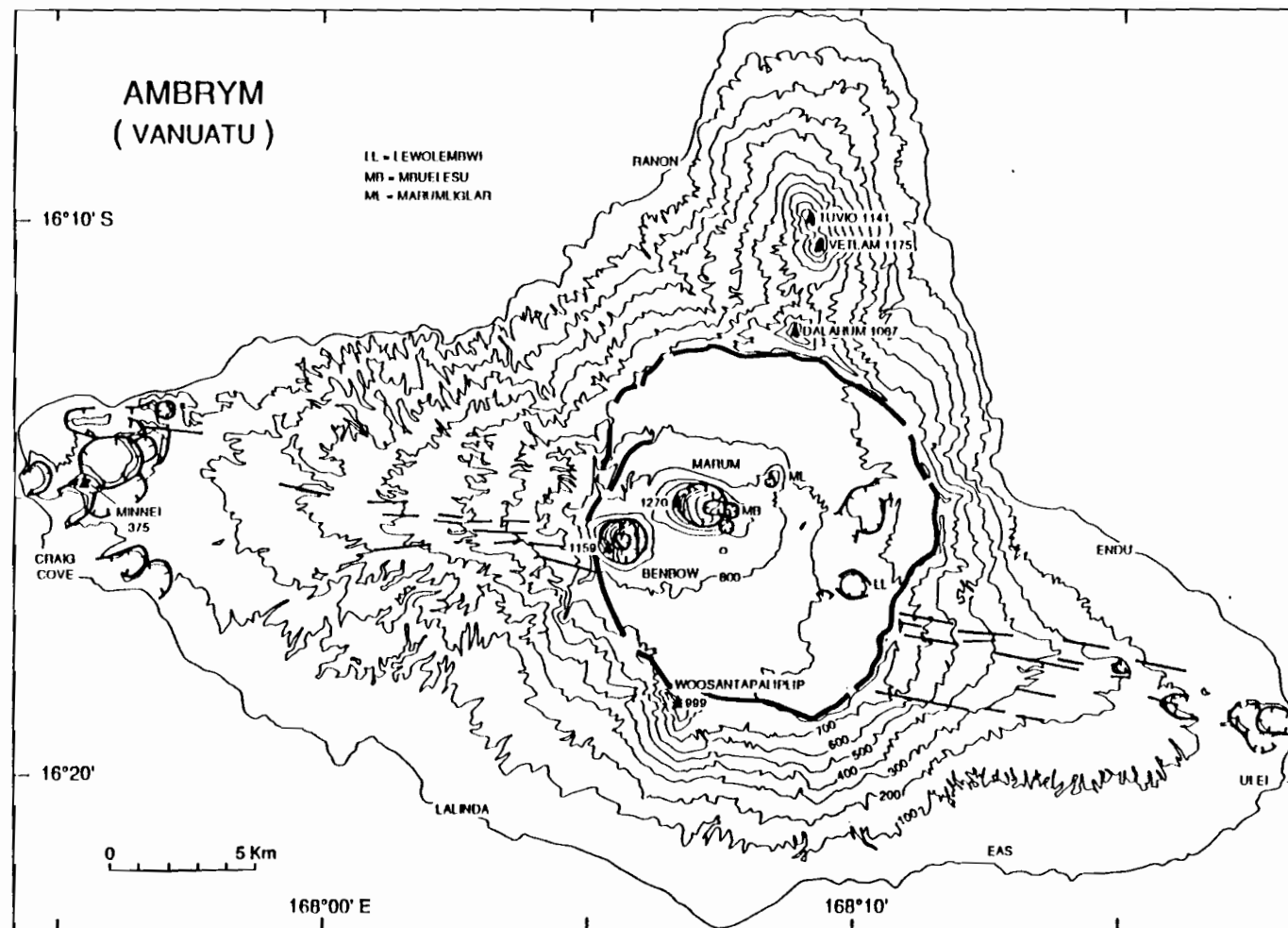


Figure 23: Topographic map of Ambrym island. In bold, the main volcanic features (caldera, cones, maars, fissures). Contour interval, 100 m. (From Robin et al. 1993).

23). Post-caldera volcanics, dominantly from the Marum and Benbow intra-caldera cones, have partly filled the depression. Post-caldera scoria cones and lava flows occur outside the caldera, along fissures oriented N105° E.

MacCall et al. (1970) stressed that the change from pre-caldera to post-caldera volcanics at Ambrym is not marked by any unusual type of deposit or any clear break in the eruptive sequence. These authors postulated that the caldera was formed by quiet subsidence accompanied by minor eruptions of scoria lapilli, i.e. following the Hawaiian model. The discovery of dacitic ash- and pumice-flow deposits on the lower flanks of the volcano, and of a subsequent voluminous series of mainly basaltic hyaloclastites which constitute an exceptionally large tuff cone around the caldera, have encouraged us to reconsider the problem of the caldera formation in this volcano.

Basal edifice

The oldest subaerial volcanics are ankaramitic lava flows and pyroclastic deposits exposed on the northern part of the island. In the main cone, pre-caldera lava flows crop out on the S, NW and E sides along or very close to the coast. They are commonly porphyritic, low viscosity basalts (pahoehoe type), which constitute a basal shield volcano with very gentle slopes (2-3°).

The Ambrym Pyroclastic Series

A series of tuffs (Ambrym Pyroclastic Series: APS) overlies the basal shield volcano and constitutes most of the volume of the cone up to the caldera rim. Deposits of the APS have been observed as far as the western end of the island, 15 km from the caldera margin. No interruption (erosional discordance or buried soil) has been observed in these pyroclastic deposits, and despite extensive erosion of the flanks of the cone, no lava flows are included in this series. The scarce lava flows exposed on the upper slopes of the cone are post-caldera basalts that have overflowed the caldera rim.

Four sequences of pyroclastic deposits comprise the Ambrym Pyroclastic Series (I to IV, Fig. 24). In the following section, the term pyroclastic flow deposit is used for all flow deposits with less than 50 % ash and with variable contents of lapilli-sized dense juvenile clasts, scoria and pumice, and xenoliths. The term ash flow deposit is used only for fine deposits essentially made of

ash (at least 50 %, commonly >70 %).

Sequence I- On the north coast, an ~60 m thick lower sequence of pyroclastic flow deposits (I, Fig. 24) fills topographic depressions on the basal shield edifice. This sequence, dacitic in composition (Column D, Table 3), consists mainly of six sub-horizontal indurated massive units of coarse ash and medium-grained lapilli (≈50%), pumice (≈15%), cauliflower bombs and glassy clasts (≈15%), and abundant basaltic accidental clasts (≈20%). This sequence also includes pumice-rich layers, surge deposits and two massive block-rich layers. An 8-10 m thick sequence of fallout ash layers bearing abundant accretionary lapilli occurs in the middle of the section and indicates that two major pyroclastic flow events occurred. Base surge deposits, accretionary lapilli and poorly vesiculated cauliflower bombs are evidence of phreatomagmatic processes during the eruption of sequence I.

Sequence II- The deposits of sequence I grade upward into a thick sequence of well-bedded, laterally continuous layers of vitric tuffs. The continuous beds are generally <3 m thick (commonly 30 cm - 1 m) and form thick deposits with intercalated lenses of agglomerates, some in excess of 8 m thick. Two dominant facies occur: a) thin and coarse ash including quenched glass fragments and accretionary lapilli, and b) agglomerates of vitric clasts and shards in a granular sideromelane matrix which also includes basaltic lithics from the basement. The sideromelane matrix is sometimes palagonitized and the vitric fragments are commonly aligned parallel to the beds. Typical shapes of juvenile clasts are: i - Light-brown basaltic blocky or platy fragments (0.5 - 5 mm in size; analysis G, Table 3), aphyric and non-vesicular, with cracks due to quenching. ii - Dark-brown to opaque basaltic glass fragments, with a low vesicularity (0 - 10 %), which can represent the major part of the matrix. iii - Irregularly-shaped, translucent basaltic or basic andesitic vitric clasts which are mainly incipiently or poorly vesicular (5 - 40 %) but show a broad vesicularity range (up to 70 %). iv - Glassy andesitic to dacitic angular fragments, also showing various degrees of vesicularity. Different types of shapes occur in the same sample; all the juvenile particles show signs of shattering, induced by interaction with water.

Ash flow deposits are interbedded with these deposits

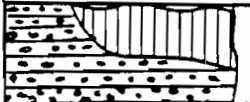
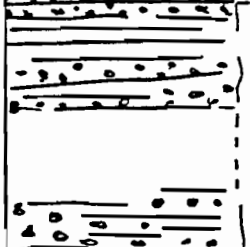
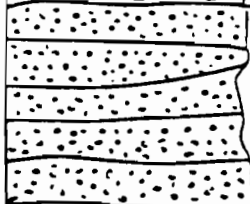
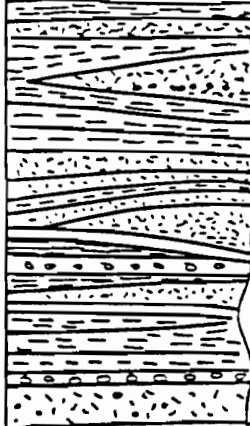
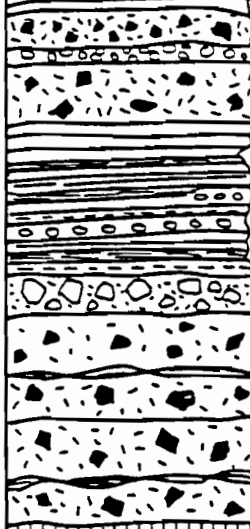

VOLCANIC SEQUENCES	COMPOSITION	ERUPTIVE STYLES	ROLE OF EXTERNAL WATER
	POST-CALDERA VOLCANICS	FALLOUT TEPHRA AND LAVA FLOWS	
	SEQUENCE IV Up to 250 m thick at Woosantapalip	BASALTIC	STROMBOLIAN and Subordinate plinian. ABSENT or marginal influence
	SEQUENCE III 10 - 25 m thick	BASALTIC	PLINIAN LOW then WEAK
	SEQUENCE II Major part of the flanks	MAINLY BASALTIC	HYDRO-MAGMATIC (Surtseyan-like) ERUPTIONS and minor Plinian eruptions PAROXYSMAL
	SEQUENCE I Up to 60 m thick	MAINLY DACITIC	PLINIAN ERUPTIONS and PHREATOMAGMATIC ERUPTIONS TRIGGERING EFFECT FOR EMPTYING THE BASALTIC RESERVOIR INCIPIENT and then Important
	PRE-CALDERA LAVA FLOWS (SHIELD VOLCANO)		

Figure 24: Composite section of the Ambrym Pyroclastic Series (APS). (From Robin et al. 1993).

Table 3: Table 1. Selected whole-rock analyses from Ambrym volcano (ICP method; analyst Jo Cotten, Université de Bretagne Occidentale).

A : ankaramitic basalt from the ancient edifice. B and C : two porphyritic basalts from the basal shield volcano. D to H : syn-caldera pyroclastic products from the tuff cone; D : juvenile clast from the lower dacitic sequence I; E, F, G : vitric clasts from the surtseyan-like deposits (sequence II); H : basaltic ash flow from sequence III. I, J, K : pre-historic basalt from the caldera floor (I), and historic lava flows of 1914 (J) and 1988 (K).

	A	B	C	D	E	F	G	H	I	J	K
	PRE-CALDERA LAVA FLOWS			SYN-CALDERA PYROCLASTIC PRODUCTS (APS)					POST-CALDERA LAVA FLOWS		
	AMB72	AMB32	AMB36	AMB60C	AMB39A	AMB60I2	AMB39B	AMB65	AMB20	AMB25	AMB8
SiO ₂	48.50	49.30	52.30	63.50	55.00	54.10	49.60	49.40	49.80	50.75	50.40
TiO ₂	0.80	0.68	0.98	0.54	0.77	0.79	0.90	0.78	0.85	0.96	0.93
Al ₂ O ₃	14.75	15.68	16.45	14.75	15.82	16.42	15.89	17.60	15.94	15.90	15.90
Fe ₂ O ₃ *	10.70	10.43	10.81	7.59	9.83	11.81	12.41	12.07	12.46	12.90	12.54
MnO	0.19	0.18	0.18	0.21	0.19	0.22	0.21	0.20	0.21	0.23	0.22
MgO	10.16	4.85	4.36	1.36	3.60	3.90	4.80	4.53	5.70	4.86	4.90
CaO	12.50	11.96	6.67	4.35	7.40	8.58	9.34	10.55	11.10	9.80	10.00
Na ₂ O	2.06	2.37	3.22	4.37	3.29	3.15	2.78	2.40	2.52	2.80	2.74
K ₂ O	0.64	1.20	2.52	2.65	2.90	1.28	1.75	0.98	1.82	1.99	1.90
P ₂ O ₅	0.19	0.23	0.42	0.19	0.28	0.25	0.32	0.22	0.30	0.35	0.34
LOI 1050°C	-0.29	0.02	-0.08	0.54	1.53	-0.03	2.29	0.70	-0.59	-0.41	-0.59
	100.20	99.70	99.63	100.05	100.61	100.27	100.29	99.43	99.93	99.33	99.28
Pb	11	19	48	51	54	24	31	19	28	35	34
Ba	418	287	480	725	522	390	358	151	342	407	393
Nb	1.00	1.35	3.40	3.75	4.50	1.95	2.70	1.60	2.35	2.30	2.60
La	4.2	7.7	12.8	15.8	13.5	6.3	10.3	7.8	9.2	11.0	11.3
Sr	304	578	838	266	488	418	572	482	588	818	815
Nd	7.5	11.0	17.5	19.0	17.5	12.0	15.0	11.0	12.8	15.0	15.5
Zr	44	51	93	142	112	68	89	51	80	76	73
Eu	0.85	0.95	1.25	1.30	1.10	1.20	1.25	1.05	0.95	1.20	1.30
Dy	2.9	2.7	3.5	6.1	4.0	3.9	3.4	3.1	3.1	3.9	3.7
Y	16.0	16.0	21.0	41.0	24.0	23.5	20.5	18.5	17.0	22.0	21.0
Er	1.60	1.50	2.10	4.10	2.00	2.90	1.70	1.60	1.70	2.30	2.50
Yb	1.57	1.42	1.87	4.07	2.27	2.52	1.77	1.70	1.60	1.97	1.92
V	279	284	360	70	245	299	330	335	340	375	350
Cr	381	65	21	31	59	5	155	56	51	10	15
Co	49	38	32	12	29	32	41	36	45	41	40
Ni	101	27	34	17	20	13	100	38	35	24	28
Sc	43	32	24	17	23	29	29	31	32	30	32

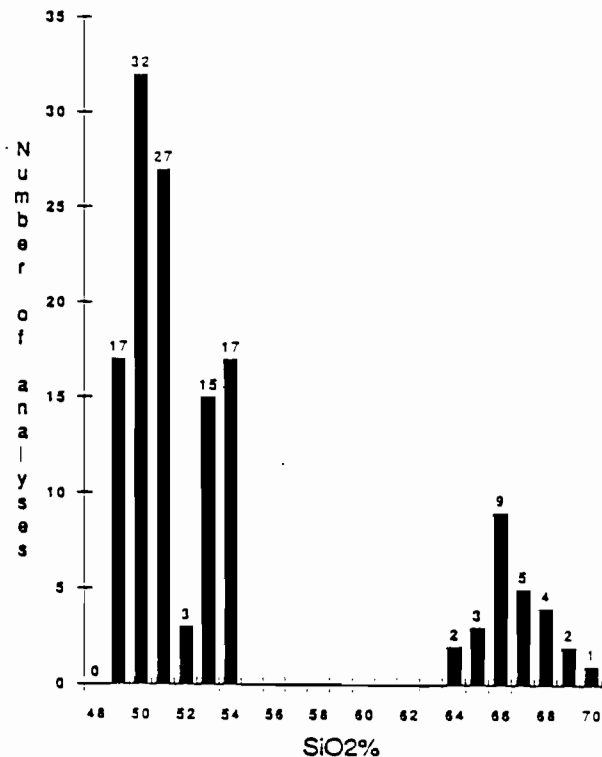


Figure 25: SiO₂ histogram of 137 microprobe analyses of vitric clasts from the syn-caldera Ambrym Pyroclastic Series (APS). Class interval: 1 %. As example, for SiO₂ = 50 %, 32 analyses from 49.5 to 50.5. (From Robin et al. 1993).

in the upper part of the sequence. Dense vegetation, which covers the flanks of the cone, makes an estimate of the total thickness difficult; nevertheless, observations in deep gullies suggest that this sequence is very thick, probably at least 200 m.

Sequence III- The following sequence, 10-25 m thick, consists mainly of grey to bluish ash flow deposits, almost free of xenoliths, in beds a few meters thick. The highly to extremely vesicular (60 - 90 %) “dry” sideromelane droplets and pumiceous lapilli are basaltic (analysis H, Table 3). Translucent ash particles show fragmentation after cooling but no reworking after deposition; other grains have a smooth appearance.

Sequence IV- On the south slope of the cone, basaltic strombolian deposits constitute this sequence. Their origin is the Woosantapaliplip vent, located on the caldera rim (Fig. 23).

On the north side of the cone, viscous basaltic andesite lavas, 20-25 m thick, overly the APS. They extruded on the caldera edge and flowed downward as far as Bogorfan Bay, forming a 2 km-wide lava tongue. Near the vent,

part of these flows remained in the caldera and has been intersected by the collapse.

Most juvenile clasts of the APS are aphyric. 137 microprobe analyses of juvenile glasses from the APS show compositions ranging from medium-K calc-alkaline basalt to dacite. A histogram for SiO₂ content (Fig. 25) shows three peaks, at 50% SiO₂ (basalts), 54% (basaltic andesites) and 66% (dacites). Dacitic compositions are restricted to products of sequence I, whereas basalts and subordinate basaltic andesites constitute the juvenile material of sequences II, III and IV.

Post-caldera volcanism

Outside the caldera, recent vents occur along fissures oriented N 105° E and appear as scoria cones and maars that fed lava flows from the lower flanks of the volcano. Within the caldera, activity from the Marum (1270 m) and Benbow (1160 m) cones and from maars located in the eastern part has infilled the depression.

Ambrym has had a large number of historical eruptions, in 1888, 1894, 1913-14, 1929, 1937, 1942, 1952-53 (Fisher 1957; Williams & Warden 1964), the latest being in 1986 and 1989. Episodic lava lakes in Benbow and Marum craters drain out as basaltic lava flows onto the caldera floor. Magma in the conduit is also frequently ejected as ash and scoria falls, which mantle the caldera and the west part of the volcano (Fig. 26).

Structure of the volcano

The APS tuffs dip at similar angles (10 - 20°) to the present upper slopes surrounding the caldera, above a break of slope at ~ 6 km away from the caldera rim. Since the dips of the underlying fluid lava flows are constant (2-3°), the APS thickens towards the caldera, as observed on the southern flank, along the track from Lalinda to the caldera edge. Thus, Ambrym differs from other oceanic volcanoes whose slopes generally expose piles of lava flows with minor interstratified tuffs. The structure of the edifice is that of a lava shield volcano, overlain by an uncommonly large tuff cone, the inner part of which has subsided (Fig. 27). Along the caldera fault, the height of the buried pre-caldera edifice is probably 200-300 m, except on the northeastern side where it is very low (~100 m). This suggests a thickness ranging from 200 - 450 m for the APS deposit near the caldera edge (up to 600 m at

Woosanapaliplip Peak) and a volume from 60 - 80 km³ (~19 - 25 km³ Dense Rock Equivalent).

The large volume of the pyroclastic edifice does not agree with the relatively small volume of the tuff cone, the central depression of which would correspond to a simple crater enlarged by explosive coring. By the volume of basalt released, the pyroclastic event at the origin of the APS is drastically different from those which led to the deposit of tuffs associated with a caldera in other large basaltic volcanoes, for example, the 1790 Keanakakoi ash member at Kilauea (Swanson & Christiansen 1973; MacPhie et al. 1990). The eruption of the Keanakakoi tuff (0.1 km³) produced only minor shape modification of the Kilauea summit caldera. At Masaya (Nicaragua), caldera collapse apparently formed in response to large scale pyroclastic eruptions of basaltic magma, including ignimbrites and surges (Williams 1983; Bice 1985). This caldera seems the only known example which resembles, in terms of mechanisms of producing Plinian basaltic eruptions, the large tuff cone of Ambrym. Vertical continuity, volume, large extent and the range in composition of the juvenile clasts are strong arguments favouring the hypothesis that the APS products erupted during a major pyroclastic event related to the emptying of a chemically zoned magmatic chamber, mainly basaltic in composition.

Tentative model of caldera formation

Products of sequences II to IV are also affected by subsidence. To construct sequence II or the Woosanapaliplip cone (sequence IV), the pyroclastic eruption at the origin of the APS must have lasted several months, or even years, and several subsidence stages probably occurred. It is notable that the composite lower sequence of dacitic ignimbrites exposes an intermediate series of phreatomagmatic fallout layers and, therefore, was emitted during a lengthy eruptive event.

(1) - *Eruption of sequence I : earlier caldera collapse.*
The volume of the dacitic pyroclastic flows from sequence I cannot be estimated, due to their unknown extent below sealevel. Based on the thickness of deposits, they represent a major plinian phase which probably occurred after a long period of quiescence, allowing magmatic differentiation. Their eruption led to collapse in the summit area of the volcano. The large percentage of accidental

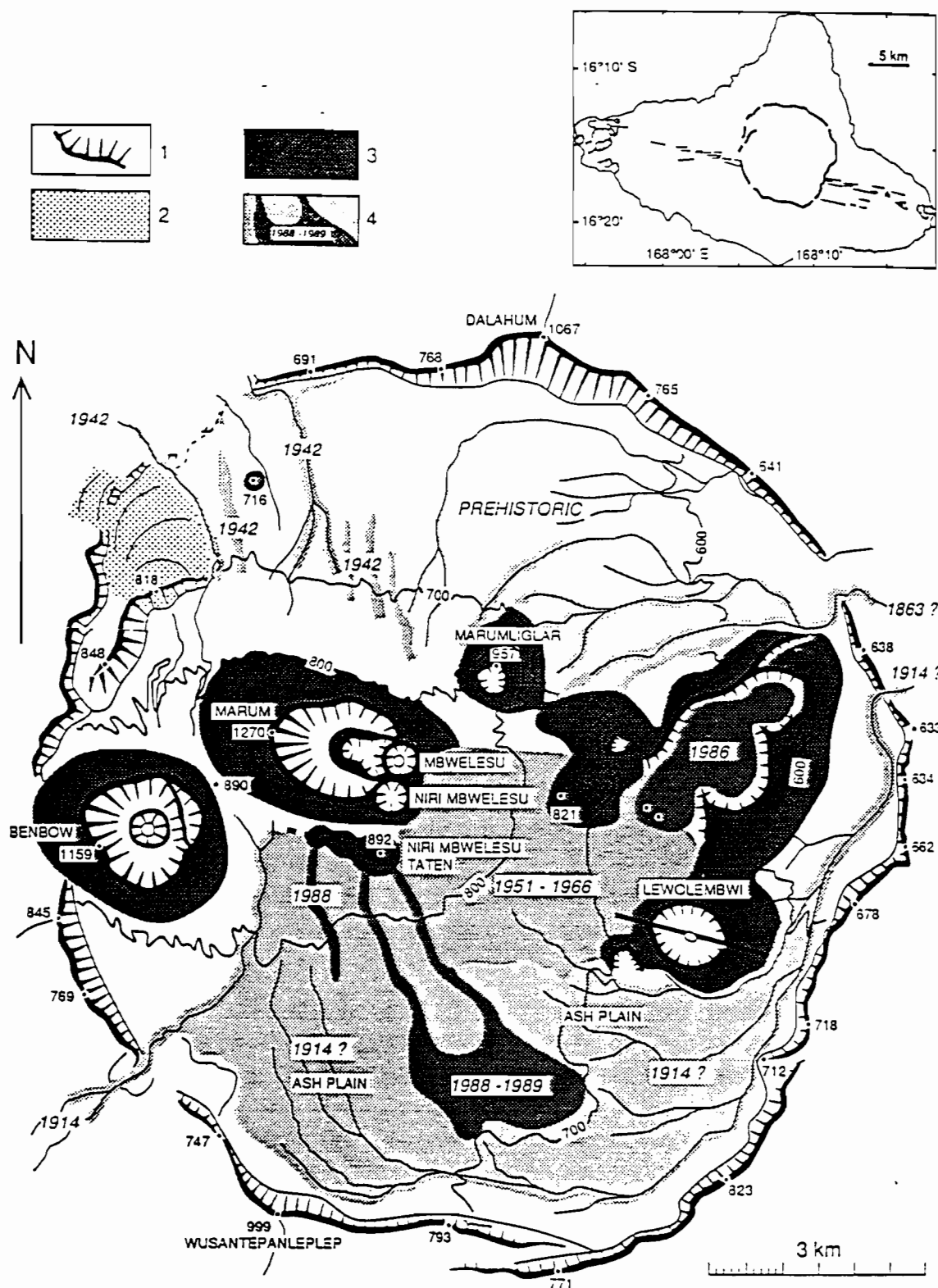


Figure 26: Sketch volcanologic map of the caldera. 1: caldera scarp. 2: Bogorfan basaltic andesite viscous lava flow. 3: volcanic cones. 4: pre-historic and historic lava flows. (From Robin et al. 1993)

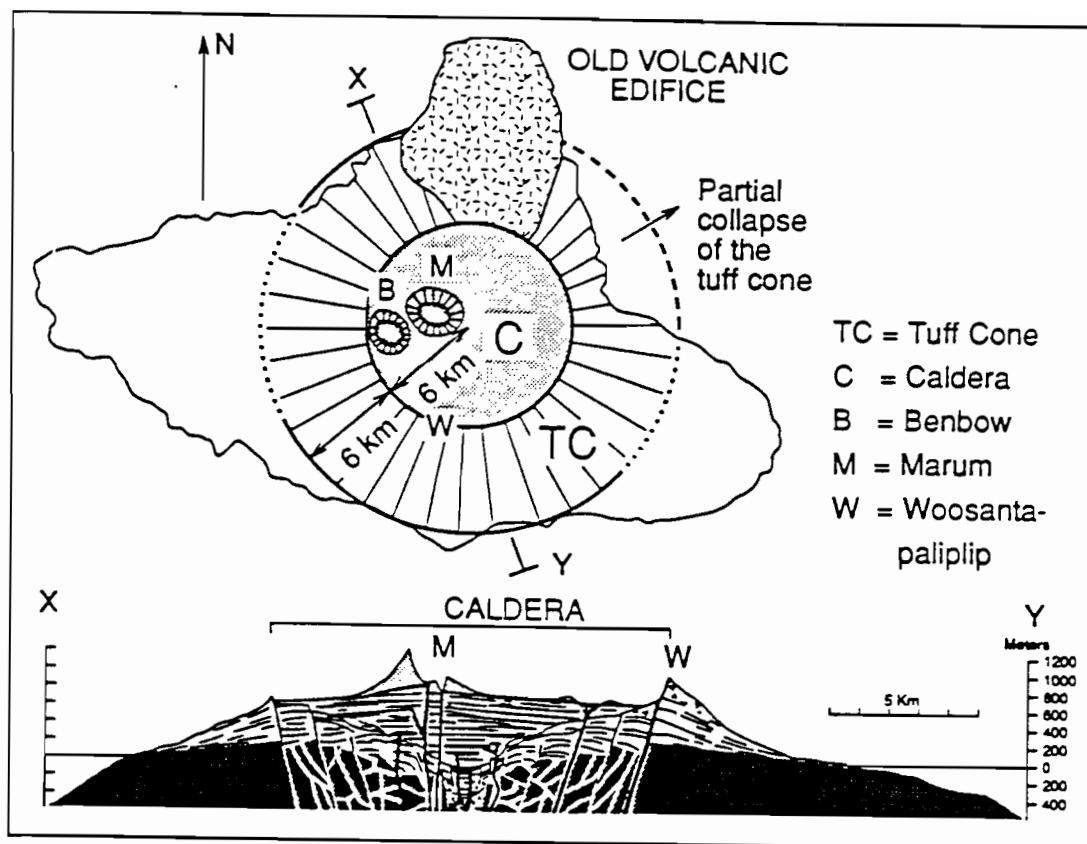


Figure 27: Inferred cross-section (X-Y) showing the basal edifice (dark grey), the tuff cone (white) and the post-caldera volcanics (light grey). Vertical exaggeration X 3. (From Robin et al. 1993).

clasts from the basal volcano incorporated in the coarse layers (Fig. 24) argues in favour of collapse of the roof into the magma reservoir, and enlargement of the vent during the eruption.

Energy released by expansion of magmatic gases may have been sufficient to initiate the eruption. Nevertheless, the lower dacitic pyroclastic flow deposits from this sequence show phreatomagmatic features and these deposits are followed immediately by typical phreatomagmatic deposits. Thus, magma/water interaction is important, even during the earliest stages of the eruption.

The formation of a caldera subsequent to eruption of sequence I does not preclude the possibility of a pre-existing caldera of the Kilauea type at the top of the shield volcano, and a lake within such a structure could explain the phreatomagmatic processes in this sequence. Introduction of seawater into the flat edifice may be an alternative mechanism for magma/water interaction.

(2) - *Construction of the tuff cone as the collapse enlarges.* The thick ring of accumulated vitric tuffs with radial dips, and the clast textures, are consistent with a hydroclastic origin. As juvenile clasts have moderate to

high vesicularity, we propose a phreatomagmatic explosive mode of fragmentation for an already vesiculated erupting basaltic magma (Cas & Wright 1987; Cas et al. 1989). The accretionary lapilli beds are also diagnostic of a wet eruptive column of extremely disaggregated material. It was at this stage of the eruption that seawater probably entered the upper levels of the magmatic reservoir.

Although the ash deposits of sequence III include noncarbonized plant fragments, the flowage of these deposits and the surface features of shards indicate a pyroclastic origin and an emplacement mode similar to that of ignimbrites.

During this second phase of the eruption, both explosive coring and collapse processes occurred. Since Surtseyan-like deposits are likely to occur in a centered eruption, and as the subsequent Woosantapaliplip deposits and Bogorfan Bay lava flows from sequence IV originated near the ring fracture, an enlargement of the collapse during eruption of sequences II and III may have occurred as the cone was growing (Fig. 27).

(3) - *Final phase: eruptive vents on the ring fracture.* Finally, the construction of the Woosantapaliplip

Strombolian cone and the eruption of lavas which flowed towards Bogorfan Bay confirm a decreasing role of water. These formations are affected by the final collapse. Probably other vents opened when the caldera enlarged, but are now buried by post-caldera volcanics.

II - PETROLOGICAL - GEOCHEMICAL SUMMARY

Considering variations of K_2O , La and Zr, three major trends characterize the geochemistry of Ambrym lavas and pyroclastics; one medium-K (MK) to high-K (HK) tholeiitic to calc-alkaline basaltic trend, and two more evolved trends, respectively MK and HK, from basaltic to dacitic-rhyodacitic compositions. These magmatic suites correspond to several volcanic phases:

1 - older MK basalts forming the Tuvio-Vetlam-Dalahum edifice;

2 - MK to HK basalts forming the basal shield volcano;

3 - MK andesites and rhyodacites forming the first pyroclastic sequence of the APS which initiated the formation of the caldera;

4 - MK to HK basalts and andesites forming Surtseyan then Strombolian pyroclastics sequences II, III and IV of the APS; and

5 - post-caldera MK to HK basalts forming the recent olivine-phyric and plagioclase-phyric suites, locally associated with more evolved HK andesitic volcanic rocks in the eastern part of the caldera.

(La/Yb)_n variations (2 to 5.9), (La/K)_n values (1.3 to 2.2) and Zr contents suggest that the parental magmas could have originated via incremental batch melting or fractional melting (21 to 25%) during diapiric ascent of a single spinel lherzolite source (from at least 60 - 45 km depth) in response to the changing tectonic environment due to collision of the d'Entrecasteaux Zone. However, K and La contents require prior subduction-related mantle metasomatism of this source. Fractionation of olivine, plagioclase, cpx and Fe-Ti oxides explain most of the major and trace element variations in the resulting liquids, and interaction between magmas rising from two distinct chambers, combined with massive introduction of seawater into the edifice appear to be the major causes of the giant eruption leading to caldera formation. More recent activity of the volcano is principally related to magma generation processes in relation with the N100° rifting.

SANTA MARIA (GAUA)

The following section is based on the report by DJ Mallick & R P Ash (1975) *Geology of the southern Banks islands, New Hebrides Geological Survey Reports 1975*, 33pp and unpublished data from the authors, collected during a five-week fieldtrip in 1992.

Santa Maria island (originally named by Queiros in 1606) or Gaua (167°30'E; 14°15'S) is about 25 km across (330 km²), and rises to a height of 797 m on the active volcanic cone, Mt Garet. Basically, the island consists of a little-dissected, low, truncated cone with an 8 x 6 km central caldera. It represents the upper part of a 40 km wide and ~3,000 m high volcano (the height of the southern flank, facing the Aoba Basin, is 3,500 m). The caldera is partly occupied by Lake Letas and by the active Garet cone (250 m high; base 3 km wide). A previous study of the geology of the island, including a geological map (Fig. 28) has been presented by Mallick & Ash (1975).

STRUCTURE OF THE VOLCANO

The structure of the volcano essentially consists of 4 major volcanic units.

1 - Dissected remnants of an earlier volcanic edifice, probably early Pleistocene or Late Pliocene in age. These rocks form an apron in the southwest corner of the island.

2 - A regular volcanic cone which is truncated between 500 and 690 m by the caldera rim. Its elevation was originally around 1,000 m. Two main directions of faulting (60° and 320°) affect this cone, the western side of the caldera being in the angle formed by these two trends. On the NE slope of the cone, the Lusal River flows in a small graben bounded by 60°-trending faults. Volcanics from this cone appear to be wholly subaerial and represent outpourings of basaltic and basic andesitic lavas with associated rubble horizons and pyroclastic beds (red cinders, agglomerates and ashes).

3 - A group of superficial small parasitic cones or vents occurring on the outer flanks of the main cone and near the caldera edge. Some lava flows derived from these cones have reached the sea, following topographic lows, or form large fans mantling the lower slopes of the

edifice. For example, in the north east, a young centre located near 300 m in elevation produced a broad fan of olivine basalt lava flows which borders the coastline between Namasari and Tarasag.

4 - The central Mount Garct volcano within the caldera. Although the construction of this cone is contemporaneous with some of the external parasitic cones, its compositional characteristics, drastically different from the entire Santa Maria volcanic series and the external cones, show that it represents a fourth distinct volcanic unit.

Mallick & Ash (1975) summarize the geological

development of Gaua as follows: 1- Growth of a basaltic and andesitic volcano in Pliocene times. 2- Disruption of this volcano (the NW-trending faults may have paralleled the margin of an early caldera, just as similar faults parallel the present caldera). 3- Renewed growth forming a symmetrical cone of basalts and basic andesites (main cone). 4- Quiet collapse of the central part of the new cone, forming the caldera (floor at least 700 m below the former summit). 5- Extensive ash eruptions after the caldera event; new cinder cones began to form in the caldera, notably Mont Garet, and on the flanks of the main cone.

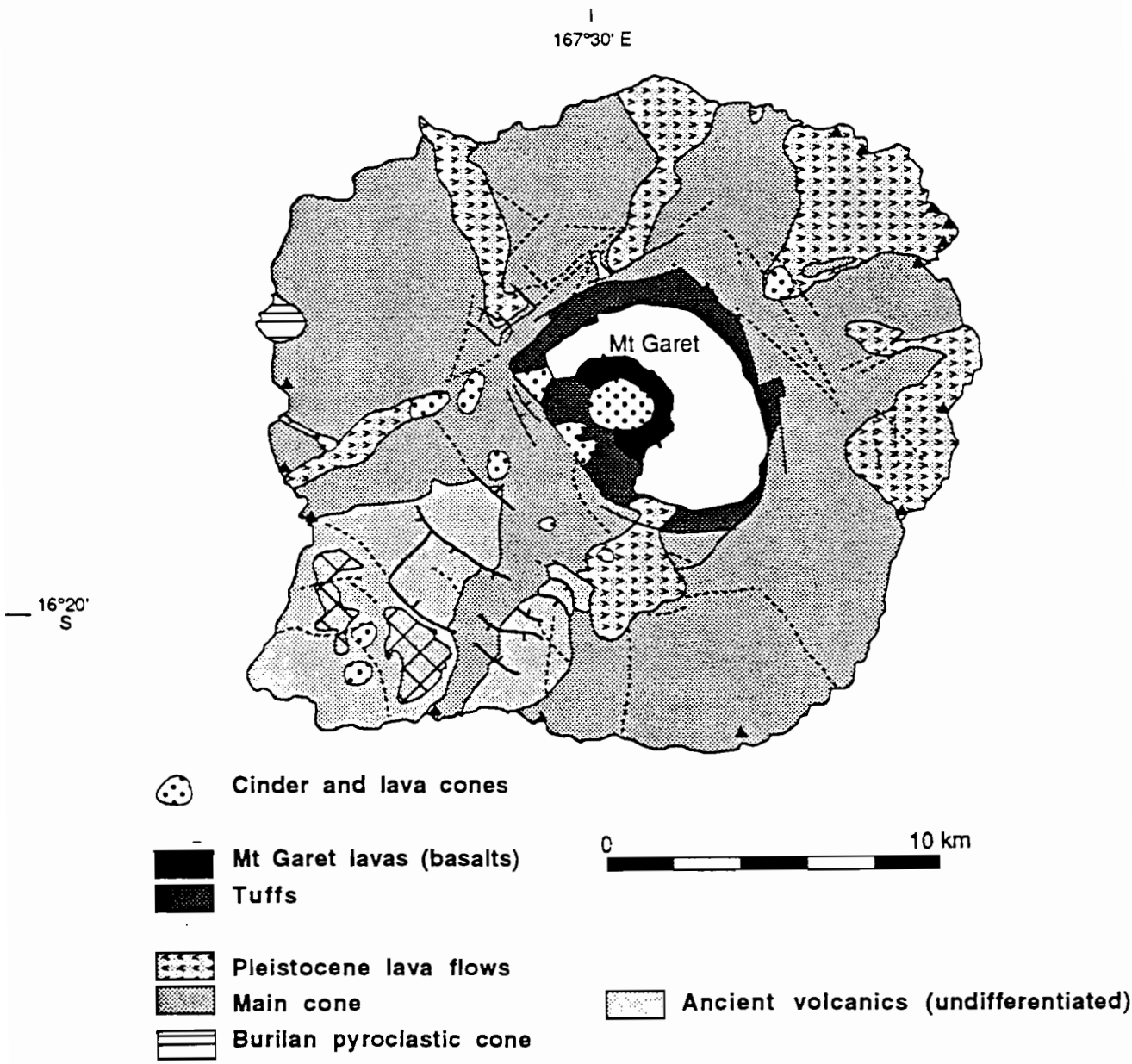


Figure 28: Geological map of Santa Maria (Gaua) volcano. (After Mallick & Ash 1975, modified).

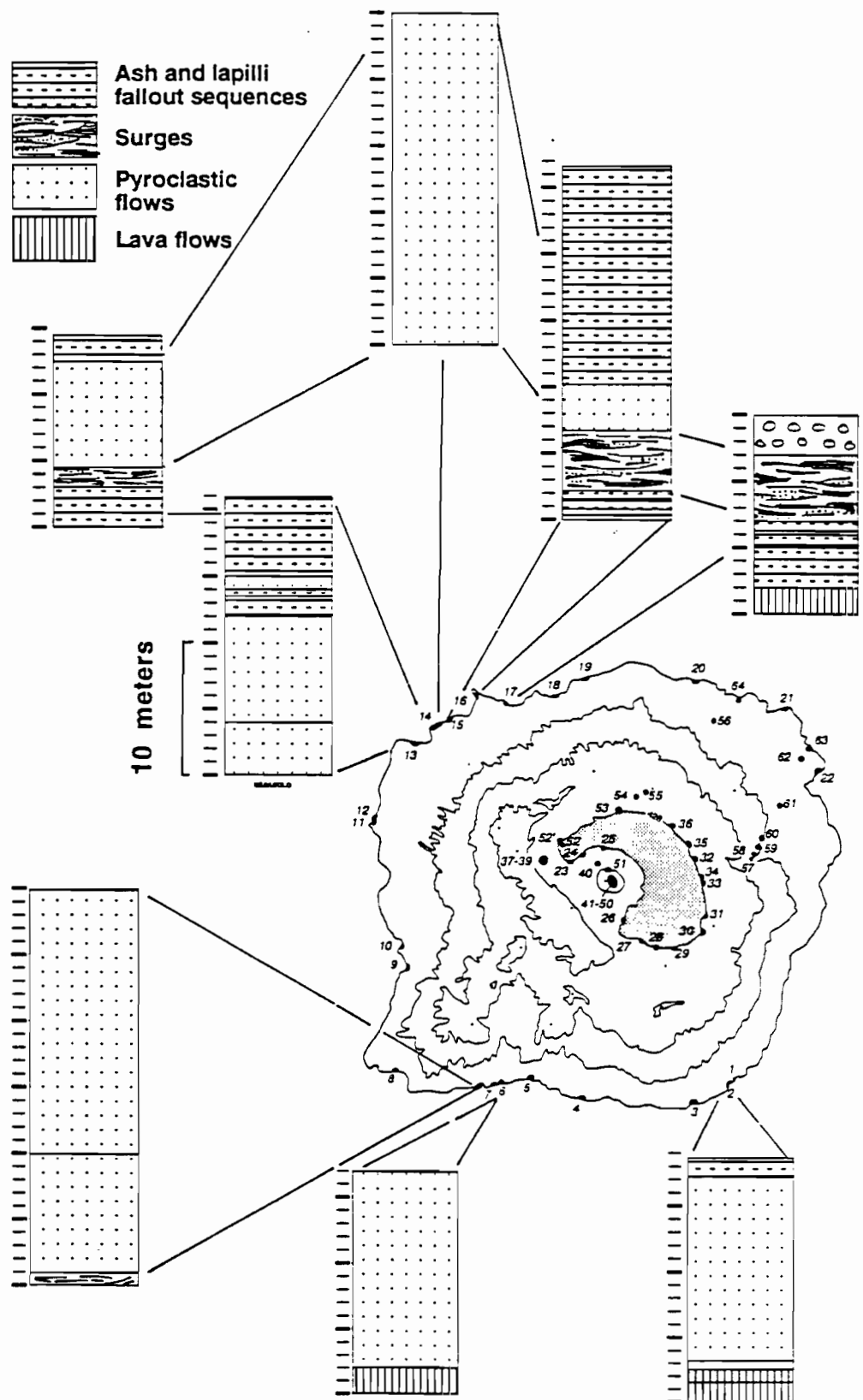


Figure 29: Location of studied sections of the Santa Maria Pyroclastic Series; sampling site numbers refer to analyses in Table 4.

THE SANTA MARIA PYROCLASTIC SERIES AND THE PROBLEM OF THE CALDERA FORMATION

Since 1992, we have carried out an extensive study of Santa Maria. A preliminary result of this study is the recognition of a thick, coherent pyroclastic series well represented on the southeast and northwest shores of the island. As for Ambrym and Tanna, this series consists of complex hydromagmatic and Plinian sequences showing an alternation of both eruptive styles.

At the base of the series, many ash flow deposits, often reworked as thick lahar deposits, have phreatomagmatic characteristics, as demonstrated by quenched juvenile clasts, cauliflower bombs, surge deposits, quenched lapilli, mud-armed lapilli and indurated or muddy matrix. A composite section of these products is presented Figure 29. The pyroclastic flow deposits are associated with sequences of Plinian fallout deposits (ash and lapilli layers) which often expose accretionary lapilli beds. At least one major Plinian episode is represented by a 3 m-thick pumice deposit. These fallout deposits,

observed along the coast, are probably chronological equivalents of a 20 - 50 m-thick sequence of yellow-brown ashes that blanket all the earlier effusive series of the main cone along the track from Namasari to Lake Letas, and that we have also observed at the top of the thick lava flow sequence dissected by the Lusal River. Towards the caldera, these ash deposits grade into stratified tuffs well exposed above the lava flows from the pre-caldera edifice on the northern and eastern shoreline of Lake Letas. These tuffs show a 10° dip to the centre of the caldera.

Thus, the large ash-fall deposits recognized within the caldera and forming the upper slopes of the cone, the brownish tuffs surrounding the caldera rim, the fallout deposits from the northwest and north coast, and the series of pyroclastic flow deposits and breccias (up to 60 m thick in some places) observed along the north and south coasts (Fig. 29), constitute a single pyroclastic series that we attribute to a large hydromagmatic and Plinian event implicated in the formation of the caldera.

Table 4: Wholerock analyses of juvenile clasts from the Santa Maria Volcanic Series

	SM 1C	SM 6C	SM 7A	SM 13A	SM 13B	SM 13D	SM 14A	SM 14B	SM 17D	SM 30A	SM 31B	SM 64A
SiO ₂	55,15	57,20	51,50	51,70	52,00	55,30	55,60	52,00	57,50	58,00	59,00	63,60
TiO ₂	0,86	0,88	0,89	0,86	0,87	0,70	0,87	0,85	0,83	0,74	0,83	0,49
Al ₂ O ₃	16,20	16,34	17,20	16,97	16,95	16,40	16,60	16,58	16,32	16,75	16,35	16,80
Fe ₂ O ₃ *	9,65	8,20	11,50	10,94	11,05	7,75	9,65	10,94	8,00	8,00	7,93	4,01
MnO	0,24	0,23	0,24	0,23	0,23	0,22	0,24	0,23	0,23	0,20	0,20	0,15
MgO	2,68	1,89	3,90	3,95	3,95	1,95	2,76	3,84	1,61	2,25	2,23	0,64
CaO	6,00	4,95	8,40	8,25	8,39	4,10	6,05	8,15	3,88	5,22	5,16	1,60
Na ₂ O	4,27	4,82	3,28	3,54	3,61	4,30	4,34	3,35	4,56	4,60	4,56	5,62
K ₂ O	3,00	4,06	1,80	2,17	2,16	3,46	3,07	1,89	3,61	3,40	3,37	5,35
P ₂ O ₅	0,52	0,69	0,38	0,41	0,42	0,37	0,55	0,37	0,52	0,40	0,40	0,16
LOI 1050°	1,26	1,04	1,45	0,88	0,47	5,28	0,87	2,33	3,13	0,41	0,30	0,53
	99,83	100,30	100,54	99,90	100,10	99,83	100,60	100,53	100,19	99,97	100,33	98,95
Mg#	0,38	0,34	0,43	0,44	0,44	0,36	0,39	0,44	0,31	0,38	0,38	0,26

MOUNT GARET VOLCANIC ACTIVITY

Until 1956, no eruptions had been recorded and this volcano was probably in a solfataric stage (Fisher 1957). Priam (1962) and Warden (1963) confirmed that a long period of dormancy ended in 1962 when the upper slopes of Mont Garet were largely denuded of vegetation, and ash spread northwestwards from a new vent on the southeast side of this cone.

Beginning in 1962, central crater explosions with frequent associated ash columns were reported nearly every year until 1977. In 1965, an eruption lasted for at least three days and a column of ash rising to over 6,000 m was emitted. In 1966 and 1967, small ash eruptions occurred. On October 1973, a small eruption involving the projection of blocks in the active crater was reported. Since such an eruption might become phreatic if water from the caldera lake gained access to the rising magma, the population was evacuated. Nevertheless, no major activity followed and only three emissions of ash occurred, during January 1974. After an increase in fumarolic activity in April 1991, strong continuous degassing was observed, forming a dense white plume from the SE crater in July. This fumarolic activity was continuing in 1992.

PETROLOGICAL - GEOCHEMICAL SUMMARY

Pre-caldera lava flows have compositions ranging from basalt to andesite. Lavas from the parasitic cones are basalts and basaltic andesites, including porphyritic (plagioclase-rich) lavas.

As for the APS on Ambrym (and also the pyroclastics from Tanna and Kuwae caldera, see below), the pyroclastic deposits from Santa Maria show a large compositional range. Wholerock analyses of 15 juvenile clasts from this series (vitric blocks from the phreatomagmatic deposits, welded blocks, scoriaceous bombs and pumices from the pyroclastic flows) are basaltic to andesite-dacite in composition ($\text{SiO}_2 = 51.5 - 63.6$; Table 4). A microprobe study of glasses in juvenile clasts shows two dominant compositions at $\text{SiO}_2 = 52 - 53\%$ and $57 - 58\%$. The pyroclastic flows are either basaltic (a rare phenomenon worldwide for pyroclastic flows of such volume, but which seem to be relatively common in the New Hebrides

arc volcanoes), or show juvenile clasts of different compositions. Preliminary data suggest that these compositions represent the magmatic signature of a layered chamber, the compositional gradient of which is the result of fractional crystallization.

VANUA LAVA

This section is from RP Ash, JN Carney & A MacFarlane (1980) *Geology of the northern Banks Islands*, New Hebrides Geological Survey Regional Reports, 52pp, and from unpublished field observations collected during three week fieldwork in 1991 by the authors, plus new analytical data.

Vanua Lava island ($13^{\circ}48' \text{ S}$; $167^{\circ}28' \text{ E}$; 331 km^2) has a near circular outline whose symmetry is offset in the south by the Ngere Kwon peninsula (Fig. 30). It corresponds to the emerged part of a low profile volcanic complex, rising to about 2500 m above sea floor, and 35 km wide.

Ash et al. (1980) recognized four main volcanic formations in the subaerial part of the edifice.

1- Older volcanics, including a series of basaltic volcanoes of Late Pleistocene age.

2- Andesitic lavas and agglomerates on the western and northern flanks, the Irsa Lion Formation.

3- A thick accumulation of laminated waterlain volcanoclastics (Pe Lav tuffs)

4- Recent volcanics, including the central Suretamatai volcano (Fig. 30), a broad, low-angled shield of predominantly andesitic and basaltic andesite lavas.

SURETAMATAI VOLCANO

Suretamatai (921 m, base: $4 \times 6 \text{ km}$) is the largest volcanic cone of a series of 5 volcanoes aligned SSW-NNE. This basaltic stratovolcano shows a main crater 1 km wide and only 100 m deep. To the north and to the south-east of the crater, two secondary vents 300 and 500 m wide are occupied by lakes at 730 m and 690 m elevation. Recent deposits consist of basaltic and basic andesite lava flows, and layered pumiceous or ashy deposits. These deposits, added to those from the four other cones (Tow Maravig, Tow Mear, Gemekeret and Kwon Saoro) refilled the large central depression of the

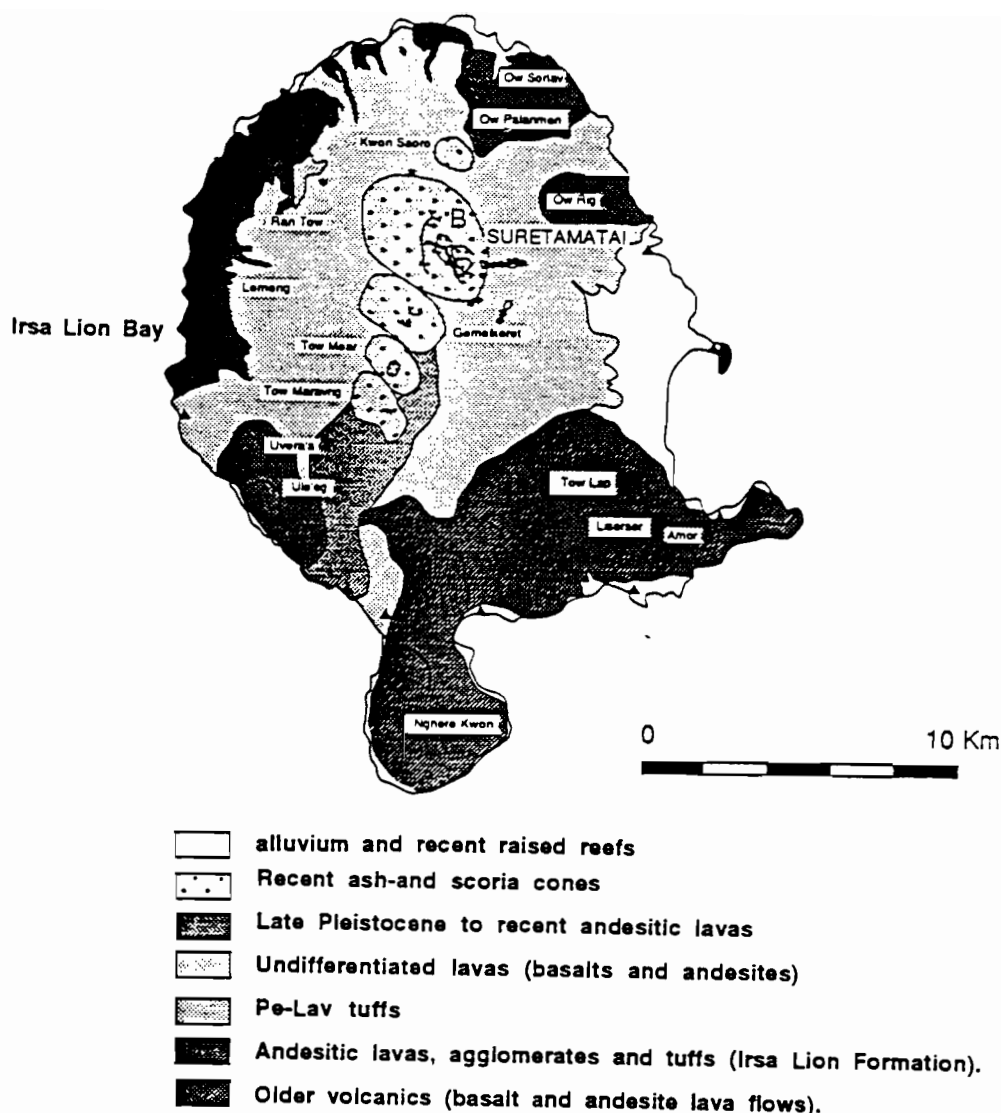


Figure 30: Geological sketch map of Vanua lava (After Ash et al. 1980).

island, from Tow Lap peak in the southeast and Ran Tow in the northeast, forming a large volcanic shield.

Suretamatai erupted in 1841, 1856 and 1861 (or 1865 ?). In 1856, "the mountain was very active: large quantities of ashes fell at Mota, ten miles to the windward". In 1868 (or 1865 ?) "flames were seen apparently from the place". In 1965, an ash plume rose from a new vent on the NW flank, followed by some other emissions over a one year period (NHGS Ann. Rept. for 1966; Blot 1976; Ash et al. 1980; Simkin et al. 1981). In 1966, small explosions occurred in the crater (phreatic activity ?). Eruptive activity is at present restricted to solfataras.

In 1991, the major geothermal area located on the east side of Suretamatai (Frenchman's Solfataras and Hell's Gate) showed slightly superheated fumaroles, hot springs and boiling ponds along the Sulfur River, an activity

which has changed little since the early descriptions by Aubert de la Rue in 1937.

A REMARKABLE VOLCANIC FORMATION: THE IRSA LION FORMATION

During field work in 1991, we studied in detail the Irsa Lion Formation, previously studied by Ash et al. (1980). This formation constitutes a 3 km wide, crescent-shaped area in the northwest of the island. A transverse section along the Pe Lav River exposed the rock facies that compose this formation.

Some lava flows occur in the lower part of the Irsa Lion formation. Nevertheless, we emphasize here the importance of the pyroclastic rocks, which volumetrically dominate this formation. Ash et al (1980) described a

common facies of these pyroclastics as "agglomerates composed of flattened ribbon bombs, poorly welded, that grade into densely welded glassy flows exposing an obvious dark and light coloured banding and showing vertical cooling joints". When poorly welded, these agglomerates are quite similar to the spatter pyroclastic flow exposed in the caldera wall at Santorini (Mellors & Sparks 1991). At Vanua Lava, these tuffs are much thicker, since coastal cliffs expose at least 80 m of these both pyroclastic agglomerates and banded flow facies.

Upstream in the Pe Lav river, layered, gently undulating hydromagmatic tuffs, at least 60 m thick, have been observed, and these consist of coarse and fine ash and pumice tuffs. Bed thickness ranges from 10 to 100 cm with an average of 30 cm. Common cross bedding and typical surge deposits occur in the series, as well as laharic formations. At the base of this tuff series are typical ash flow deposits, including pumice, of acidic composition. Relationships between the ash flows and phreatomagmatic layers on one hand, and the agglomerates and welded tuffs on the other, are uncertain, but probably the ash flows and hydromagmatic sequence underlie the typical Irsa Lion welded facies.

Further upstream, this pyroclastic sequence is succeeded by soft clayey tuffs: the Pe Lav Tuffs. Typically, they are "well bedded, pale yellow to green in colour, and vary from slightly reworked coarse and medium grained pumice lapilli tuffs to finely laminated volcanic mudstone with blue-grey clay bands" (Ash et al. 1980). Wet deformational structures are present and include load casting, slump folding and convoluted lamination. The contact of the Pe Lav Tuff and the Irsa Lion Formation is sharp, since the tuffs were deposited in water-filled lows, against the east-facing fault scarp of the Irsa Lion Formation. The Pe Lav Tuff post dates the Irsa Lion Formation and is overlain by the younger volcanics of Suretamatai complex. An inferred age for the Irsa Lion Formation is upper Pleistocene.

Considering (i) the geographic distribution of the Irsa Lion Formation over a crescent-shaped area, (ii) the pyroclastic origin of its main deposits, (iii) the presence in these pyroclastics of the most differentiated rocks of the edifice (up to 66.5% SiO₂ as shown by our new analyses), (iv) the fault contact between the outer pyroclastic series and the inner waterlain tuffs, and the

depression at the centre of the island (now filled by the Suretamatai volcanic complex), and (v) similarities with the other pyroclastic series encountered in Ambrym and Santa Maria, we suggest as a working hypothesis that the Irsa Lion Formation may be related to a cataclysmic volcanic event (the formation of a caldera ?) and that faults probably delimit a central collapse structure.

Aoba

Since the visit to Aoba will focus primarily on the petrography and geochemistry of its lavas, only a brief summary of its volcanology is presented here, reporting some of the descriptions by AJ Warden (1970) *Evolution of Aoba Caldera volcano, New Hebrides. Bull. Volcanol.* 34: 107-140, and more recent work by S. M. Eggins (1993): *Origin and differentiation of picritic arc magmas, Ambae (Aoba), Vanuatu. Contrib Mineral Petrol* 114: 79-100

Aoba is an almost ellipsoidal, voluminous Hawaiian-like shield volcanic island about 38 km long and 16 km wide, elongated along a N 50° E axis, and located in the central section of the flexural Aoba Basin (Fig. 31). The island (1496 m) forms the upper part of the most voluminous volcano of the archipelago (3900 m above the sea floor, about 2,500 km³). Its summit area shows two concentric calderas, the smallest including three lakes: Manoro-Ngoru (300 m in diameter), Vui (2.1 km in diameter) and Monoro (about 1.3 km). Lake Monoro is located in the eastern part of the caldera against the caldera wall. Lakes Manoro-Ngoru and Vui are two near circular crater lakes. Lake Vui is at the summit of a new cone built on the caldera floor, and may therefore represent a third caldera (Fig. 31). Renewed fumarolic activity was observed by the authors in 1991.

Two magmatic rift zones radiating from the summit have promoted elongated growth of the volcano toward the SW and NE. These rifts have been the sites of fissure-style eruptions, now marked by scoria ramparts, and are flanked by gently dipping slopes formed by extensive lava flows. The rift zones and their flanks are dotted in places with scoria cones up to hundreds of metres high.

Thin pyroclastic units comprising scoria and ash are interleaved between the more voluminous lavas. One relatively thick sequence (~50-100m) of pyroclastics occurs on the northern flank of the central volcanic cone, and is of significance because it marks an abrupt change in magma chemistry and mineralogy. Below this pyroclastic unit occur plagioclase+clinopyroxene+olivine-phyric lavas which have relatively high HFSE concentrations (High-Ti Suite of Eggins 1993), whereas the overlying lava sequence is dominated by olivine

+clinopyroxene-phyric lavas with low HFSE concentrations (Low-Ti Suite). The latter mantle most of the island (at least 90%) and are of particular interest due to their primitive compositions (from ~5 to ~20 wt% MgO).

Development of this volcano includes:

1- A construction stage corresponding to the pre-caldera volcano, including: a- A basal group of basaltic lava flows, interstratified with pyroclastics (250-300 m); b- The Lomala pyroclastics (60-70 m) interbedded with scarce lava flows; c- A series of picritic basalts (about 400 m ?); d- The Manoro pyroclastics (130 m ?): agglomerates and tuffs exposed in the caldera wall, interbedded with rare basaltic lava flows.

2- Formation of the calderas.

3- Post-caldera volcanic activity. Building of the central cone and formation of Lake Vui and Monoro Ngoru. A radiocarbon dating suggests an age of 354 ± 54 years B.P. for the related hydromagmatic products. Subsequently, a small palagonite tuff cone has grown in Lake Vui.

4- Activity in recent times: Eruption of widespread buff-coloured ash deposits with layers of accretionary lapilli mantling pre-caldera rocks. Possible lahars annihilating villages on the SE flanks, about 120 years ago (?).

In addition, activity at flank fissures, spatter cones and formation of phreatic craters along the coast, especially at both extremities of the island, occurred during both the pre-and post-caldera stages of development.

Three anomalous "boiling" areas with large bubbles and burned vegetation were observed at Lake Vui on July 1st, 1991 by a VANAIR pilot. It was the first time he had observed such a phenomenon, and he noted that the vegetation had still been green in May. On 24 July, an aerial survey by the authors revealed no strong degassing, but three areas of discolored water were noticeable in the crater lake. Burned vegetation was observed up to the crater rim, 120 m above the water. Anomalously strong SO₂ degassing is believed to have occurred between May and July. This event went un-noticed by island residents, but since Aoba has been quiet for at least 120 and probably 350 years, as a precaution, a seismological station was installed in July this year on the SW flank of the volcano.

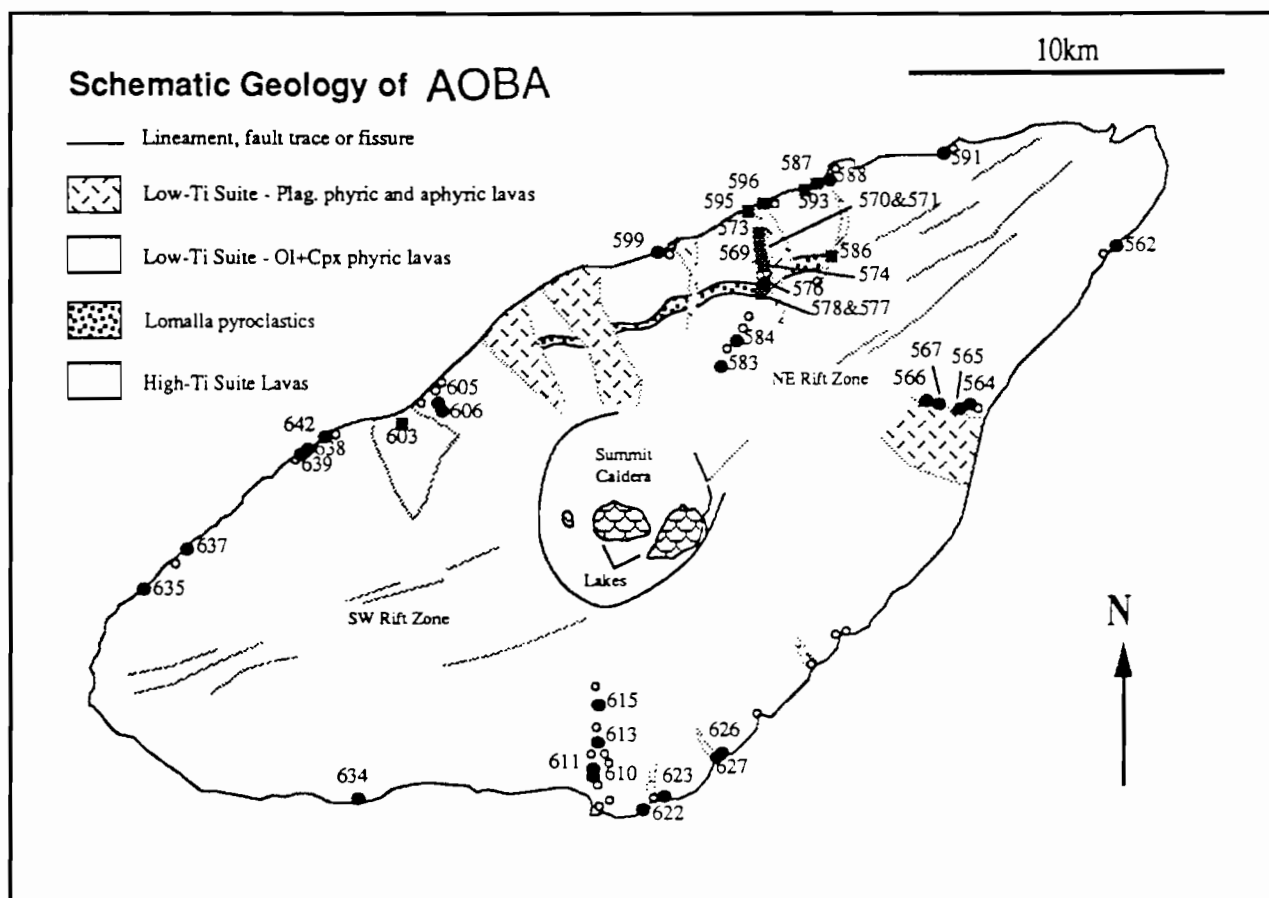
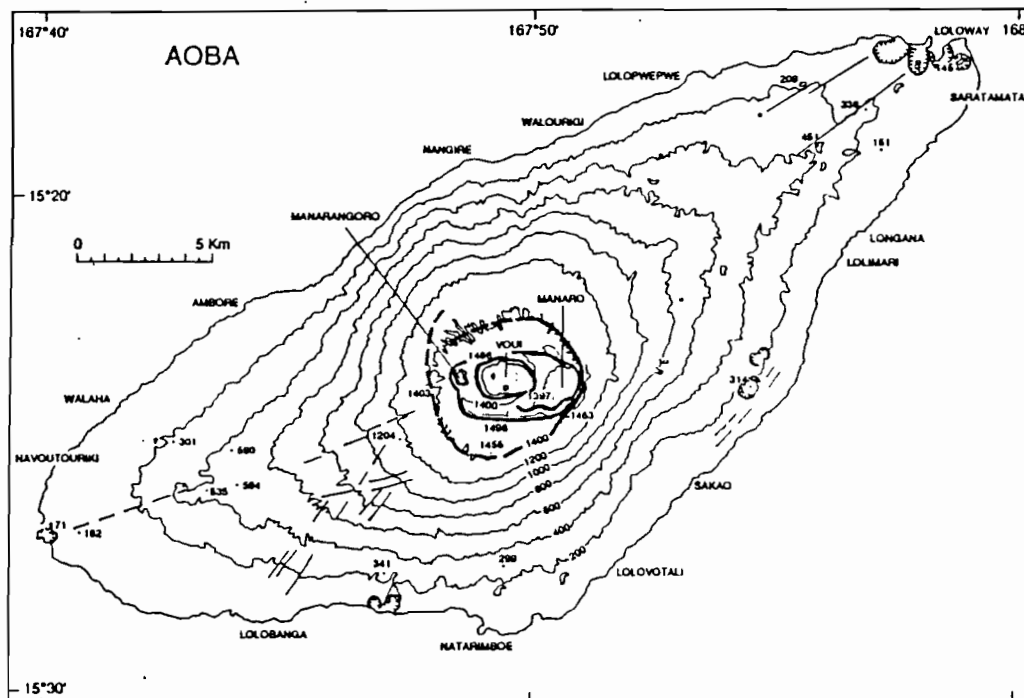


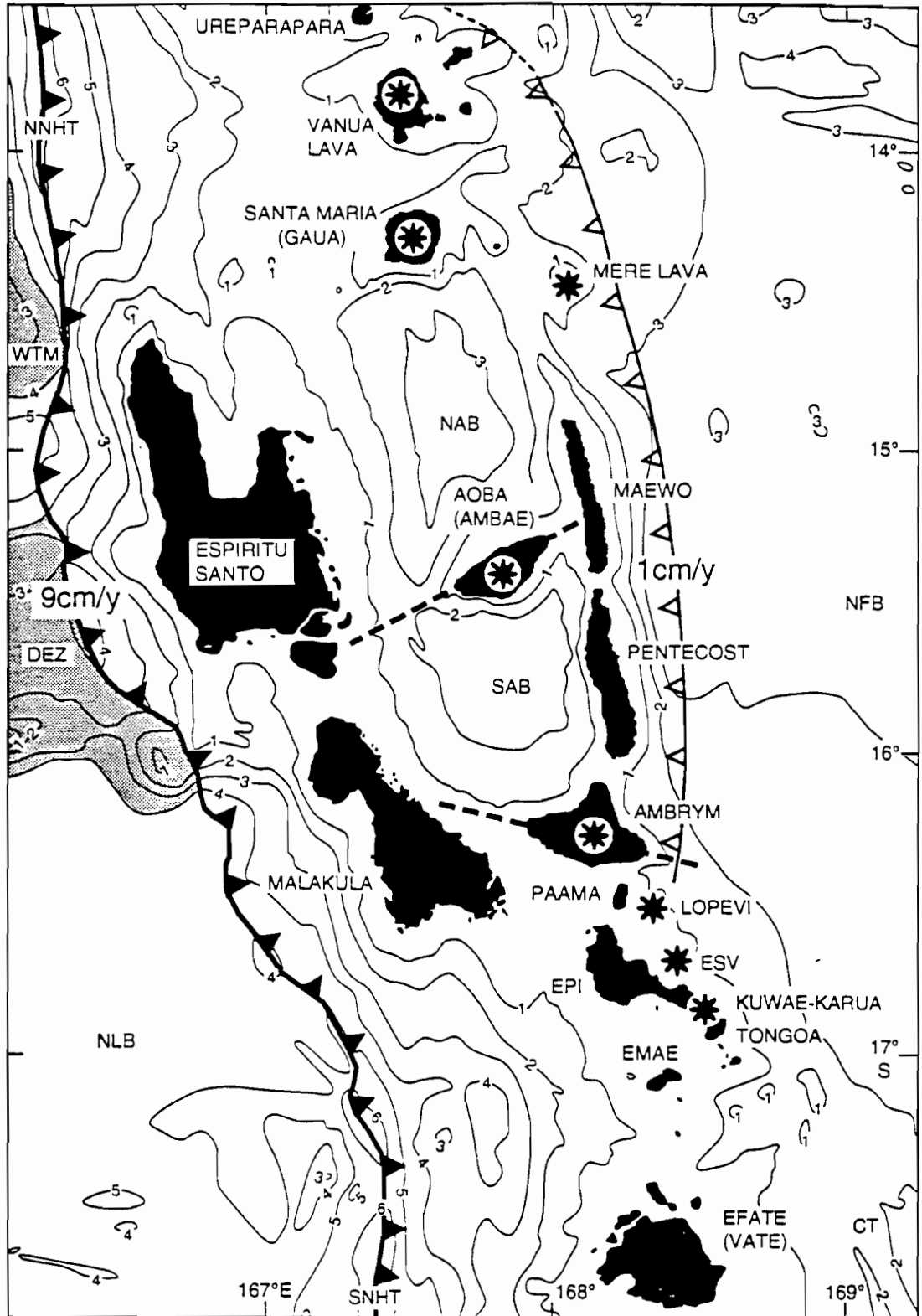
Figure 31: Topographic (a) and geological (b) maps of Aoba volcano showing the main structural features, summit calderas and faults. Contour interval, 100 m.

Crystallisation and differentiation of the Aoba Magmas

The Low-Ti suite lavas range from olivine+clinopyroxene-rich magnesian magmas to aphyric and sparsely phyrlic high-Al basalt compositions. Small plagioclase phenocrysts and Ti-magnetite occur in some high-Al basalts. The crystallisation sequence begins with magnesian olivine ($\text{Fo}_{93.5}$) and Cr-spinel, joined by magnesian diopside ($\text{Mg\#} \sim 92$) when olivine reaches Fo_{89} . Plagioclase and Ti-magnetite are late crystallising in high-Al basalt compositions, together with relatively evolved clinopyroxene ($\text{Mg\#} \sim 85$) and olivine.

Olivine and clinopyroxene phenocrysts have euhedral forms, commonly exceed 1 cm in length and can reach 2-3 cm. Olivine phenocrysts have abundant Cr-spinel inclusions (visible in hand specimen) and often also melt inclusions. Clinopyroxene phenocrysts are characterised by complex growth zoning patterns (for example; mottled magnesian cores containing large melt inclusions, probably reflecting rapid growth from highly undercooled magma, overgrown by intense oscillatory zonation).

Compositional variation in the Low-Ti suite lavas is largely consistent with fractionation of the observed phenocryst phases, and also with experimentally-determined phase relationships. However, variation in magnesian compositions with >10 % MgO conforms to addition/subtraction of olivine and clinopyroxene in the ratio 3:1, where otherwise control by olivine alone is expected. This apparent control by clinopyroxene in addition to olivine may be accounted for by either mixing very primitive olivine-saturated magmas/melts with more evolved olivine+clinopyroxene-saturated magmas, or by rapidly crystallising the primitive magmas before fractionation takes place. Petrographic and mineral chemical evidence for magma mixing and rapid crystallisation occur in the Ambae lavas, in the form of multi-modal phenocryst populations and clinopyroxene zoning characteristics (consistent with initial skeletal growth) respectively. Rapid crystallisation may further explain the development and common eruption of crystal-rich magmas, by producing a more evolved, higher viscosity, and crystal-rich system on a time scale insufficient to enable effective fractionation to take place.



KUWAE

THE FORGOTTEN CALDERA

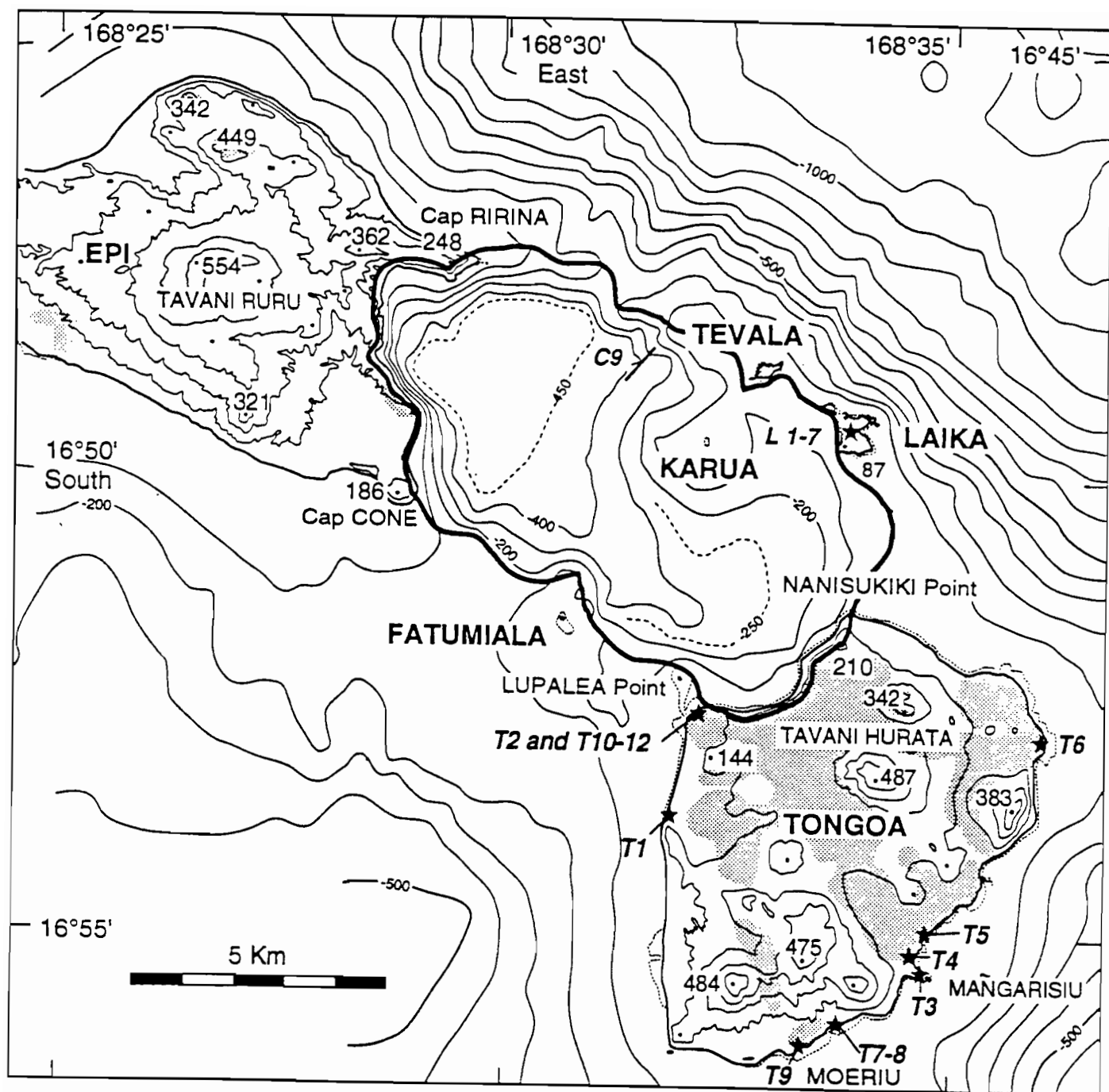


Figure 32: The Kuwae submarine caldera and surrounding islands. Location of sections and sites of sampling referenced in the text. Topographic or bathymetric contour interval =100m. Dotted zones show the extent of PFD 1 and PFD 2 on Tongoa.

DAYS 2 and 3: Tongoa and Laika islands. Eruptive products of Kuwae Caldera.

KUWAE CALDERA

This section derives from two papers presently submitted for publication. M Monzier, C Robin & J-P Eissen. *Kuwae (mid-fifteenth century:) the forgotten caldera*. Submitted to J. Volcanol. Geotherm. Res., and C Robin, M Monzier & JP Eissen. *Formation of the 550 year-old Kuwae caldera (Vanuatu) by an initial hydroclastic and subsequent ignimbritic eruption*. Submitted to Bull. Volcanol.

BACKGROUND

In central Vanuatu, there is a local legend that Tongoa island once formed part of a larger landmass, Kuwae, partly destroyed during a cataclysmic seismo-volcanic event (Garanger 1966; 1972; Hebert 1966; Espirat et al. 1973). When embellishments common to oral folklore are filtered out, it appears that after several strong earthquakes of increasing magnitude, Kuwae tilted and broke into pieces while a gigantic eruption was occurring. Many people escaped death, fleeing southward as far as Efate island at the first signs of the cataclysm. Most inhabitants remaining on Kuwae were killed, but a few reached Tongariki island, and among them was the young Ti Tongoa Liseiriki who first resettled Tongoa shortly after the eruptions ceased.

This cataclysmic event has been well known to archaeologists and ethnologists, as well as to geologists over the last few decades. Nevertheless, inadequate geological data and the misinterpretation of ¹⁴C dates quoted by archaeologists have previously prevented the determination of the age and size of the event, the nature and volume of the erupted products, and the precise morphology of the resulting caldera. As a consequence, there is no report of this major eruption, which was probably of the same order of magnitude as that of the Santorini Minoan event in 3600 B.P. or that of Mount Mazama (Crater Lake) in 6845 B.P.

PREVIOUS STUDIES

Warden (1967) and Warden et al. (1972) related the dacitic pumiceous agglomerates which cover most of the high ground of Tongoa, Laika, Tongariki, and the Valea islands, and also the southeastern part of Epi island, to the major volcanic event recorded in oral tradition. Previous workers (Aubert de la Rüe 1956; Espirat 1964; Geze 1966) postulated that this cataclysm might correspond to the formation of a large-scale caldera, somewhere between Epi and Tongariki islands. Warden (1967) disputed this hypothesis, but Carney & Macfarlane (1977) recognized an oval-shaped caldera between Epi and Tongoa from new bathymetric data. Crawford et al. (1988) defined five large, mainly submerged calderas between Epi and Efate islands and proposed that Kuwae was destroyed and largely submerged during paroxysmal eruptions of one or more of the adjacent calderas, between 3,000 and 400 years ago.

MORPHOLOGY OF THE CALDERA

The scalloped rim of the caldera is conspicuously delimited by Epi, Tevala, Laika, Tongoa and Fatumiala (Sail Rock) islands. As a whole, the caldera is a NW-SE elongated depression, 12 km-long and 6 km-wide, with an area of ~60 km² at the level of the rim, and a floor 250 m to 450 m below sea-level, from SE to NW (Fig. 32).

The inner wall of the caldera is steep, from about 200 m high between Laika and Tongoa to 700 m high along the shore of Epi. From seismic reflection data, "well layered, flat lying reflectors" that partly fill the structure (Crawford et al. 1988) -i.e. the ignimbrites (and minor ash from the intra-caldera Karua active volcano; see below) trapped within the caldera- are 225 m thick. If the "basinward dipping and chaotically bedded reflectors" observed below are also part of the pyroclastic series, the fill reaches 380 m in thickness. Thus, the minimum estimate for collapse near the caldera edge ranges from 650 m along the Tongoa coastline to 950 m along southeastern shore of Epi, and may range from 800 to 1100 m.

For volume calculation, a simplified caldera shape is considered to take into account probable slope modification during collapse, which enlarged the caldera

to its present size and created its scalloped outline. This simplified shape covers an area of 45 km². On this basis, the volume of the depression is estimated to be 17 km³ and the volume of the intracaldera tuffs is in the range 10 to 17 km³. In addition, an undocumented volcanic edifice vanished during the eruption. Considering a hypothetical previous topography, quite similar to that of Epi and Tongoa islands (i.e. 500-600 m in elevation; see discussion below), of two cones 5 km in diameter and respectively 0.5 and 0.6 km-high, the volume of rocks above sea-level was ~7 km³. Part of this volume (~2 km³ ?) can be accounted for as lithics in the proximal pyroclastic deposits. Thus a total of ~32-39 km³ of rock were engulfed during the caldera formation.

AGE

Frederick (1893) first mentioned the cataclysm and Hébert (1966) summarized information collected by European missionaries and travellers about the tectono-volcanic event. Rough estimates based on the number of generations of chiefs place the event between 1540 and 1654 A.D. According to Garanger (1972), these estimates appear too recent in view of two ¹⁴C age determinations carried out on burned wood included in deposits related to the cataclysm, and one collagen age determination carried out on the skeleton of Ti Tongoa Liseiriki, suggesting that the cataclysm occurred in the first decades of the Fifteenth century.

New ¹⁴C data

The sequence of deposits related to the caldera collapse includes two thick pumice flow deposits which occur extensively on Tongoa. Three radiocarbon dates have been determined at the Centre des Faibles Radioactivités (Gif sur Yvette, France) from pieces of charcoal from sites T4, T7 and T9. Carbonised tree trunks are abundant in the lower deposit near Moeriu (sites T7 and T9).

- T4D, is a completely carbonised pandanus trunk, 7 cm in diameter, from the upper pumice flow deposit at Mangarisiu, with a conventional radiocarbon age of 430 ± 50 years B.P. (Gif-8958), that reduces to a calibrated date of CAL A.D. 1414 - 1619 (calibration according to Pazdur & Michczynska (1989); 95% confidence level, range based on 2 sigmas).

- T7D, is a completely carbonised "ironwood" trunk, 20 cm in diameter, from the lower pumice flow deposit at Mocriu, with a conventional age of 560 ± 50 years B.P. (Gif-8959), or CAL A.D. 1295 - 1430.

- T9A, is a completely carbonised "ironwood" trunk, 25 cm in diameter, from the lower pumice flow deposit at Mocriu, with a conventional age of 430 ± 40 years B.P. (Gif-8960), or CAL A.D. 1420 - 1611.

As the exact positions of the dated samples within the carbonised logs have not been recorded (outermost rings or core ?), some of these dates could predate the eruption by some years or tens of years. This may be the case for sample T7D, which gave an older age than samples T4D and T9A; furthermore, the tree corresponding to this sample could have died before the main eruption (perhaps during a previous eruption?). As both samples T4D and T9A (from two distinct sites) give a maximum probable date of 1445 A.D., the cataclysmic eruption of Kuwae probably took place in the mid-Fifteenth century. This result agrees well with previous ¹⁴C dates (Garanger 1972).

PRODUCTS OF THE TERMINAL MAAR PHASE OF THE PRE-CALDERA EDIFICE, AND PRODUCTS RELATED TO THE CALDERA EVENT

Effusive and Strombolian, mainly basaltic, products characterize the pre-caldera edifice. Basalt and andesite lava flows and agglomerates may be observed and sampled on Tongoa (sites T1, T3, T5, T8 and T9. Table 5 shows three representative analyses from these series.

Three detailed cross-sections from Tongoa-Laika will be observed during our field trip, and these illustrate the tephrostratigraphy of the entire series of tuffs surrounding the caldera and overlying the pre-caldera formations (Fig. 33). Two sections are located on the caldera wall, at Lupalea Point on Tongoa (sites T2 and T10-12, Fig. 32) and on the small island of Laika (L1-7), and the third is a composite section from the SE coast of Tongoa, near Moeriu and Mangarisiu (T4 and T7-9).

Lupalea point section (day 2, morning)

1 - At Lupalea Point, the first 33 m of deposits which overlie the pre-caldera lava flows show a complex association of pyroclastics which correspond to alternating hydromagmatic (HD 1-4) and Plinian eruptive styles. At

Table 5: Kuwae - Wholerock analyses. Major elements geochemistry in wt% summed to 100% volatile free; FeO*=total iron as FeO; LOI=loss on ignition; Mg # determined on the basis of $\text{Fe}^{2+}/(\text{Fe}^{2+} + \text{Fe}^{3+})=0.9$.

Sample n°	PRE-CALDERA			SYN-CALDERA PYROCLASTIC SERIES																	Out. Extr.	KARUA
	Mg β T9C	Al β T2A	And. C9B	HD1 T2C	HD5 T2J	T2K	PFD1		PFD2			HD6		WFD3		WFD4		WFD5 L7B	lava fl. T6A	C10A		
							T7F	T4A	T4B	T2N	T10C	L1A	L1B	L6A	L6G	L7A	L7F					
SiO2	51.60	52.08	58.74	51.92	64.33	62.48	64.11	64.43	63.91	62.49	61.67	64.41	64.71	64.51	64.37	64.40	65.68	64.38	63.88	53.04		
TiO2	0.70	0.79	0.64	0.83	0.60	0.60	0.60	0.60	0.61	0.61	0.62	0.59	0.58	0.58	0.59	0.59	0.56	0.59	0.61	0.67		
Al2O3	14.06	18.60	15.68	18.31	15.37	16.00	15.62	15.53	15.61	16.00	16.24	15.49	15.20	15.45	15.52	15.42	15.29	15.47	15.62	16.85		
FeO*	10.17	9.65	8.27	10.45	6.35	6.68	6.16	6.25	6.28	6.69	8.86	6.06	6.04	6.08	6.15	6.16	5.69	6.12	6.48	10.77		
MnO	0.20	0.17	0.18	0.19	0.15	0.16	0.16	0.15	0.15	0.16	0.16	0.29	0.15	0.15	0.15	0.15	0.14	0.15	0.16	0.12		
MgO	8.12	3.96	3.48	3.87	1.71	2.05	1.69	1.68	1.78	2.05	2.23	1.64	1.70	1.66	1.87	1.66	1.46	1.82	1.73	5.67		
CaO	12.00	10.50	7.54	9.86	4.80	5.74	4.88	4.80	5.04	5.73	6.07	4.68	4.61	4.77	4.75	4.80	4.33	4.74	4.90	8.96		
Na2O	2.13	2.69	3.37	2.99	3.93	3.76	3.98	3.80	3.91	3.77	3.61	4.04	4.18	3.93	3.95	3.99	4.03	4.03	3.95	3.28		
K2O	0.81	1.29	1.81	1.28	2.51	2.29	2.56	2.50	2.47	2.27	2.33	2.57	2.58	2.62	2.60	2.59	2.58	2.46	2.43	0.48		
P2O5	0.20	0.27	0.29	0.30	0.24	0.23	0.24	0.25	0.24	0.23	0.22	0.23	0.25	0.25	0.24	0.24	0.25	0.24	0.24	0.15		
LOI 1050°C	-0.21	0.07	-0.36	2.21	0.02	-0.06	0.59	0.10	-0.12	-0.02	0.62	0.04	0.98	-0.09	-0.03	0.10	-0.10	0.57	-0.15	1.62		
Initial tot.	98.62	98.96	99.40	98.51	98.73	99.17	99.63	98.96	98.85	99.03	99.54	99.18	98.79	99.58	99.87	99.64	99.25	99.05	98.94	98.62		
Mg#	0.61	0.45	0.45	0.42	0.35	0.38	0.35	0.35	0.36	0.38	0.39	0.35	0.36	0.35	0.35	0.35	0.34	0.37	0.35	0.51		

the base, a first sequence of hydromagmatic deposits (HD 1), 3.5 m-thick, consists mainly of surge layers grading upward into ash flow deposits bearing basaltic scoriae. This sequence is followed by a rhythmic 1.5 m-thick sequence of ash and lapilli fallout layers. Above, two sequences of yellowish layered hydromagmatic deposits, HD 2 (7.5 m-thick) and HD3 (4 m-thick) are intercalated with two massive (2.5 and 6 m) beds of grey airfall lapilli. Ash layers show conspicuous cross bedding or wavy fine "laminites", intercalated with ash and vitric lapilli layers cemented by a coarse or fine muddy matrix consisting of sideromelane clasts with palagonite, mainly basaltic andesite in composition. An 8 m thick sequence of yellowish layered hydromagmatic deposits HD 4, quite similar to HD 2-3, ends these 33 m of deposits, which may be interpreted as a terminal maar phase of the pre-caldera edifice, and which includes drier Plinian episodes. The hydromagmatic deposits grade upwards into two major sequences, which mainly consist of Plinian deposits, and are clearly related to the caldera event.

The upper part of the Lupalea Point section (26 m) exposes: (i) 7 m of massive yellow hydromagmatic tuffs, with quenched black, vitric blocks and flattened bombs, dacitic in composition, in an indurated muddy matrix of coarse ash cemented by fines (layer HD 5); (ii) a co-ignimbrite breccia including about 10% of juvenile clasts, 5 m thick; (iii) an additional lenticular yellow layered tuff

sequence, 3 m-thick; (iv) a 4 m-thick lithic-and pumice-rich unwelded flow deposit (PFD 1), and (v) a 6 m-thick unwelded pumice flow deposit (PFD 2) with 80 to 90% pumice (sample T2N, Table 5). An 80 cm-thick ashfall layer crowns this section.

Moeriu-Mangarisiu composite cross-section (day 2, afternoon).

The two major ignimbritic units PFD 1 and PFD 2 reached the SE coast of Tongoa:

- Near Moeriu, a lower unwelded pumice flow deposit is exposed over 9 m at the base of the coastal cliffs. This deposit includes 50 to 80% of pumice fragments (sample T7F) up to 15 cm in size, but commonly 3 to 7 cm, 20 - 50% of lithic blocks up to 20 cm, but usually 2 to 8 cm, and scarce quenched glassy blocks a few cm in size. At sites T4 and T9, this unit commonly shows bigger (30 cm) and more frequent glassy blocks (sample T4A). Completely carbonised "ironwood" trunks, frequently oriented in the direction of flow (NW-SE), are so frequent in this lower pumice flow deposit that local people use them to cook food. A 1m-thick ashfall layer crowns this deposit.

- The middle and upper parts of the Moeriu-Mangarisiu composite section are exposed near Mangarisiu. The upper ignimbrite unit exposes a 50 cm to 2m-thick basal layer of welded vitric tuff with glassy blocks up to 80 cm

Mangarisiu on Tongoa, and including carbonised trunks, were observed on Epi island. Observation of the Fatumiala rock showed that this 15 m high islet consists of red welded tuffs similar to WFD 5. On Figure 34, a composite log of the complete pyroclastic series related to the caldera is shown. In general terms, the lower tuff series exposes alternating hydromagmatic (HD 1-4) and Plinian fallout deposits, whereas the upper tuff series mainly consists of four thick welded or unwelded ignimbrite units (PFD 1, 2, WFD 4 and 5), minor ash flow deposits and two sequences of hydromagmatic deposits (HD 5-6).

Volcanics from outer vents (day 3, afternoon).

On the eastern coast of Tongoa, at site T6, we will examine two silica-rich glassy lava flows, erupted from volcanic centers that are located on a fracture, radial to the caldera. These turned to hyaloclastites when they entered the sea. Although if these lavas are covered by pumice fallout deposits, their petrology and composition (dacites, sample T6A) suggests that they must be considered as lavas erupted from outer vents, just preceding the caldera event.

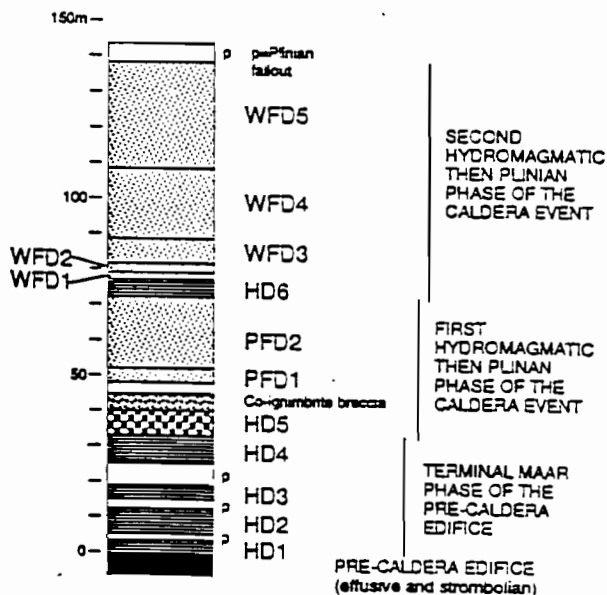


Figure 34: Summary log of the whole Kuwae pyroclastic series (KPS) preceding the caldera event (maar phase) and directly related to it (two main phases).

PETROLOGY OF THE TUFFS

In the welded tuffs, minerals generally represent 4-7% of volume, the matrix being constituted by glassy shards, some of them totally aphyric. Surtseyan-like deposits are constituted by abundant vitric clasts and scarce lithics set in a very fine and palagonitized matrix. Some samples are crystal-enriched. All studied samples are characterized by a phenocryst mineralogy very close to that of the pre-caldera acid andesites. Bytownite phenocrysts (An_{72-88}) are frequent in the vitric fragments from the basal and lower hydromagmatic layers HD 1-4, in association with less abundant clinopyroxene and scarce olivine phenocrysts. The ignimbrite deposits PFD 1-7 and their associated hydromagmatic deposits HD 5-6 show, in decreasing order of abundance: dominant andesine-bytownite (An_{43-89}), subordinate augite ($En_{35-43}Wo_{39-42}Fs_{15-25}$), Ca-poor pyroxene ($En_{49-68}Wo_{3-4}Fs_{29-47}$), minor olivine (Fo_{63-67}) and Ti-magnetite.

Fifteen wholerock analyses are given in Table 5. In addition, microprobe analyses of minerals, 257 glassy clasts, and 10 interstitial glasses from the groundmass of lava T6A were performed on 12 thin sections.

Basal and lower hydromagmatic tuffs HD 1-4:

One wholerock analysis has been made on sample T2C from the basal hydromagmatic deposits HD 1. There are no wholerock analyses for the lower deposits HD 2-4, but microprobe analyses were carried out on a population of 100 glass shards from samples T2E, T2F, T2G, T2H (Fig. 35). No correlation exists between physical characteristics (color and vesicularity) and chemical compositions of the shards. Analyses range from 48 to 61% SiO_2 , but interestingly SiO_2 distribution is bimodal, with one peak at 53.9% mainly formed by glasses from HD 3, and a second at 55.8% mainly formed by glasses from HD 2. In addition, sample T2F includes a few basaltic glass fragments, whereas sample T2H contains a few acid andesite vitric clasts.

Intermediate and upper hydromagmatic deposits (HD 5-6) and ignimbrites

Wholerock compositions of ignimbrites and associated hydromagmatic deposits from the upper part of the series range from acid andesites to dacites (62 to 66% SiO_2 ; Table 5), but are mainly dacitic. Taking into account the

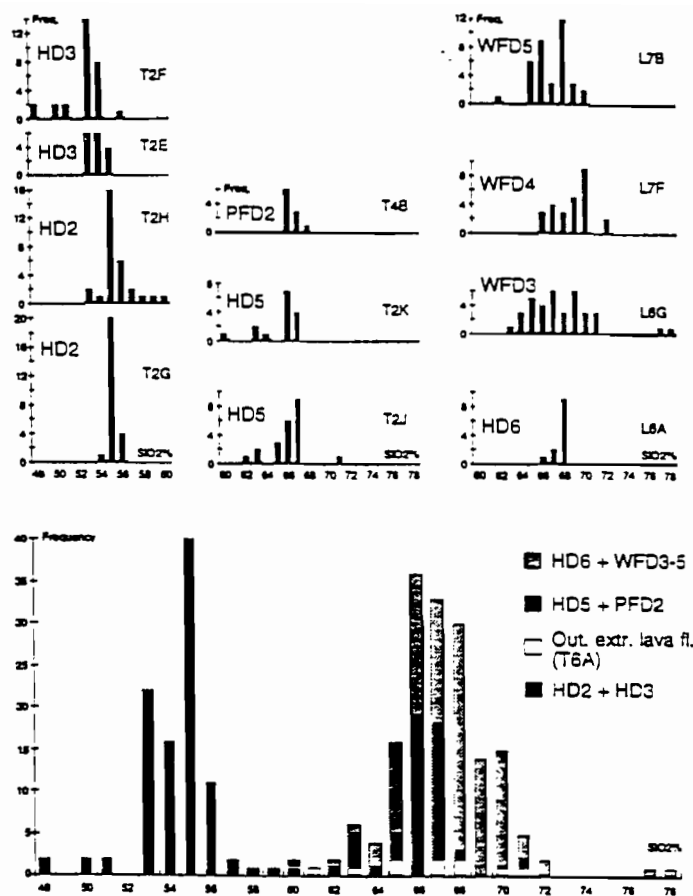


Figure 35: Frequency histogram for SiO₂ values in glasses from the entire tuff series. Microprobe analyses on studied samples and generalised frequency histogram. Class 48 = 48.00% to 48.99% SiO₂.

phenocrysts contents, microprobe analyses of glasses are in good agreement, in term of major elements, with corresponding wholerock analyses (Fig. 36).

Taken individually, each sample from the welded tuffs of Laika (L6G, L7B or L7F) shows a glass population characterized by a wide, dacitic to rhyolitic, and not unimodal SiO₂ distribution (Fig. 35). In comparison, samples from the upper hydromagmatic deposits of Laika display glass populations with a restricted dacitic range in SiO₂ around 68% (L6A). Black glassy blocks from HD 5 and PFD 2 deposits of Tongoa (T2J, T2K, T4B) show glasses with a wide SiO₂ compositional range, but with a definite peak around 66-67% SiO₂. Interstitial glass patches from the groundmass of sample T6A display a wide compositional range in SiO₂ from 61 to 71%.

Taken together, these glass analyses (60.2 - 78.5% SiO₂) display a fairly well defined unimodal distribution around a marked peak near 66-68% SiO₂. For each group of hydromagmatic deposits and their following pumice flow deposits (HD 5 + PFD 1-2 and HD 6 + WFD 1-5),

an average composition has been calculated (Table 6). Vitric clasts in tuffs from Laika (i.e. the upper group) are slightly more silicic than those of Tongoa (lower group corresponding to flows PFD 1-2 and bombs from the massive hydromagmatic layer HD 5).

DISCUSSION

Comparison with other caldera-forming eruptions

The total volume of material released by the Kuwae event cannot be measured, as most of its products entered the sea. However, as for the Crater Lake (Bacon 1983) and Tambora eruptions (Self et al. 1984), the "lost" volume (i.e. the ~32-39 km³ of rock engulfed during the caldera formation) should equal the DRE (Dense Rock Equivalent) erupted volume. The emission of 4 main units of thick unwelded and welded tuffs (PFD 1, 2 and WFD 4, 5) associated with lesser ash flows agrees well with such a large magma output.

A comprehensive idea of the Kuwae eruption

Table 6: Averages and standard deviation of microprobe analyses (recalculated to 100%) of glasses. HD 2 and HD 3: av. of 80 analyses of basalt andesite glass fragments in samples T2E, F, G, H from the basal hydro magmatic deposits (Lupalea Point, Tongoa); HD5 etc: av. of 143 analyses of dacitic glass fragments in samples T2J, T2JK, T4B, L6A, L6G, L7B, L7F from unwelded or welded ignimbrites and related rocks (Tongoa and Laika) and intermediate hydromagmatic deposits (Laika); C9G is a feeder dyke from Kuwae caldera wall; see Fig. 32 for sample locations.

	HD2		HD3		HD5+PFD2		HD6+WFD3,4,5		DYKE
Samples	T2G-T2H		T2E-T2F		T2J-T2K-T4B		L6A-L6G-L7F-L7B		C9G
SiO2 range	55,00 to 56,99		53,00 to 54,99		65,00 to 68,99		64,00 to 71,99		
No of analyses	46	sd	34	sd	39	sd	104	sd	1
SiO2	55,86	1,20	53,96	1,31	66,73	2,09	68,79	2,88	67,70
TiO2	0,97	0,30	0,90	0,19	0,69	0,15	0,59	0,02	0,52
Al2O3	14,93	1,24	14,98	1,69	14,75	0,10	13,94	0,16	14,79
FeO*	10,82	1,87	11,22	2,73	5,72	1,49	4,62	1,62	4,84
MnO	0,24	0,07	0,24	0,05	0,14	0,04	0,08	0,07	0,12
MgO	3,83	0,24	4,69	0,18	1,20	0,20	1,28	1,25	1,08
CaO	7,97	0,05	9,74	0,97	3,63	0,40	2,91	0,50	3,58
Na2O	3,37	0,20	2,74	0,22	4,91	1,08	4,25	0,23	4,23
K2O	1,91	0,14	1,51	0,93	2,24	1,06	3,55	0,21	2,95
Cr2O3	0,10	0,07	0,03	0,04	0,00	0,00	0,00	0,00	0,19
Initial Total	98,30	0,86	98,39	0,26	99,79	1,03	99,41	0,77	99,77

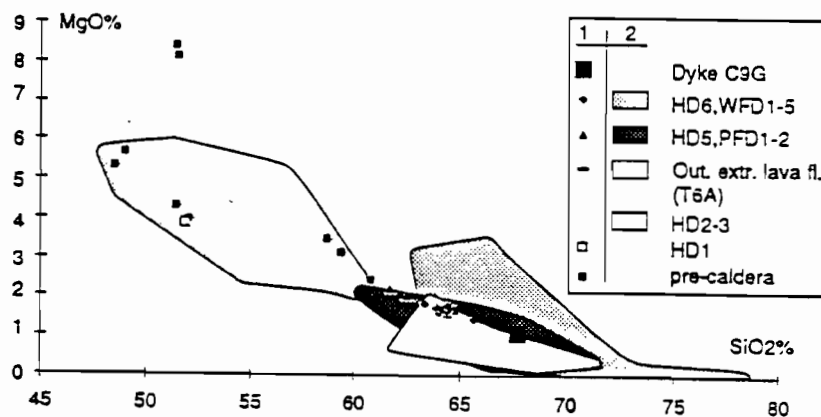


Figure 36: MgO vs SiO₂ variation diagram for whole-rock analyses (dots) and microprobe analyses (areas) from Kuwae caldera. Glass analyses from tuffs are grouped following the three eruptive phases (Figure 34). Note the spread of microprobe analyses from the unhomogenized sample C9G (feeder dyke).

magnitude may be simply arrived at by comparing this erupted volume with the volume released by the largest eruptions (i.e. exceeding 25 km³ of magma output) recorded during the past 10,000 years. The DRE volume of the Kuwae event, the Taupo rhyolitic event (186 A.D.; Walker 1980) and the Santorini Minoan event (3600 B.P.; Druitt & Francaviglia 1992) are quite similar (30 - 40 km³), and are only surpassed by those of the Tambora (1815 A.D.; Self et al. 1984; Sigurdsson & Carey 1989), Kikai-Akahoya (6300 B.P.; Machida & Arai 1983) and

Mount Mazama (Crater Lake; 6845 B.P.; Bacon 1983) events (50 to 60 km³). The age of the caldera event at Ambrym is not well constrained, but this event should also be included in the list, since it is believed to be very young (less than 2,000 B.P.; Mc Call et al. 1970), and released at least 19 - 25 km³ DRE of products (Robin et al. 1993).

Thus, together with the Crater Lake, Kikai-Akahoya, Santorini (Minoan), Ambrym, Taupo and Tambora events, the Kuwae event is among the seven biggest caldera-

forming events of the last 10,000 years. Furthermore, the Kuwae eruption appears second in importance amongst the eruption witnessed during the present era, just after the Tambora eruption (Self et al. 1984). Considering recent events in the SW Pacific, the great eruption on Long Island (11-12 km³ calculated volume of tephra) which occurred about 250 years ago and provoked a "Time of darkness" in the highlands of Papua New Guinea (Blong 1982), should also be mentioned. As for Kuwae, oral folklore has provided accurate accounts of this eruption.

Duration and triggering of the event: model of caldera formation

The lower part of the pyroclastic series shows increasing amounts of hydromagmatic deposits at the expense of Plinian fallout deposits, both types of deposits being mainly of basaltic andesite composition. Conversely, the upper part of the series exposes a thick pile of dacitic ignimbrites, all emitted during the climactic stage of the eruption. This latter phase was probably short, as similar eruptions such as Tambora in 1815 and Krakatau in 1883 seem generally to have lasted for two-three days or less. The time separating the eruption of the hydromagmatic deposits from the climactic stage and the collapse is not known. Nevertheless, the eruption of the whole pyroclastic sequence was of short duration as, in spite of the wet tropical climate, no soils are developed between the different units of tuffs and there are also no lava flows.

The lack of temporal discontinuity, added to the intimate association between hydroclastic and Plinian products and the progressive evolution in the eruptive styles, leads us to consider that these pyroclastics form a *coherent volcanic series, the climactic stage of which provoked the caldera collapse*. This is one of the original characteristics of the Kuwae caldera, compared to other calderas of similar size which originate in a sudden, major, essentially Plinian eruption. Association between hydromagmatic and Plinian eruptive styles is a second remarkable characteristics of the Kuwae caldera. Thus, a model for the Kuwae cataclysmic eruption must take into account (i) temporal considerations, and (ii) eruptive style evolution and (iii) petrologic considerations.

(i) - The numerous eruptive events that preceded the ignimbrite eruptions suggest months or even years of relatively moderate activity before the collapse paroxysm. Probably, this initial phase was accompanied by earthquakes and radial faulting, allowing construction of the outer cones observed on Tongoa. On the other hand, all oral folklore seems to suggest that earthquakes and tsunamis started clearly before the paroxysmal phase.

(ii) - An unusual sequence of hydromagmatic and Plinian deposits and evolution from one type of volcanism to the other are evidenced in some places: a- at Lupalea Point on Tongoa, the lower sequence of deposits shows increasing hydromagmatism with time at the expense of Plinian fallout deposits. b- This evolution leads to the emission of hydromagmatic deposits HD 5 at the start of the cataclysmic event, i.e. an eruptive phase in which water played an important role; c- higher in the ignimbritic sequence, a second burst of hydromagmatism (HD 6) occurs, testifying that water-magma interactions still occurred between two episodes of the major Plinian eruptive phase. This strongly argues for triggering of the Plinian eruptions by magma-water interaction.

(iii)- Glasses from the caldera tuff series are usually not of homogeneous composition, but rather show a wide compositional range. These compositions, together with wholerock compositions, display well defined trends on oxide-SiO₂ variation diagrams. Considering the major elements, all caldera tuffs can be readily interpreted in terms of fractional crystallization, the vitric clasts in the tuffs representing variable compositions from an early differentiated magma chamber. Thus, as for Tanna (see below), the caldera event of Kuwae is characterized by a large compositional range of magmas and the intimate association of hydromagmatic and Plinian products.

Glass compositions represent liquids quenched from differentiated layers in the magmatic chamber just before the eruption. During the eruption, these layers disintegrated and droplets of various compositions were mechanically mixed, but usually without homogenization of the resulting product. A striking similarity is evident between averages of glass compositions and the wholerock composition of sample C9G, a porphyritic dacite with fine-grained groundmass from a probable feeder dyke, dredged on the

caldera wall (site C9, Fig. 32). Other feeder dykes were observed in coastal cliffs on Laika and Fatumiala islet.

The preliminary seismo-tectonic crisis and the pronounced hydromagmatic features of the lower deposits provide evidence that external water (probably seawater) reached mafic andesite magma. Such a magma does not usually stay in the upper central part of a differentiated chamber. Therefore, earlier magma-water interaction probably occurred under a lateral submarine part of the volcanic field, where basic andesite magma was rising, either from an intermediate level of the chamber or from a secondary magma chamber, through a fissure swarm opened during the seismic crisis. At this time, a volatile-charged acid cap, dacitic in average composition, and potentially self-explosive, was stored under the roof of a magma chamber located beneath the central part of the volcanic field, pending eruption. This stock of evolved magma may have been produced by generation of dacitic liquids in a sheath of magma adjacent to the walls of the chamber, ascending by boundary-layer convection and progressive concentration at the top of the chamber, as proposed by Wheller & Varne (1986).

As water played an important role in the first stage of his eruption, the following mechanism is suggested: opening of vents related to earlier hydromagmatic eruptions (maar phase) weakened the rock-pile at the top of the central magma chamber, which progressively failed. This allowed water to reach the volatile-charged cap. At this stage, magma water interaction resulted in the overflow of hydrovolcanic dacitic products poured out, as a mixture of gas and dense vitric and vesiculated blocks (layer HD 5). This was followed by co-ignimbrite breccia corresponding to the initiation of the caldera collapse and enlargement of the vents. Then, depressurization and a turbulent convective regime induced in the differentiated cap produced expansion and eruption of heterogeneous dacitic magma. New infiltration of seawater during a volcanic lull is responsible for the upper hydromagmatic sequence HD 6 and, perhaps, for the triggering of the second Plinian phase (PFD 3-7 on Laika island).

Kuwae caldera: two probable coalescent collapse structures

The oval and lobate shape of the depression, with two

basins at different depths, does not accord well with the existence of a single large volcano before the cataclysm. In addition, the caldera is located on a very narrow volcanic ridge, where a strip of land, at most 6-km wide, previously joined Epi and Tongoa islands, and this also precludes the existence of a large-sized pre-caldera volcano. For comparison, the 12-km wide Ambrym caldera is at the top of a 35 x 50 km-wide volcano, and the caldera of Santa Maria in the north of the archipelago, only 6 x 8 km-wide, is at the top of a 30 km-wide volcano.

Additional observations are in favour of a previous topography rather similar to that of Epi and Tongoa: the 200 m-high cliff along Epi exposes a pile of thin lava flows intercalated with agglomerates (Warden 1967), which suggest a nearby vent approximately at the center of the NW basin. Along Tongoa, the caldera wall exposes in some places thick sequences of coarse scoria, also suggesting a volcanic center near the present shoreline. Moreover, it is worth noting that both basins on the caldera floor are quite similar in diameter to Mounts Tavani Ruru and Tavani Hurata on Epi and Tongoa (Fig. 32). Thus, two small-sized volcanoes in the same places as the present basins probably produce a good approximation to the pre-caldera morphology. In addition, these volcanic centres would be precisely aligned with the Tavani Ruru and Tavani Hurata cones.

Therefore, the elongate shape of the caldera may be explained by an elongated magma chamber with several discrete (or unconnected) apophyses. The fact that dacitic products from the second Plinian phase are systematically higher in SiO₂ than those from the first phase supports such an hypothesis. Moreover, upper ignimbrites PFD 3-7 have never been observed on Tongoa.

Post-caldera activity during the last 500 years includes the development of the basaltic Karua cone on the floor of the caldera (Crawford et al. 1988). Karua has been periodically active since the first documented eruption in 1897 (Warden 1967; Simkin et al. 1981). This cone has produced basaltic lavas and scoria quite different from precaldra basalts. At many times, it has emerged as a small island. It is interesting to ask why these small islands, up to 100 m in elevation in 1948-1949, and often made of scoriaceous pyroclastics, disappeared. Did this disappearance result only from wave action, or from movements of the still-young caldera floor?

TANNA

OLD TANNA IGNIMBRITES AND THE SIWI IGNIMBRITE

The following section is from "C Robin, J-P Eissen & M Monzier (1993) *Ignimbrites of basaltic andesite and andesite compositions from Tanna, New Hebrides Arc*. *Bull. Volcanol. (In press)*, and from new field observations by the authors during recent fieldwork in June 1993. During the fieldtrip, we will encourage discussion about the exact location of the Siwi caldera and about the respective roles of the regional tectonics and magmatic resurgence over the structural pattern of the Yasur - Port Resolution area.

STRUCTURE OF THE TANNA VOLCANIC COMPLEX

Tanna (19°30'S - 169°20'E; 561 km²) is the main island in the southern Vanuatu archipelago, rising 1084 m elevation at Mount Tukosmeru (Fig. 37). Present volcanic activity is restricted to the small Yasur scoria cone (350 m high) in the southern part of the island. Carney & McFarlane (1979) divided Tanna's volcanics into three groups of lavas and pyroclastics: two ancient groups of Late Pliocene and Pleistocene age, the Green Hill and Tukosmeru Groups, and the younger Late Pleistocene to Present Siwi Group, the deposits of which cover the southeastern part of the island. The latter includes the presently active Yasur cone, the volcanics from Ombus, another scoria cone recently extinct, and the Yenkahe volcanics which comprise a remarkable ignimbrite sheet, the Siwi ignimbrite (Nairn et al. 1988).

The Eastern Tanna Volcano and the Old Tanna Ignimbrite Sequence (OTI) .

Carney & McFarlane (1979) recognized two volcanic centres in the former Green Hill Group, respectively the Green Hill centre in the north and the Waesisi-Lowniel centre in the south, near the eastern coast. They also included in this Group the thick pyroclastic deposits which lie between these two centres, along the eastern coast and

over the central part of the island, but they were uncertain of their origin. According to Carney & McFarlane's observations, regional eastward dips of these deposits suggest an origin in the west, but there is no morphological evidence to support a volcanic edifice in the central area of the island. As suggested by these authors, an eastward increase in grain size of the pyroclastics would represent a lateral transition to coarser deposits closer to a centre located in the east, and the observed regional dip may not be primary. Such a hypothesis is sustained by the presence of raised limestones in the NW part of the island.

Bathymetric data obtained during a recent marine survey (ORSTOM Calis Cruise, May 1991, Fig. 38) revealed that the crescent-shaped island belongs to a Plio-Pleistocene volcanic complex, about 40 km wide and some 1800 m high, relative to the arc basement. Field observations show that part of the volcanic sequence assigned to the Green Hill and Tukosmeru Groups, especially the lava flows and pyroclastics exposed along the eastern coast (i.e. pyroclastics from sites 16, 22 and 23, Fig. 37) and in the central part of the island, form the western slope of a large edifice. This edifice, now collapsed below sealevel, we name the *Eastern Tanna Volcano* (ETV). A pile of lava flows and intercalated agglomerates (scoria, ash and lapilli fallout deposits), forming the 100 to 150 m high coastal cliff near Waesisi represent the remains of the southwest flank of this cone. Thick massive to lenticular units of coarse scoria and breccia, numerous dykes intruding scoria and lavas, and the general dips of these lavas, suggest that the vent was located not far to the north-east, probably near 19°26' S and 169° 25' E.

At sites 16, 22 and 23, a complex series of ash flow deposits, scoria-rich pyroclastic flow deposits and massive, poorly welded bomb-rich pumice flow deposits, associated with fallout tephra, overlies the lavas from ETV (Fig. 39). Here, this series is named the Old Tanna Ignimbrites (OTI) to distinguish them from the Late Pleistocene Siwi ignimbrite. As for the associated lavas, local dips (W-SW at sites 22-23, and W-NW at site 16) and their distribution along the coast suggest that the source of these pyroclastics is the ETV.

We will not have enough time to visit outcrops on the eastern coast. As these tuffs extend over most of the island, examination of these tuffs will be possible in the Bethel area, where they underlie recent raised limestones.

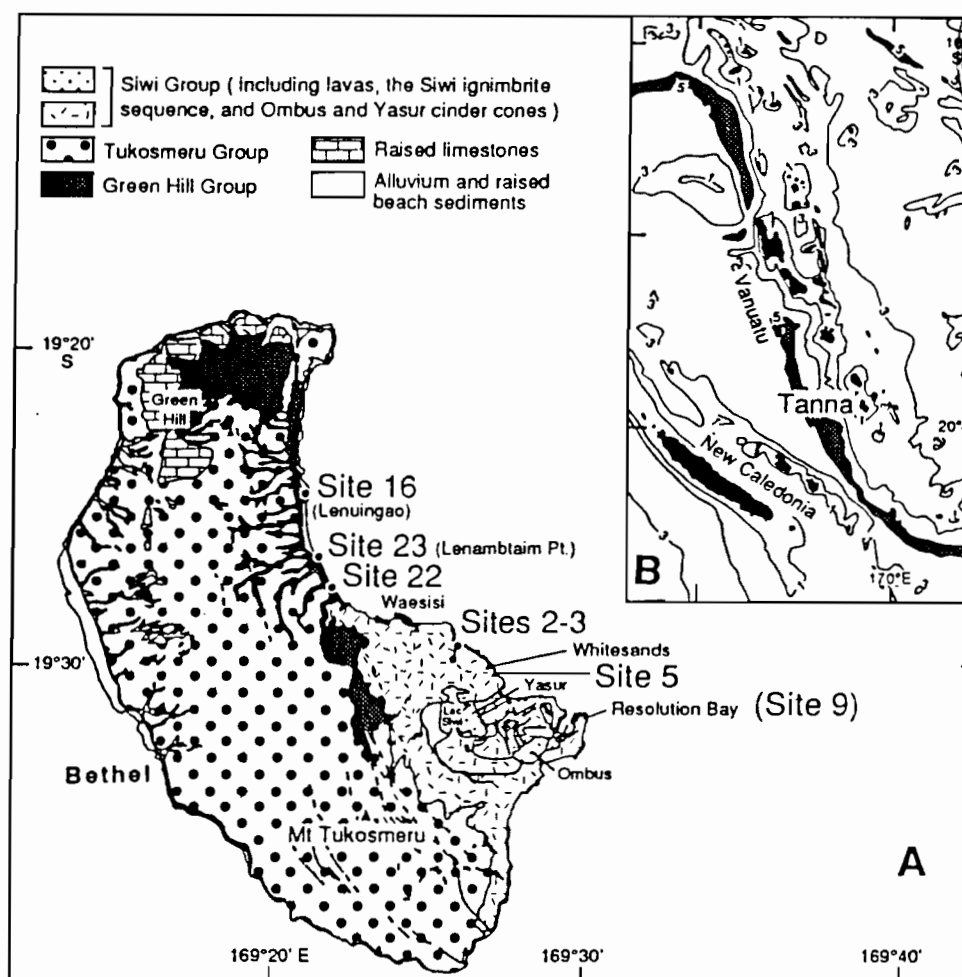
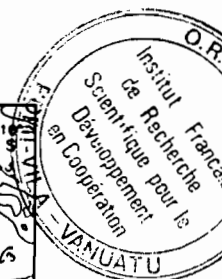


Figure 37: A - Geological sketch map of Tanna island, from Carney & McFarlane (1979), showing the main units and location of outcrops to be visited during the fieldtrip. B - Location of Tanna in the New Hebrides Arc. Dotted area: New Hebrides Trench. Bathymetry in kilometers.

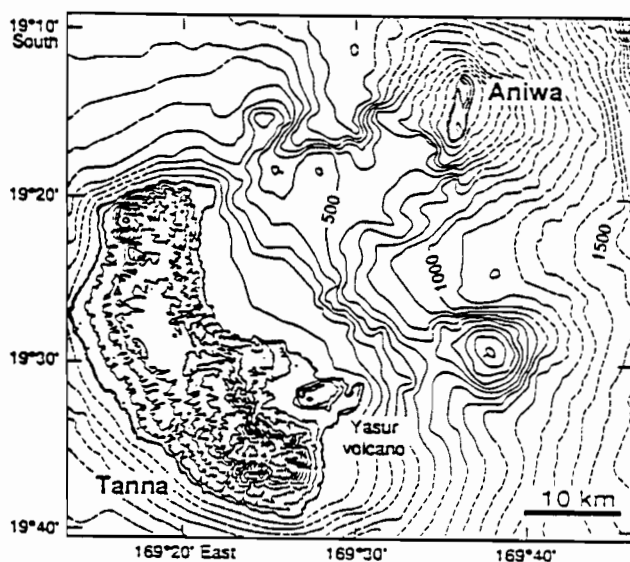


Figure 38: Bathymetric data obtained during the ORSTOM Calis Cruise, May 1991, north-east of Tanna Island. Topographic and bathymetric interval contour: 100 meters.

Upper Pleistocene volcanics and the Siwi ignimbrite sequence

Nairn et al. (1988) investigated the Upper Pleistocene volcanics and emphasized the presence of the Siwi ignimbrite, which covers a large area in the southeast part of the island. These authors attribute to this ignimbrite an approximative age of a few tens of thousands of years and relate the pyroclastic event to the collapse area in which the Ombus and Yasur cones and the Lake Siwi are located (see Fig. 43). The deposits are well exposed at Waesisi along the northeast coast, at sites 2, 3, 5 and in the region of Resolution Bay. On the northeast coast, the intimate association between ash flow deposits and thick underlying phreatomagmatic deposits led us to reconsider the Siwi ignimbrite as part of a complex sequence including these

phreatomagmatic deposits. At site 5, a 4 m-thick densely welded tuff is present at the base of the main pumice flow and overlies the phreatomagmatic deposits (Fig. 39).

Thus, at least four main volcanic units comprise the Tanna volcanic complex: 1 - the Green Hill centre in the north; 2- the Tukosmeru centre in the southwest; 3- Late Pleistocene Yenkahe volcanics in the south-east, and 4- the Eastern Tanna Volcano, in a more central position, but now collapsed below sea-level and dissected by conjugate NW-SE and SW-NE faults, as suggested by the bathymetry (Fig. 38). Scarce ages do not presently allow development of a useful geochronology: three radiometric datings from the Green Hill, Tukosmeru and Yenkahe volcanics give ages of 2.45, 0.65 and 0.23 Ma respectively (Dugas et al. 1976; Carney & MacFarlane 1979). Since the OTI (that overlie the Green Hill volcanics) have their source in the east, Eastern Tanna Volcano was probably as volumetrically large as Tukosmeru volcano, although confirmation is still required.

FIELD CHARACTERISTICS OF IGNIMBRITES

The OTI series is divided into three parts:

1- A lower part consists of brown to yellowish ash flow deposits (up to 2 m thick) and bedded tuffs that show alternating thin and coarse ash, including centimetre sized quenched glass fragments, pumice and lithics (layers 2 and 3, Fig. 39). These deposits reach 9 m in thickness at site 16, where they are overlain by a 5 m thick ash and scoria unit of the intermediate part of the deposits (layer 4). At site 22, only the upper 3 m of this lower sequence (ash flow bearing quenched vitric clasts, layer 3) are observed. No sharp discontinuity is present and the ash flow deposits grade into the intermediate pyroclastic flow deposits.

2- The intermediate pyroclastic flow deposits (layer 4), enriched in scoria and bombs, occur at all three sites. At site 22, transverse sections to the west directed flows show lenses (up to 6 m thick and a few tens of meters long) mantled by a 6 m thick fallout ash and lapilli scoria layers. The lenses comprise unsorted massive beds of coarse ash, 2-3 meters thick, bearing dense and pumice lapilli, scoria and small cauliflower bombs that form up

to 60% of the volume. These deposits locally develop slightly wavy bedded structures some metres long. The dense lapilli are commonly quenched vitric clasts from disaggregated bombs. Accidental clasts are rare.

3- At Lenambaim Point (site 23), three indurated pumice flow units were emplaced almost simultaneously, forming a single cooling unit. They represent the major flows of the OTI (layer 5). They form the cliff along the coast and dip slightly to the S-SW. These tuffs include 30-40% of glassy collapsed pumice blocks and bombs, mainly poorly vesicular and obsidian blocks, generally 10 - 25 cm across, but up to 1 m. Some of the dense fragments are elongate and ribboned lenses 5-10 cm thick and 20-80 cm long, made of compacted scoria and pumice lapilli. Xenoliths are represented by limestone, lavas from the basement, and blocks of a plagioclase-rich andesite.

At all three sites, the upper part of deposits consists of bedded fallout tephra (layers 6), and a lava flow overlies the pyroclastic sequence at site 22.

The Siwi ignimbrite sequence

At sites 3 and 5, the lower deposits of the Siwi sequence exposed along the coast are agglomerates of light brown coarse-grained ash, bearing vitric fragments 2-3 mm to 2 cm across, dense vitric bombs (up to 60 cm) and scoria (2-3 mm to 20 cm) and accidental clasts. Locally, more fine-grained surge deposits occur. The lower half (about 3 m) of these typical phreatomagmatic deposits is indurated. In the upper part of the deposit, bombs become more abundant and interfingering between these deposits and the succeeding ignimbrite sheet can be seen. The following layer is a 4 m-thick densely welded layer (layer 2 at site 5, Fig. 39). The top of this welded tuff grades into the base of the unwelded flow, which is over a few metres thick and rich in poorly vesicular glassy lenses showing bread crusts. The latter become less abundant and then disappear from the pumice deposit. At the lower part of the pumice flow deposits, a block-rich layer separates the lower part of the pumice flow from the rest of the flow, about 30 m thick, which becomes homogeneous. In the latter, the pumices (generally cm-sized, but up to 15 cm across) and the ash are in equal volume. Accidental clasts are scarce.

Along the coastline between Telekey (site 5) and

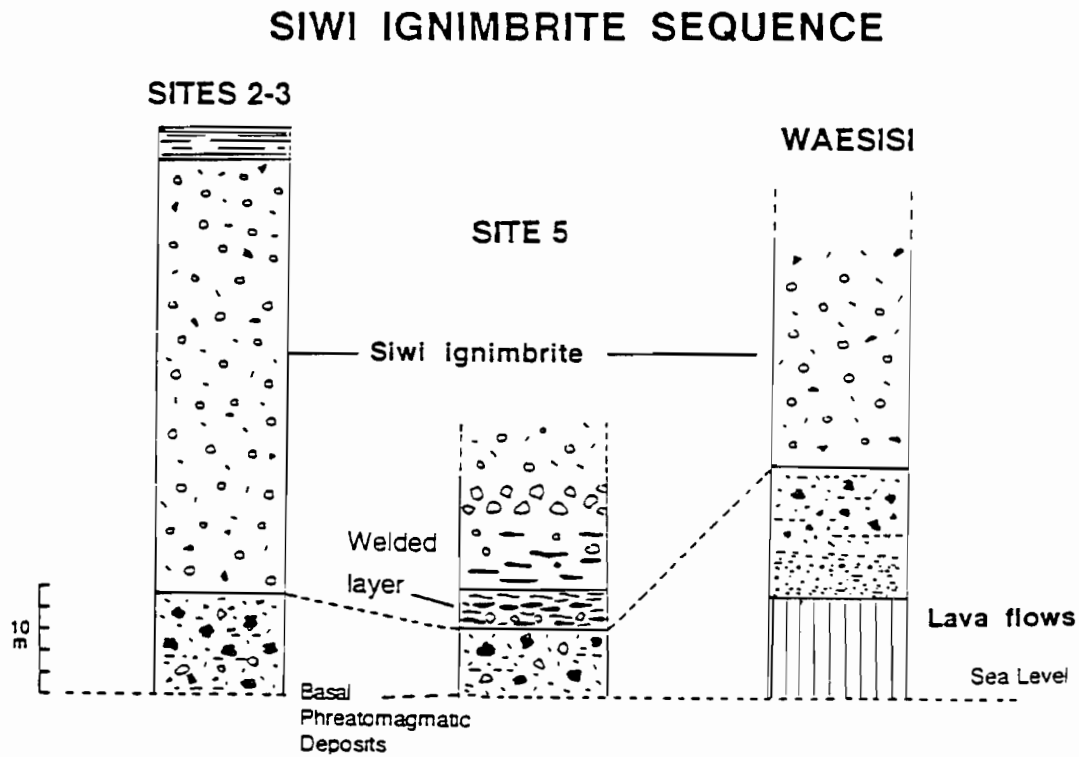
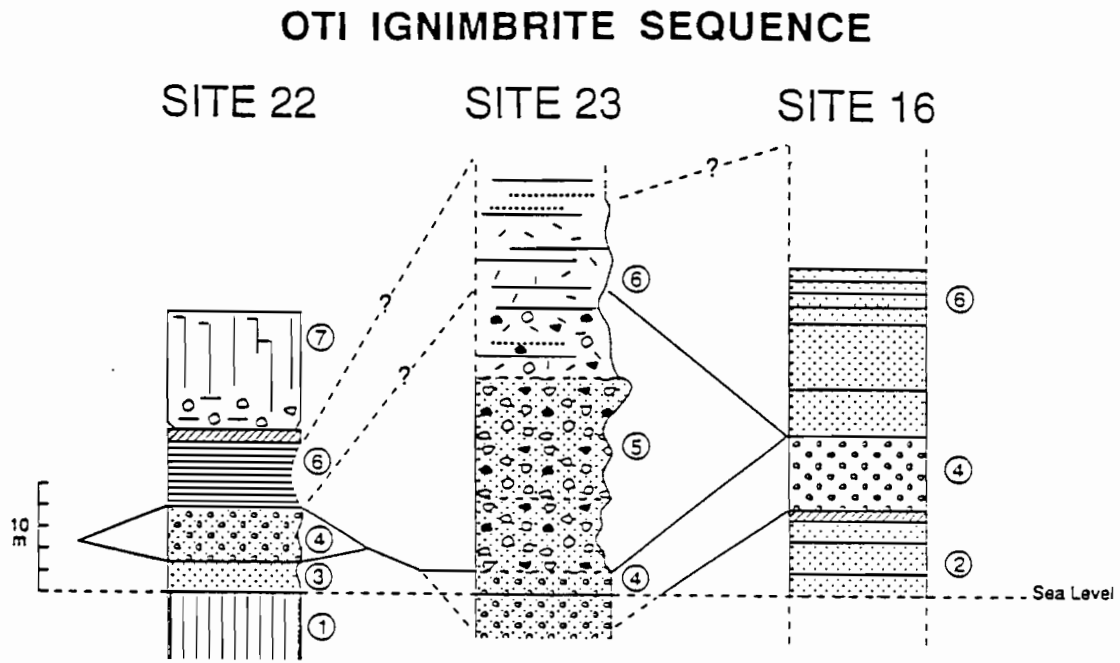


Figure 39: Synthetic sections of OTI and Siwi ignimbrite sequences. Location of sites in Figure 37.

OTI sequence: 1- Lava flows. 2 and 3- Phreatomagmatic ashy deposits bearing vitric clasts. 4- Ash and scoria flow deposits bearing cauliflower bombs, juvenile vitric clasts and accidental clasts. 5- Main ignimbritic deposits of the OTI. 6- Ash and lapilli fallout layers. 7- Lava flow.

Siwi sequence: At site 2, recent fallout ash and lapilli layers from Yasur overlie the ignimbrite sequence.

Sulfur Bay, a complete section of the Siwi ignimbritic sequence will be observed. Here, the Siwi ignimbrite sequence s.s. consists of (i) basal surge deposits (to 1 m thick); (ii) a hydromagmatic layer bearing vitric fragments, dense vitric bombs, scoria, and accidental clasts. This deposit grades into (iii) an initial layer of densely-welded tuff (3-4 m thick) overlain by a 6 m-thick unwelded ignimbrite; (iv) a second succession of welded and unwelded tuffs (4 and 6 m thick, respectively). This sequence lies on a composite sequence of hydromagmatic (maar type) deposits and at least two pyroclastic flows from a probable initial pyroclastic event heralding the caldera forming event. At the base of the section, a feldsparphyric lava flow from the pre-caldera edifice outcrops.

On the eastern side of Port Resolution, two ignimbritic units (2 and 5 m thick respectively) are separated by a complex sequence (~4 m) of block-rich hydromagmatic layers.

In addition, at the northeastern end of the Yenkahe horst, we will observe waterlain pumice tuffs which are obviously the stratigraphic equivalents of the Siwi ignimbrite. Their areal distribution defines the initial location of the caldera and their subsequent tilting (from 30 to 80°) at the periphery of the horst allows definition of the resurgent zone. In our opinion, the main part of the caldera is at present below sea-level, and it would include only the northeastern part of the Yenkahe horst. This proposed location, and our interpretation of the resurgent zone differ from that of Carney & MacFarlane (1979) and Nairn et al. (1988,) who suggested that the caldera corresponds to the entire Siwi area. For us, the present structural pattern of the Siwi area seems controlled by the pre-and post-caldera regional tectonics rather than by volcanotectonic movements.

Interpretation of the OTI and Siwi ignimbrites

In both sequences, the lower deposits (layers 2 and 3 for the OTI sequence, layer 1 for the Siwi sequence) have phreatomagmatic characteristics, as demonstrated by quenched juvenile clasts, cauliflower bombs, surge features, coated lapilli, and indurated or muddy matrix.

For the upper deposits, those from the Siwi sequence are easily interpreted, since the spatial lithologic relationships and distinct textures from base to top

represent a classical facies model from a single pyroclastic flow.

This is not the case for the deposits from the OTI sequence. The volcanologic significance of the main flow deposits at site 23 (layers 5) may be deduced from the following characteristics: 1- Rare accidental clasts. 2- Large juvenile fragments (max. 1 m), commonly bread-crust bombs (up to 40% of the volume). 3- Massive indurated or poorly-welded beds without stratification. 4- Matrix consisting of lapilli that range from pumiceous to scoria, and sparse coarse ash. At Lenambaim Point, these deposits resemble the Acatlan and Campanian poorly vesiculated bomb deposits (Wright & Walker 1981; Rosi et al. 1983). The dense material is too heavy to have been transported far from the source, and we suggest an origin from a collapsed, fines depleted, dense eruptive column. These deposits characterize the proximal deposits of a typical ignimbrite eruption dominated by a complex flux regime.

PETROLOGICAL SUMMARY

Old Tanna Ignimbrites.

Most obsidian blocks and pumices are aphyric or poorly porphyritic. The juvenile blocks show eutaxitic textures (banded and welded matrix, flattened glassy shards). The compositions of 9 samples from sites 16, 22 and 23 range from 53.3 - 58.8% SiO₂ (Table 7). Juvenile clasts in the lower and intermediate OTI deposits show a wide range in plagioclase composition (An₉₀₋₅₈) whereas plagioclase from the upper pyroclastic flows at Lenambaim Point clearly shows less anorthitic compositions and a narrow range (An₅₈₋₄₂). These data are consistent with the compositional evolution of clinopyroxene toward more Fe-enriched augite from the basal deposits to the upper layers, also marked by an evolution of the M# from 49 to 36. Low Ca-pyroxene only occurs in dense vitric lapilli from lower andesitic ash flow deposits (layer 2; analysis TA 15) at site 16. Olivine (Fo₆₀) is scarce.

Our 144 microprobe analyses of glassy shards and welded laminations from the OTI vary from 54 to 69% SiO₂ (Fig. 40, 41, 42), with two main peaks at 56 - 57% SiO₂ and 60 - 61% SiO₂, and minor peaks at 54-55, 59, 61-62 and 69% SiO₂. It is notable that the whole range of

compositions may be represented within a single flow deposit of the upper sequence, or even within a single sample from this flow deposit (Fig. 41).

Siwi Ignimbrite:

Seven wholerock analyses of juvenile clasts from the three parts of the Siwi sequence were carried out. Three samples from the basal layer include a basaltic andesite and two andesites, whereas the upper ignimbrite is mainly andesitic ($\text{SiO}_2 = 59\text{-}60\%$).

Glass compositions (152 analyses), including the lower phreatomagmatic deposits, range from 51 to 65.5% SiO_2 (Fig. 42). The lower phreatomagmatic deposits show a multi-modal distribution, with 3 main peaks at $\text{SiO}_2 = 54 - 55$, $57 - 58$ and $61 - 62$, and also a minor dacite peak at 64% SiO_2 . In contrast, the welded layer, as well as the upper non-welded pumice flow deposit, are characterized by a unimodal compositional distribution of the glass, at 61 - 62% SiO_2 .

Such variations in the vitric phase are matched by the mineralogical data. A very wide range of plagioclase (An_{92-40}) and olivine (Fo_{56-72}) compositions exists in the lower deposits, whereas more narrow compositional ranges for these phases occur in the upper ash flow deposit.

Petrological significance

An important question raised by the large compositional range for the wholerock samples and vitric components, is to know if these compositions were produced by mixing, or by various degrees of differentiation of the same parental magma. The absence of features typical of magma mixing argues in favour of the second process. To address this question, and to constrain the petrologic and volcanologic significance of these pyroclastics, both mixing and crystal fractionation models were tested using wholerock and vitric compositions, and may be summarized as follows:

Wholerock : In a few cases, tests of mixing applied to the near-homogeneous samples clearly indicate that these samples may result from the homogenization of the heterogeneous ones. Nevertheless, such successful tests are rare and although the sum of the squares of residuals for major elements is <1 , high residuals for most trace element tests show that mixing is unlikely to have produced

the different compositions.

Glasses : The compositional gaps in many samples strongly suggest that the dominant process producing these diverse glass compositions is crystal fractionation, and that these compositions are representative of various layers in a zoned magma chamber. Mixing tests applied to the average glass compositions from Table 8 show that mixing cannot explain the data. On the other hand, crystal fractionation gives excellent results from basaltic andesite BA to andesite A3, through intermediate andesites A1 and A2.

Results for the Siwi ignimbrite are comparable. Mixing calculations give poor results, whereas fractionation models fit very well, in agreement with the modal mineralogy and the wholerock and glass compositions throughout the sequence.

Because the overall composition of most of the OTI and Siwi products is andesitic, the mechanics of the eruption must differ from that of a potentially self-explosive acidic magma (dacite or rhyolite), for which gas overpressure may be sufficient to cause eruption. Since our results preclude a mixing process between a deep mafic and a silicic magma, a hypothesis invoking triggering of the eruption by introduction of basalt into a differentiated magma chamber must be rejected. For each sequence, mineralogical data and fractionation models suggest that these compositions represent the magmatic signature of a voluminous layered chamber, the compositional gradient of which is the result of fractional crystallization. Thus, Figure 42 gives a quantitative representation of the zoned chamber just before the explosive events, and we conclude that these two sequences of phreatomagmatic products and ignimbrites resulted from rapid emptying of a large magma body with a strong compositional gradient imposed by crystal fractionation.

The intimate association between lower phreatomagmatic deposits and upper ignimbrite deposits suggests the following model of eruption.

- 1- Phreatomagmatic processes during the earlier stages of eruption.
- 2- Welded textures indicating hot emplacement in a subaerial environment for the main deposits.
- 3- Induration and glassy blocks in the upper pumice

flow deposits, that also indicate magma-water interaction, probably to a lesser extent than for the lower ash flows.

4- Simultaneous eruption of mafic and intermediate magmas at all stages of the OTI sequence and at the beginning of the Siwi sequence.

5- Homogenization of the composition during the outpouring of the Siwi ignimbrite.

In both cases, the successive eruptive dynamics, from phreatomagmatic to Plinian, emphasize the role of water in initiating the eruptions, without which the mafic and intermediate magmas would probably not have erupted.

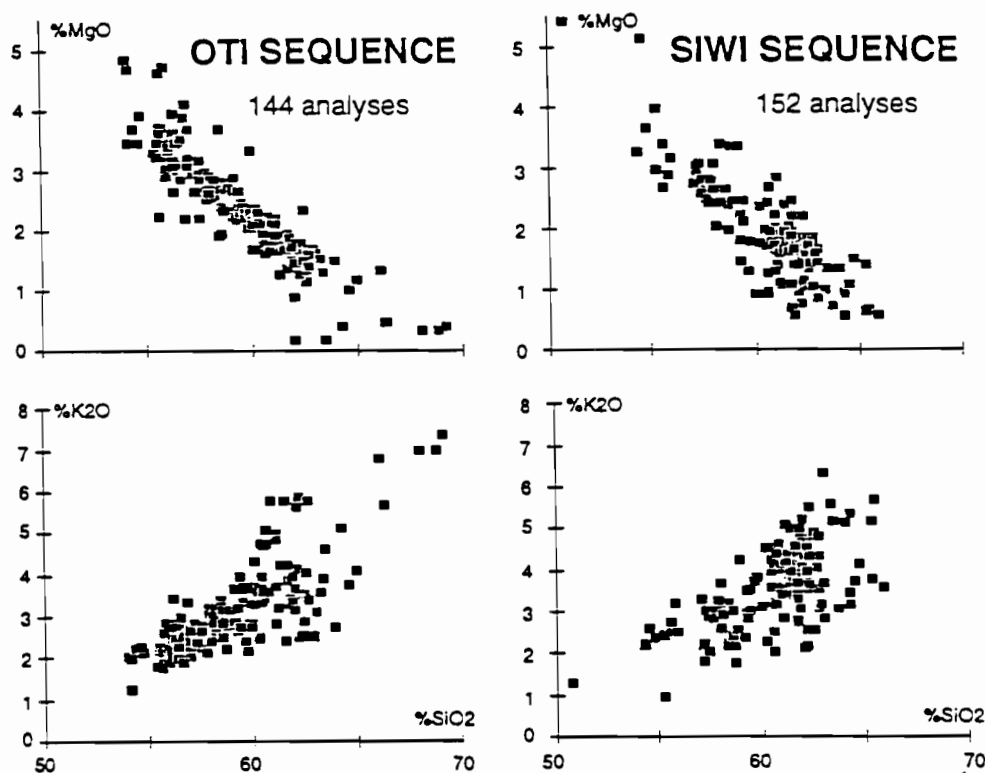


Figure 40: MgO and K₂O vs SiO₂ diagrams of analysed glasses from the OTI and Siwi sequences.

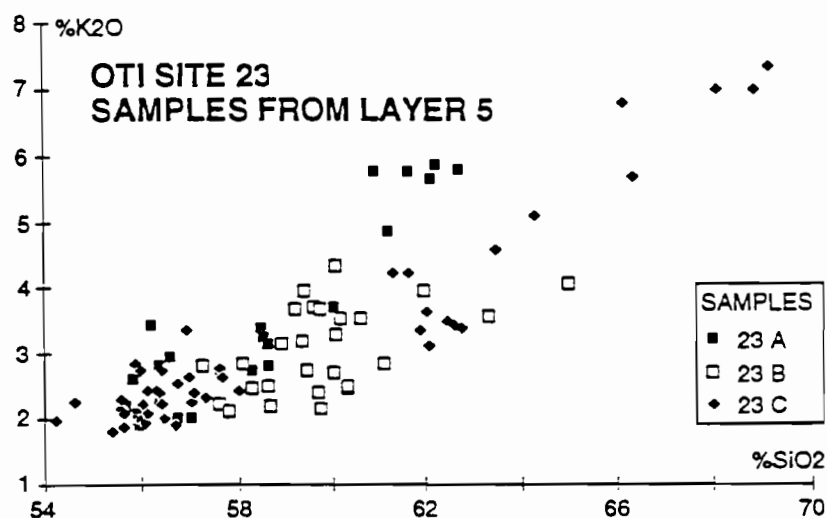


Figure 41: K₂O vs SiO₂ diagram for analysed glasses within 3 juvenile clasts from the OTI ignimbrite at site 23.

Table 7: Whole rock analyses of juvenile clasts from OTI and Siwi ignimbrites, Tanna.

Sample	SIWI IGNIMBRITE							OTI SEQUENCE													
	SITES 2-3-5					SITE 9	SITE 10	SITE 16		SITE 22				SITE 23							
	TA 2B	TA 3B	TA 5A	TA 5B	TA 5C	TA 9B	TA 10B	TA 15	TA 16	TA 22A	TA 22B	TA 22C	TA 22D	TA 23A	TA 23B	TA 23C	TA 23G				
SiO2	60,00	59,80	59,40	58,65	56,30	59,20	53,70	59,30	57,30	55,20	58,80	57,30	54,55	53,30	58,60	55,80	57,00				
TiO2	0,89	0,77	0,89	0,88	0,76	0,88	0,70	0,69	0,78	0,89	0,81	0,81	0,74	0,79	0,79	0,78	0,80				
Al2O3	15,33	15,57	15,12	14,93	17,56	15,19	17,45	16,68	16,18	16,03	15,98	16,41	16,33	16,68	15,87	15,92	15,69				
Fe2O3*	8,60	7,99	8,65	8,77	9,16	8,57	9,66	7,68	9,15	10,83	8,51	8,87	9,23	10,36	8,91	9,91	9,43				
MnO	0,20	0,19	0,19	0,19	0,23	0,19	0,17	0,18	0,16	0,20	0,17	0,17	0,17	0,21	0,19	0,19	0,18				
MgO	1,92	2,04	1,97	2,02	3,07	1,89	3,87	1,99	2,61	3,70	2,38	2,89	4,05	3,80	2,58	3,49	3,15				
CaO	4,50	4,80	4,56	4,71	6,65	4,41	8,94	5,68	6,00	7,77	5,66	6,48	7,51	7,82	5,84	7,43	6,52				
Na2O	4,10	4,30	4,36	4,20	4,35	4,25	3,31	4,13	4,08	3,32	4,05	3,81	3,18	3,24	4,13	3,65	3,72				
K2O	3,93	3,20	4,00	3,80	1,90	3,96	1,83	2,10	2,74	2,09	3,13	2,80	2,21	1,90	2,93	2,32	2,59				
P2O5	0,69	0,50	0,67	0,65	0,47	0,67	0,33	0,32	0,42	0,35	0,52	0,47	0,39	0,42	0,46	0,38	0,43				
LOI	-0,01	0,18	0,22	0,60	0,19	0,28	0,23	0,88	0,53	-0,17	-0,19	0,02	1,01	1,60	-0,16	0,39	-0,02				
	100,15	99,34	100,03	99,40	100,64	99,49	100,19	99,63	99,95	100,21	99,82	100,03	99,37	100,12	100,14	100,26	99,49				
Pb	59	47	58	56	31	59	26	30	38	32	48	42	34	29	44	46	39				
Ba	745	765	740	722	580	1445	432	248	1140	436	600	545	453	422	577	454	524				
Nb	1,60	1,50	2,00	1,50	1,35	1,90	1,00	1,35	1,05	0,90	1,50	1,50	0,90	1,00	1,40	0,50	1,60				
La	21,50	15,25	19,25	18,40	15,25	18,80	9,00	9,50	13,50	10,00	14,80	13,40	11,20	9,80	13,60	10,80	12,40				
Sr	445	476	440	443	547	438	647	468	537	495	536	583	580	567	530	567	548				
Nd	29,0	23,0	28,0	29,0	21,0	28,0	12,5	15,5	19,5	16,0	24,0	21,0	18,0	17,0	21,0	19,0	20,0				
Zr	144	122	151	141	101	148	65	78	99	89	118	105	88	81	110	84	99				
Eu	1,75	1,55	1,70	1,70	1,45	1,85	1,05	1,15	1,55	1,10	1,60	1,50	1,30	1,25	1,40	1,30	1,25				
Dy	5,9	5,1	5,8	5,7	4,4	5,8	3,5	4,6	4,3	4,2	4,9	4,3	3,9	3,7	4,6	4,3	4,5				
Y	35,0	30,5	36,0	35,0	27,0	36,0	20,0	28,0	26,8	29,0	31,0	29,0	24,0	23,0	29,0	25,0	27,0				
Er	3,6	3,1	3,7	3,7	3,0	3,6	2,2	2,7	2,6	3,0	3,0	2,7	2,5	2,1	3,2	2,0	2,4				
Yb	3,40	3,05	3,50	3,35	2,65	3,40	2,00	2,65	2,58	2,65	2,93	2,60	2,23	2,30	2,85	2,35	2,58				
V	175	157	177	179	238	168	281	130	238	330	198	237	246	320	222	296	258				
Cr	4,5	4,5	2,5	4,0	22,0	10,0	22,5	43,0	3,3	20,0	15,0	26,0	90,0	37,0	12,0	17,0	21,0				
Co	17,0	17,0	16,5	17,0	21,0	16,0	27,0	16,0	20,0	26,0	19,0	21,0	26,0	28,0	20,0	25,0	23,0				
Ni	6,5	6,0	3,5	6,0	16,0	7,0	20,0	22,0	9,0	26,0	11,0	16,0	47,0	24,0	10,0	18,0	17,0				
Sc	15,0	16,0	14,5	15,0	18,0	15,0	23,0	17,7	19,0	26,0	17,0	19,0	22,0	26,0	19,0	23,0	21,0				
Mg#	0,33	0,36	0,33	0,34	0,42	0,33	0,47	0,36	0,39	0,43	0,38	0,42	0,49	0,45	0,39	0,44	0,42				
Mg# on the basis of Fe2+/(Fe2+ + Fe3+)=0,9																					

Table 8: Averages of glass compositions from microprobe data, calculated following the peaks observed in Figure 42.

OTI IGNIMBRITES						AVERAGES OF GLASS COMPOSITIONS					
No an.	BA		A1		A2		A3		AA		D
	6		21		15		18		12		2
		sd		sd		sd		sd		sd	
SiO2	54,40	0,24	56,47	0,29	58,50	0,28	60,44	0,28	62,36	0,26	68,46
TiO2	1,04	0,18	0,81	0,16	0,80	0,12	0,78	0,05	0,73	0,19	0,88
Al2O3	15,09	1,12	16,03	0,80	16,16	0,83	15,74	0,33	15,93	1,74	13,14
FeO*	10,61	1,35	8,54	0,80	7,72	0,89	7,24	0,47	6,14	1,65	4,34
MnO	0,20	0,07	0,20	0,07	0,15	0,07	0,19	0,09	0,16	0,09	0,08
MgO	4,00	0,81	3,28	0,44	2,60	0,43	2,02	0,24	1,35	0,52	0,32
CaO	7,87	0,72	7,07	0,79	6,13	0,53	4,79	0,82	3,82	0,87	1,45
Na2O	3,73	0,15	3,85	0,22	4,01	0,38	4,14	0,40	4,44	0,99	2,79
K2O	1,96	0,39	2,46	0,44	2,85	0,35	3,87	0,87	4,25	1,15	7,01
Cr2O3	0,03	0,03	0,03	0,04	0,02	0,04	0,03	0,05	0,03	0,04	0,00
	98,92	1,04	98,74	0,51	98,94	0,82	99,24	0,57	99,21	0,52	98,23

SIWI IGNIMBRITES						AVERAGES OF GLASS COMPOSITIONS					
No an.	BA		A		AA		D				
	6		12		47		6				
		sd		sd		sd		sd			
SiO2	55,63	0,30	57,56	0,28	61,54	0,32	64,40	0,22	BA =		
TiO2	0,85	0,15	0,82	0,11	0,83	0,13	0,74	0,10	Basaltic Andesite		
Al2O3	15,46	0,47	15,73	1,01	15,74	0,91	16,11	0,87	A =		
FeO*	9,14	1,13	8,31	0,86	6,81	0,96	4,69	1,04	Andesite		
MnO	0,22	0,11	0,21	0,08	0,18	0,07	0,14	0,09	AA =		
MgO	3,17	0,46	2,74	0,20	1,72	0,41	1,04	0,34	Calc Andesit		
CaO	6,33	1,10	5,82	0,31	4,14	0,53	3,21	0,31	D =		
Na2O	3,69	0,46	4,21	0,51	4,07	0,88	4,14	0,97	Dacite		
K2O	2,38	0,76	2,75	0,48	3,99	0,58	4,14	0,91			
Cr2O3	0,06	0,05	0,03	0,03	0,01	0,02	0,07	0,08			
	96,93	1,18	98,19	1,50	99,04	1,07	98,68	1,15			

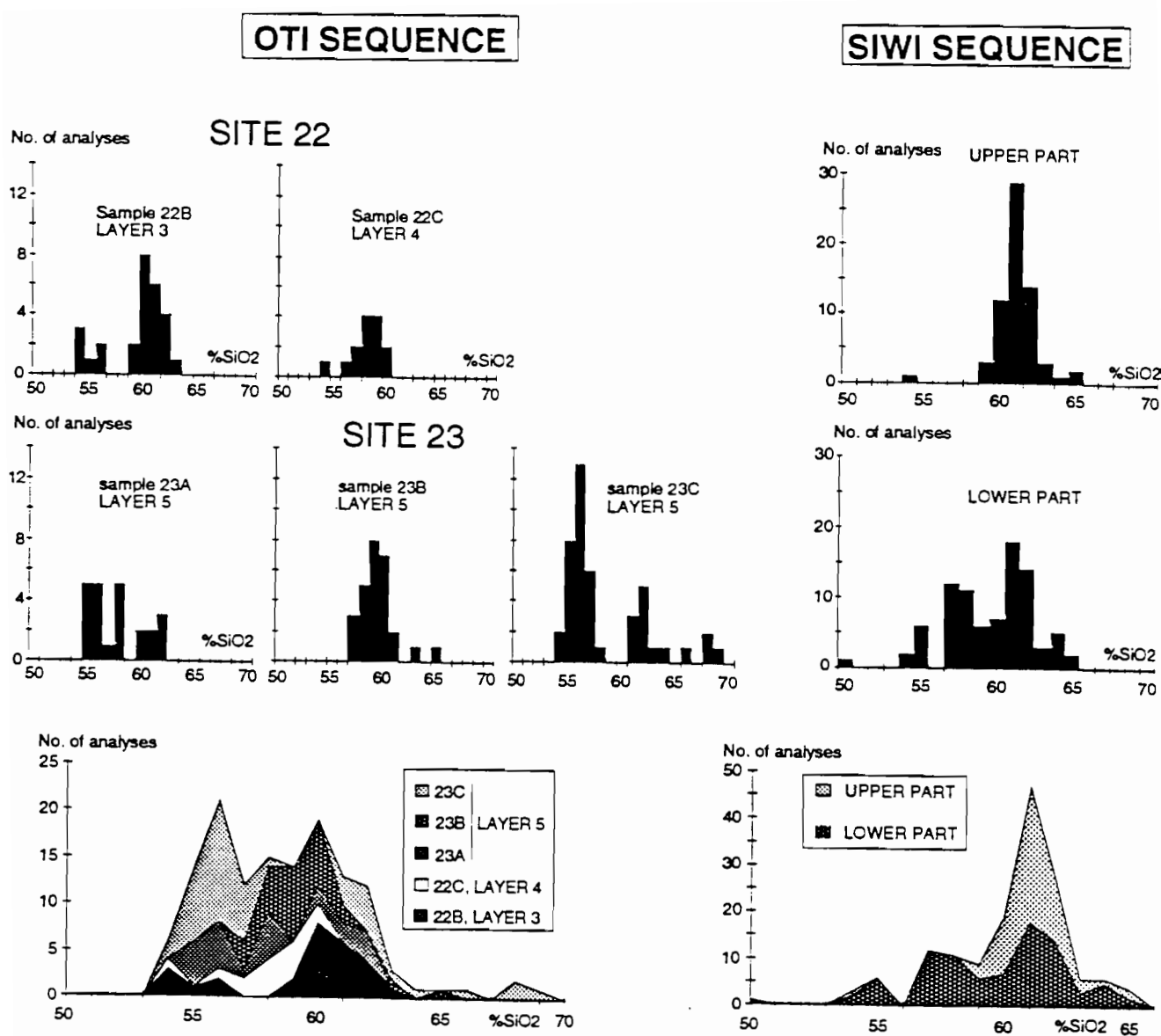


Figure 42: Frequency histogram for microprobe glass compositions in juvenile clasts from the OTI and Siwi ignimbrite sequences. Class 55 = 55.00 - 55.99% SiO₂.

YASUR VOLCANO

This section reports descriptions by IA Nairn, BJ Scott & WF Giggenbach (1988) *Yasur Volcano investigations, Vanuatu, Sept 1988*; Publ. New Zealand Geological Survey, Dept of Scientific and Industrial Res., plus observations made by Gérard Granger, (L'Association Volcanique Européenne) reported by the Global Volcanic Network Bulletin, by M. Lardy and D. Charley (ORSTOM), and our own observations.

STRUCTURE AND VOLCANIC PRODUCTS

Yasur is an active volcanic cone, 365 m high, with a base 3 km wide, located in the southeastern part of Tanna island. It is the youngest of several volcanic vents which occupy the Siwi area (including the Ombus cone). It lies at the western end of a 6 km long and 3 km wide WSW-ENE directed horst, the Yenkahe horst (Nairn et al. 1988). Uplift of the horst is demonstrated by the recent raised reef deposits up to 180 m above sea-level and by finely laminated marine volcanoclastic beds which have been tilted to 65-70° on the south shore of Sulfur Bay (Fig. 43). There are several other young (Holocene) vents on the western end of the Yenkahe horst and the present Yasur cone overlies remnants of an older cone, composed of strongly-altered coarse pyroclastics, which has been affected by somma ring collapse and erosion.

Lavas erupted prior to the formation of the present Yasur cone flowed from vents within the south somma across the Siwi ash plain.

A cliff section (8-m thick) on the north shore of Lake Siwi (2 km from Yasur) and a more distal section at Lownasunen, 4 km NNW of the cone, expose bedded medium to coarse grey-black ashes considered to have been associated with the recent activity of Yasur. Fine ash layers are of apparent phreatomagmatic origin. Charcoal from the base of an upper ash layer gave an age of 800 years B.P. and a coarser scoria bed which underlies these fine ash layers itself lies on a palcosol dated at 1400 yr B.P. (Nairn et al. 1988). Clasts from the scoria fall are of basaltic andesite composition.

VOLCANIC HISTORY AND PRESENT ACTIVITY.

Yasur was observed by Captain Cook in 1774, and its activity is regarded as having been fairly constant since that times (Fisher 1957). Yasur activity between 1959 and 1978 is summarized by Carney & Macfarlane (1979) with variations in the level of continuous eruptive activity, ash and bomb emission, crater depth and number of active vents. Particularly intense activity was reported in 1974, 1975 and in 1977. Nairn et al. (1988) described the crater morphology in 1986 and 1988. In 1986, the crater contained three distinct, vertical-walled and deep sub-craters broadly aligned in a N-S direction. The minimum depth of subcraters A and B has been determined to be about 230 m below the south crater rim, indicating retreat of the magmatic column. Five eruptive vents were distinguished in aerial photographs, although only 2 of these vents could be observed from the crater rim.

In 1991, observations showed active lava lakes and/or strombolian activity were visible at four vents (A, B, B', and B'': Fig. 44) within the large pit crater located at the center of the main crater. (Granger 1991; descriptions reported in GVN Bulletin). The fifth summit vent (C) northeast of the central pit crater, was inactive. Vent A, located within a deep nearly vertical cylindrical pit, was not visible from the rim but continuous lava fountaining ejected material several meters above the rim. Rare explosions (3 observed in two days) threw lava clots more than 50 m above the rim. In addition, Strombolian activity occurred at vent B, a small ash cone (several tens of degassing explosions per hour, occasionally with 7-8 explosions in rapid succession. The eruptive plume rose above the rim of the main crater. Located within a cinder cone at the NW base of the central pit crater, the 10 m-wide vent B was the most active. A small, continuously bubbling lava lake was periodically visible within the cone. Approximately one explosion was heard per second, accompanied by ejection of fluid lava. Several times per hour, a large explosion sent a fountain to 100 m high.

Vent B'' is located within a continuously incandescent crater. Loud explosions occurred at a rate of 3 to 4 per hour, dropping ballistics and large quantities of ash.

In October 1992, observations revealed low-level activity in zone A and substantial gas emission with faint explosions in zone B. Zone C showed significant activity with large explosions and lava ejections.

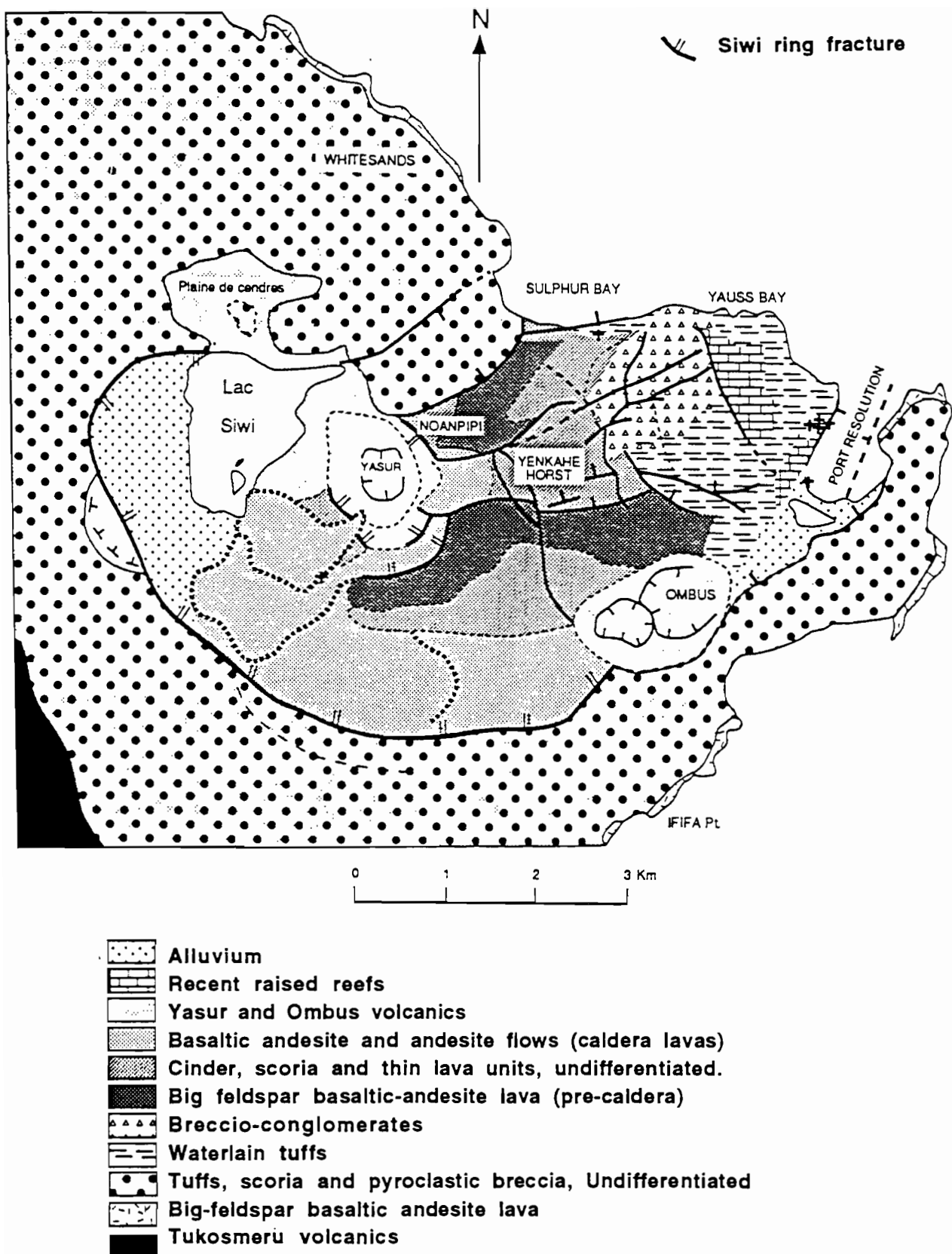


Figure 43: Geological sketchmap of the Siwi-Yenkahe area, southeast Tanna. Shows the Yenkahe horst and the Siwi ring fracture. (After Carney & Macfarlane 1979).

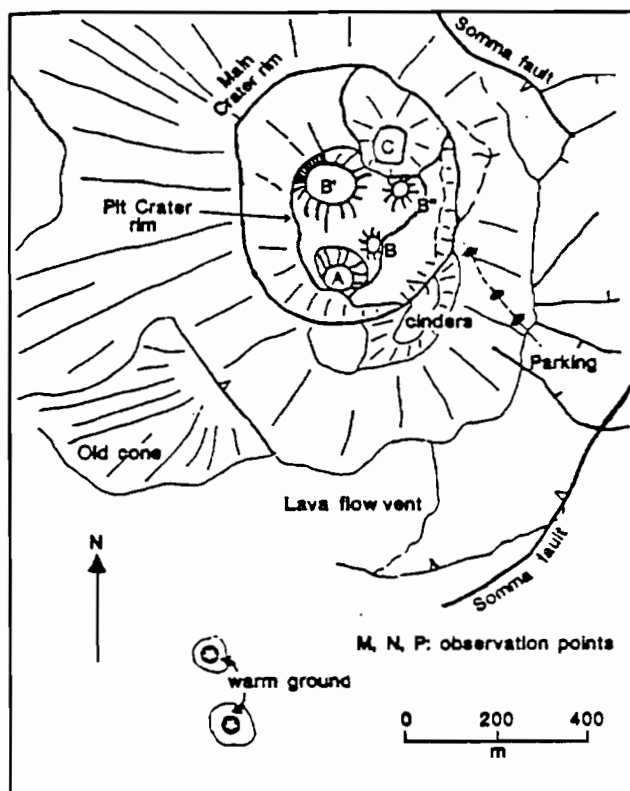


Figure 44: Sketch map of the summit of Yasur showing the eruptive vents in August 1991. (From GVN, vol 16-11).

REFERENCES

- Andrews JE, Packham GH et al. (1975) Site 286. In: Initial Repts DSDP 30: US Govt. Printers, Washington. 69-131
- Ash RP, Carney JN, Macfarlane A (1980) Geology of the northern Banks islands; New Hebrides Geol. Surv. Reports, 52 pp
- Aubert de la Rue E (1937) Le volcanisme aux Nouvelles Hébrides (Mélanesie). Bull. Volcanol. Napoli, 2: 79-142
- Aubert de la Rue E (1956) La géologie des Nouvelles-Hébrides. Volcanisme. J. Soc. des Océanistes XII: 89-93
- Auzende JM, Eissen JP, Lafoy Y, Gente P & Charlou JL (1988) Seafloor spreading in the North Fiji Basin (SW Pacific). Tectonophysics 146: 317-351
- Bacon CR (1983) Eruptive history of Mount Mazama and Crater Lake caldera, Cascade Range, USA. J. Volcanol. Geotherm. Res. 18: 57-115
- Ballhaus CG, Berry RF & Green DH (1991) High pressure experimental calibration of the olivine-orthopyroxene-spinel oxygen barometer: implications for the oxidation state of the upper mantle. Contrib. Mineral. Petrol. 107: 27-40
- Barsdell M (1988) Petrology and petrogenesis of clinopyroxene-rich tholeiitic lavas, Merelava Volcano, Vanuatu. J. Petrology 29: 927-964
- Barsdell M & Berry R (1990) The petrology and geochemistry of Western Epi. J. Petrology 31: 747-777
- Barsdell M & Smith IEM (1989) Petrology of recrystallized ultramafic xenoliths from Merelava volcano, Vanuatu. Contrib. Mineral. Petrol. 102: 230-241
- Barsdell M, Smith IEM & Sporli KB (1982) The origin of reversed geochemical zoning in the northern New Hebrides volcanic arc: Contrib. Mineral. Petrol. 81: 148-155.
- Bellon H, Marcelot G, Lefevre C & Maillat P (1984) Le volcanisme de l'île d'Erromango (Republique de Vanuatu): Calendrier de l'activité (données ^{40}K - ^{40}Ar): Académie des Sciences, Comptes Rendus 299 series 2: 257-262.
- Bice DC (1985) Quaternary volcanic stratigraphy of Managua, Nicaragua: correlation and source assignment for multiple overlapping plinian deposits. Geol. Soc. Am. Bull. 96: 553-566
- Blong RJ (1982) The time of darkness. Australian National University Press, Canberra, 257 pp
- Blot C (1976) Volcanisme et sismicité dans les arcs insulaires: prévision de ces phénomènes. Paris. ORSTOM Géophys. 13, 206 pp
- Briqueu L, Bougault H & Joron J-L (1984) Quantification of Nb, Ta, Ti and V anomalies in magmas associated with subduction zones: petrogenetic implications. Earth Planet. Sci. Lett. 68: 297-308
- Carney JN (1982) Efate geothermal project, phase 1. Geology and reconnaissance hydrology of the project area: Institute of Geological Sciences, Overseas Division Report no. 82/11
- Carney JN (1985) Geology and mineralisation of north and central Malekula: Vanuatu Dept. of Geology, Mines and Rural Water Supplies Regional Report: 57 pp
- Carney JN (1988) Geology of Maewo: Vanuatu Dept. of Geology, Mines and Rural Water Supplies Regional Report: 119 pp
- Carney JN & Macfarlane A (1977a) Volcano-tectonic events and pre-Pliocene crustal extension in the New Hebrides, in International Symposium on Geodynamics in South-West Pacific, Noumea, New Caledonia, 1976: Paris, Editions Technip
- Carney JN & Macfarlane A (1977b) Submarine geology, Epi-Tonga. In: Macfarlane A ed. Annual report of the Geological Survey for the year 1975, New Hebrides Geol. Surv., 11-13
- Carney JN & Macfarlane A (1978) Lower to middle Miocene sediments on Maewo, New Hebrides, and their relevance to the development of the Outer Melanesian Arc system. Austr. Soc. Exploration Geophys. Bull. 9: 123-130
- Carney JN & Macfarlane A (1979) Geology of Tanna, Anneytum, and Futuna. New Hebrides Geol. Surv. Report: 71 pp
- Carney JN & Macfarlane A (1980) A sedimentary basin in the central New Hebrides Arc. UN ESCAP, CCOP/SOPAC Technical Bulletin 3: 109-120
- Carney JN, Macfarlane A & Mallick DIJ (1985) The Vanuatu island arc: an outline of the stratigraphy, structure and petrology. In: Nairn AEM, Stehli FG and Uyeda S eds. The ocean basins and margins, the Pacific. New York, Plenum Press, 7: 683-718
- Cas RAF, Landis CA & Fordyce RE (1989) A monogenetic, Surtla-type, Surtseyan volcano from the Eocene-Oligocene Waiareka-Deborah volcanics, Otago, New Zealand: a model. Bull. Volcanol. 51: 281-298
- Cas RAF & Wright JV (1987) Volcanic successions: modern and ancient. A geological approach to processes, products and successions. Allen & Unwin, London, 528 pp

- Chase TE & Seekins BA (1988) Submarine topography of the Vanuatu and southeastern Solomon Islands regions. In Greene HG and Wong FL eds. *Geology and offshore resources of Pacific island arcs-Vanuatu region*. Circum-Pacific Council for Energy and Mineral Resources Earth Science Series, 8: 35-36
- Coleman PJ (1969) Derived Eocene larger foraminifera on Maewo, eastern New Hebrides, and their southwest Pacific implications: New Hebrides. *New Hebrides Geol. Surv. Annual Report for 1967*: 36-37
- Colley H & Ash RP (1971) The geology of Erromango. *New Hebrides Geol. Surv. Report*: 112 pp
- Collot JY, Daniel J & Burne RV (1985) Recent tectonics associated with the subduction/collision of the D'Entrecasteaux zone in the central New Hebrides: *Tectonophysics* 112: 325-356
- Collot J-Y, Lallemand S, Pelletier B, J-P Eissen, Glaçon G, Fisher MA, Greene HG, Boulin J, Daniel J and Monzier M (1992) Geology of the d'Entrecasteaux New Hebrides arc collision zone: results from a deep submersible survey. *Tectonophysics* 212: 213-241
- Coulon C, Maillet P & Maury R (1979) Contribution à l'étude du volcanisme de l'arc des Nouvelles-Hébrides: données pétrologiques sur les laves de l'île d'Efate. *Soc. Géologique de France, Bull.* 7: 619-629
- Crawford AJ, Falloon TJ & Eggins S (1987) The origin of island arc high-alumina basalts. *Contrib. Mineral. Petrol.* 97: 417-430
- Crawford AJ, Greene HG & Exon NF (1988) Geology, petrology and geochemistry of submarine volcanoes around Epi island, New Hebrides island arc. In Greene HG and Wong FL eds. *Geology and offshore resources of Pacific island arcs - Vanuatu region*, Circum-Pacific Council for Energy and Mineral Resources Earth Science Series, 8, Houston, Texas, 301-32
- Daniel J (1978) Morphology and structure of the southern part of the New Hebrides island arc system. *J. Phys. Earth* 26: S181-S190
- Daniel J, Collot J-Y, Monzier M, Pelletier B, Butscher J, Deplus C, Dubois J, Gerard M, Maillet P, Monjaret MC, Recy J, Renard V, Rigolot P & Temakon J (1986) Subductions et collisions le long de l'arc des Nouvelles-Hébrides (Vanuatu): résultats préliminaires de la campagne SEAPSO (Leg 1). *C. R. Acad. Sci. Paris* 303, II: 805-810.
- Druitt TH & Francaviglia V (1992) Caldera formation on Santorini and the physiography of the islands in the late Bronze Age. *Bull. Volcanol.* 54: 484-493
- Dubois J, Dugas F, Lapouille A & Louat R (1978) Troughs at the rear of the New Hebrides arc; possible mechanisms of formation. *Can. J. Earth Sci.* 15: 351-360
- Dugas F, Carney JN, Cassagnol C, Jezek PA & Monzier M (1977) Dredged rocks along a cross section in the Southern New Hebrides Island Arc and their bearing on the age of the arc. In *Geodynamics in South-West Pacific*. Technip Ed. Paris: 105-116
- Dupuy C, Dostal J, Marcelot G, Bougault H, Joron JL & Treuil M (1982) Geochemistry of basalts from central and southern New Hebrides arc: implications for their source rock composition. *Earth Planet. Sci. Lett.* 60: 207-225
- Eggins SM (1993) Origin and differentiation of picritic arc magmas, Ambae (Aoba), Vanuatu. *Contrib. Mineral. Petrol.* 114: 79-100
- Eissen J-Ph, Blot C & Louat R (1991) Chronologie de l'activité volcanique de l'arc insulaire des Nouvelles Hébrides de 1595 à 1991. *Rapports Scient. et Techn., ORSTOM, Géol.-géophys.*: 69 pp
- Espirat J-J (1964) Etude géologique de l'île Tongariki et observations sur la géologie des îles Shepherd, Rapport du Bureau des Recherches Géologiques et Minières, Nouméa: 41 pp
- Espirat J-J, Guiart J, Lagrange M-S. & Renaud M (1973) Système des titres, électifs ou héréditaires, dans les Nouvelles-Hébrides centrales d'Efate aux îles Shepherd, Museum National d'Histoire Naturelle, Mémoires de l'Institut d'Ethnologie 10: Paris, 491 pp
- Falvey DA (1978) Analysis of palaeomagnetic data from the New Hebrides. *Austr. Soc. Exploration Geophys. Bull.* 9: 117-133
- Falvey DA & Greene HG (1988) Origin and evolution of the sedimentary basins of the New Hebrides Arc. In: Greene HG and Wong FL eds. *Geology and offshore resources of Pacific island arcs - Vanuatu region*, Circum-Pacific Council for Energy and Mineral Resources Earth Science Series, 8, Houston, Texas: 413-442
- Fisher NH (1957) Catalogue of the active volcanoes of the world including solfataras fields, Part V, Melanesia. *Int. Volcanol. Ass., Naples*, 106 pp
- Frederick GC (1893) Geological notes on certain islands in the New Hebrides. *Q. J. Geol. Soc.* 49: 227-232
- Garanger J (1966) Recherches archéologiques aux Nouvelles-Hébrides, *L'Homme* 6: 59-81
- Garanger J (1972) Archéologie des Nouvelles-Hébrides, ORSTOM, Publications de la Société des Océanistes, n°30, Musée de l'Homme, Paris, 405 pp
- Gèze B (1966) Sur l'âge des derniers cataclysmes volcanotectoniques dans la région centrale de l'arc des Nouvelles-Hébrides. *Bull. Soc. Géol. France* (7), VIII: 329-333
- Global Volcanism Network (1991) Yasur volcano (Vanuatu) *GVN* 16, 11: 7
- Gorton MP (1974) The geochemistry and geochronology of the New Hebrides. Australian National University, Canberra, Ph.D dissertation: 300 pp
- Gorton MP (1977) The geochemistry and origin of Quaternary volcanism in the New Hebrides. *Geochim. Cosmochim. Acta* 41: 1257-1270
- Greenbaum D, Mallick DIJ & Radford N (1975) Geology of the Torres Islands. *New Hebrides Geol. Surv. Report*: 44 pp
- Greene HG, Macfarlane A, Johnson DP & Crawford AJ (1988) Structure and tectonics of the central New Hebrides arc. In: Greene HG and Wong FL eds. *Geology and offshore resources of Pacific island arcs - Vanuatu region*, Circum-Pacific Council for Energy and Mineral Resources Earth Science Series, 8, Houston, Texas: 377-412
- Hamburger MW & Isacks BL (1987) Deep earthquakes in the southwest Pacific: a tectonic interpretation. *J. Geophys. Res.* 92: 13841-13854
- Hébert B (1966) Contribution à l'étude archéologique de l'île d'Efate et des îles avoisinantes. *Etudes Mélanésiennes* 18-20, déc. 1963-décembre 1965, Nouméa: 71-98
- Isacks BL, Cardwell RK, Chatelain JL, Barazangi M, Marthelot J-M, Chinn D & Louat R (1981) Seismicity and tectonics of the central New Hebrides island arc. In: Simpson DW and Richards PG, eds., *Earthquake prediction; a international review: American Geophysical Union, Maurice Ewing Series* 4: 93-116.
- Jezek PA, Bryan WB, Haggerty SE & Johnson HP (1977) Petrography, petrology, and tectonic implications of Miue Island, northern Fiji Plateau. *Marine Geol.* 24: 133-148

- Jouanne C, Taylor FW, Bloom AL & Bernat M (1980). Late Quaternary uplift history from emerged reef terraces on Santo and Malekula Islands, central New Hebrides island arc UN ESCAP, CCOP/SOPAC Tech. Bull. 3: 91-108
- Kelemen P, Dick HJB & Quick JE (1992) Formation of harzburgite by pervasive melt/rock reaction in the upper mantle. *Nature* 358: 635-641
- Kress VC & Carmichael ISE (1991) Compressibility of silicate liquids containing Fe₂O₃ and the effect of compositions, temperature, oxygen fugacity and pressure on their redox states. *Contrib. Mineral. Petrol.* 108: 82-92
- Kroenke LW (1984) Vanuatu and the Eastern Outer Solomons Islands—formation of the New Hebrides and Vitiaz Arcs and development of the North Fiji Basin. In: Cenozoic tectonic development of the southwest Pacific: UN ESCAP CCOP/SOPAC Tech. Bulletin 6: 63-75
- Lafay Y, Auzende J-M, Ruellan E, Huchon P & Honza E (1990) The 16°40' triple junction in the North Fiji Basin (SW Pacific). *Marine Geophys. Res.* 12: 285-296.
- Lemaire B (1965) Etude géologique de l'île Erromango (Nouvelle Hébrides). Métallogénie locale du manganèse: Mem. Bureau Recherche Geol. et Min. 38: 183 pp
- Louat R & Pelletier B (1989) Seismotectonics and present day relative plate motions in the New Hebrides - North Fiji Basin region. *Tectonophysics* 167: 41-55
- Louat R, Hamburger MW & Monzier M (1988) Shallow and intermediate-depth seismicity in the New Hebrides arc: constraints on the subduction process. In: Greene HG and Wong FL eds. *Geology and offshore resources of Pacific island arcs - Vanuatu region*, Circum-Pacific Council for Energy and Mineral Resources Earth Science Series, 8, Houston, Texas: 329-356
- McCall GJH, LeMaitre RW, Malahoff A, Robinson GP and Stephenson PJ (1970) The geology and geophysics of the Ambrym caldera, New Hebrides. *Bull. Volcanol.* 34: 681-696
- Macfarlane A (1976) Volcanic activity during 1974. *New Hebrides Geol. Surv. Annual Rept. for 1974*: 11-13
- Macfarlane A, Carney JN, Crawford AJ & Greene HG (1988) Vanuatu - a review of onshore geology. In: Greene HG and Wong FL eds., *Geology and offshore resources of Pacific island arcs - Vanuatu region*, Circum-Pacific Council for Energy and Mineral Resources Earth Science Series, 8, Houston, Texas: 45-91
- Machida H & Arai F (1983) Extensive ash falls in and around the Sea of Japan from large, late Quaternary eruptions. *J. Volcanol. Geotherm. Res.* 18: 151-164
- MacPhie J, Walker GPL & Christiansen RL (1990) Phreatomagmatic and phreatic fall and surge deposits from explosions at Kilauea volcano, Hawaii, 1790 AD: Keanakakoi Ash Member. *Bull. Volcanol.* 52: 334-354
- Maillet P, Monzier M & Lefevre C (1986) Petrology of Matthew and Hunter volcanoes, south New Hebrides island Arc (SW Pacific). *J. Volcanol. Geotherm. Res.* 30, 1-27
- Maillet P, Monzier M, Eissen J-P & Louat R (1989) Geodynamics of an arc-ridge junction: the case of the New Hebrides arc - North Fiji Basin. *Tectonophysics* 165: 251-268
- Malahoff A, Feden RH & Fleming HS (1982) Magnetic anomalies and tectonic fabric of marginal basins north of New Zealand. *J. Geophys. Res.* 87: 4109-4125
- Mallick DIJ (1973) Some petrological and structural variations in the New Hebrides. In: Coleman PJ ed., *The western Pacific: island arcs, marginal seas, geochemistry*: Univ Western Australia Press, Perth, 193 - 211
- Mallick DIJ & Ash RP (1975) Geology of the southern Banks islands. *New Hebrides Geol. Surv. Report*, 33 pp
- Mallick DIJ & Greenbaum D (1975) The Navaka fossiliferous sands and the Kere shell bed. *New Hebrides Geol. Surv. Annual Report for 1973*: 8-12
- Mallick DIJ & Greenbaum D (1977) Geology of southern Santo. *New Hebrides Geol. Surv. Report*: 84 pp
- Mallick DIJ & Neef G (1974) Geology of Pentecost. *New Hebrides Geol. Surv. Report*: 103 pp
- Marcelot G, Dupuy C, Girod M & Maury RC (1983a) Petrology of Futuna Island lavas: an example of calc-alkaline magmatism associated with initial stages of back-arc spreading. *Chem. Geol.* 38: 3-37
- Marcelot G, Maury RC & Lefevre C (1983b) Mineralogy of Erromango lavas (New Hebrides): evidence of an early stage of fractionation in arc basalts. *Lithos* 16: 135-161
- Marthelot JM & Isacks BL (1985) Space-time distribution of shallow and intermediate depth events in the Vanuatu (New Hebrides) island arc from 1961-1981. *J. Geophys. Res.* 90: 8641-8650
- Marthelot JM, Chatelain BL, Isacks BL, Cardwell RK & Coudert E (1985) Seismicity and attenuation in the central Vanuatu (New Hebrides) islands: a new interpretation of the effect of the D'Entrecasteaux fracture zone. *J. Geophys. Res.* 90: 8641-8650
- Mawson D (1905) The geology of the New Hebrides. *Linnean Soc. New South Wales, Proc.* 30: 400-485
- Mellors RA & Sparks RSJ (1991) Spatter-rich pyroclastic flow deposits on Santorini, Greece. *Bull. Volc.* 53: 327-342
- Mitchell AHG (1966) Geology of south Malekula. *New Hebrides Geol. Surv. Report*: 41 pp
- Mitchell AHG (1971) Geology of northern Malekula. *New Hebrides Geol. Surv. Report*: 56 pp
- Mitchell AHG & Warden AJ (1971) Geological evolution of the New Hebrides island arc. *J. Geol. Soc. London* 127: 501-529
- Monjaret MC, Bellon H and Maillet P (1991) Magmatism of the troughs behind the New Hebrides island arc (RV Jean Charcot SEAPSO Cruise 2): K-Ar geochronology and petrology. *J. Volc. Geotherm. Res.* 46: 265-280
- Monzier M, Collot J-Y & Daniel J (1984) Carte bathymétrique des parties centrale et méridionale de l'arc insulaire des Nouvelles Hébrides: Paris, ORSTOM.
- Monzier M, Maillet P & Dupont J (1991) Carte bathymétrique des parties méridionale de l'arc insulaire des Nouvelles Hébrides et du Bassin Nord Fidjien: Paris, ORSTOM.
- Monzier M., Danyushevsky L, Crawford AJ, Bellon H & Cotten C (1993) High-Mg andesites from the southern termination of the New Hebrides island arc. *J. Volc. Geotherm. Res.* (In press)
- Monzier M, Robin C & Eissen J-P (1993) Kuwae (mid-fifteenth century): the forgotten caldera. Submitted to *J. Volc. Geotherm. Res.*
- Monzier M, Danyushevsky LV, Crawford AJ, Bellon H & Cotten J (1993) High-Mg andesites from the southern termination of the New Hebrides island arc (SW Pacific). *J. Volc. Geotherm. Res.* (In press)
- Musgrave RJ (1992) Magnitude and timing of New Hebrides arc rotation: palaeomagnetic evidence from Nendo, Solomon Islands. *J. Geophys. Res.*
- Nairn A, Scott BJ & Giggensbach WF (1988) Yasur volcano investigations, Vanuatu, Sept. 1988. *New Zealand Geol. Surv. Report G134*: 74 pp
- Neef G (1980) Mode of formation of an earliest Pliocene-latest Miocene basaltic pillow-lava pile present at Pentecost Island, New Hebrides, and its bearing on the formation of basaltic rudite. *Bull. Volcanol.* 43: 505-510

- Neef G (1982) Plate tectonic significance of late Oligocene/early Miocene deep sea sedimentation at Maewo, Vanuatu (New Hebrides). In: Puckham, G.H., ed., *Evolution of the India-Pacific plate boundaries*. Tectonophysics 87: 177-183
- Neef G, Plimer IR & Bottrill RS (1985) Submarine-fan deposited sandstone and rudite in a mid-Cenozoic interarc basin in Maewo, Vanuatu (New Hebrides). *Sedimentology* 32: 519-542
- Obellianne JM (1961) Contribution a la connaissance geologique de l'archipel des Nouvelles-Hebrides (iles Vate, Pentecote, Maewo, Santo). *Sci. de la Terre* 6: 139-368
- Pascal C, Isacks BL, Barazangi M & Dubois J (1978) Relocations of earthquakes, and seismotectonics of the New Hebrides island arc. *J. Geophys. Res.* 83: 4957-4973
- Pazdur M-F & Michczynska D-J (1989) Improvement of the procedure for probabilistic calibration of radiocarbon dates. *Radiocarbon* 31: 824-832
- Picard C, Monzier M, Eissen JP, Robin C. (in press) Concomitant evolution of tectonic environment and magma geochemistry, Ambrym volcano (Vanuatu - New Hebrides arc). In: JL Smellie ed. *J Geol Soc London, Spec. Issue "Volcanism associated with extension at consuming plate margins"*
- Pollitz FF (1986) Pliocene changes in Pacific plate motion. *Nature* 320: 738-741
- Prevot R, Roecker SW, Isacks BL & Chatelain JL (1991) Mapping of low P wave velocity structures in the subducting plate of the central New Hebrides, SW Pacific. *J. Geophys. Res.* 96: 19825-19842
- Priam R (1962) Mission d'études volcanologiques. *Cond. des Nouvelles Hébrides. Serv des Mines Port Vila. Rapp. Dept* 798-M
- Recy J, Pelletier B, Charvis P, Gerard M, Monjaret MC & Maillet P (1990) Structure, age et origine des fosses arriere-arc des Nouvelles-Hebrides (Sud-Ouest Pacifique). *Oceanologica Acta Spec. Vol.* 10: 165-182
- Robin C, Eissen J-P & Monzier M (1993) Giant tuff cone and 12km wide associated caldera at Ambrym volcano (Vanuatu, New Hebrides Arc). *J. Volc. Geotherm. Res.* 55: 225-238
- Robin C, Eissen J-P & Monzier M (In press) Ignimbrites of basaltic andesite and andesite compositions from Tanna, New Hebrides arc. *Bull Volcanol.*
- Robin C, Monzier M & Eissen JP (1993) Formation of the 550 year-old Kuwae caldera (Vanuatu) by an initial hydroclastic and subsequent ignimbritic eruption. Submitted to *Bull. Volcanol.*
- Robinson GP (1969) The geology of north Santo: New Hebrides Geol. Surv. Report: 77 pp
- Roeder PL & Emslie RF (1970) Olivine-liquid equilibrium. *Contrib. Mineral. Petrol.* 29: 275-289
- Rosi M, Sbrana A & Principe C (1983) The Phlegraean fields: structural evolution, volcanic history, and eruptive mechanisms. *J. Volcanol. Geotherm. Res.* 17: 273-288
- Self S, Rampino MR, Newton MS & Wolff JA (1984) Volcanological study of the great Tambora eruption of 1815. *Geology* 12: 659-663
- Sigurdsson H & Carey S (1989) Plinian and co-ignimbrite tephra fall from the 1815 eruption of Tambora volcano. *Bull. Volcanol.* 51: 243-270
- Sigurdsson IA, Kamenetsky VS, Crawford AJ, Eggins SM & Zlobin SK (1993) Primitive island arc and oceanic lavas from the Hunter Ridge-Hunter Fracture Zone: evidence from glass, olivine and spinel compositions. *Mineral. Petrol.* 47: 149-169
- Simkin T, Siebert L, McClelland L, Bridge D, Newhall C & Latter JH (1981) *Volcanoes of the world*. Smithsonian Institution, Hutchinson Ross, Pennsylvania, 233 pp
- Swanson DA & Christiansen RL (1973) Tragic base surge in 1790 at Kilauea volcano. *Geology* 1: 83-86
- Taylor FW, Jouannic C & Bloom AL (1985) Quaternary uplift of the Torres Islands, northern New Hebrides frontal arc; comparison with Santo and Malekula Islands, central New Hebrides frontal arc. *J. Geol.* 93: 419-438
- Walker GPL (1980) The Taupo pumice: Products of the most powerful known (ultraplinian) eruption? *J. Volcanol. Geotherm. Res.* 8: 642-646
- Warden AJ (1963) Investigation of eruption at Mt Gharat, Gaua island. *New Hebrides Geol. Surv. Report*: 4 pp
- Warden AJ (1967) The geology of the Central Islands, New Hebrides Geol. Surv. Report 5: 108 pp
- Warden AJ (1970) Evolution of Aoba caldera volcano, New Hebrides. *Bull Volcanol* 34: 107-140
- Wheller G & Varne R (1986) Genesis of dacite magmatism at Batur volcano, Bali - implications for the origin of stratovolcano calderas. *J. Volc. Geotherm. Res.* 28: 363-378
- Williams CE & Curtis R (1964) The eruption of Lopevi Volcano, New Hebrides, July 1960. *Bull. Volcanol.* 27: 423-433
- Williams CEF & Warden AJ (1964) Progress report of the Geological Survey for 1959-1962. *New Hebrides Geol. Surv. Report*: 75pp.
- Williams SN (1983) *Geology and eruptive mechanisms of Masaya Caldera complex, Nicaragua*. PhD thesis, Hannover, New Hampshire, Darmouth College: 169 pp
- Wright JV & Walker GPL (1981) Eruption, transport and deposition of ignimbrite: a case study from Mexico. *J. Volcanol. Geotherm. Res.* 9: 111-131.

Appendix A - Vanuatu basalt geochemistry

Volcano Sample	Merig Mig6	Merig Mern7	Merig Mern11	Van'Lava VL6	Van'Lava Vmac006	Merclava 31541	Merclava 31547	Merclava BC13	Gaua G20	Gaua G21	Gaua G24	Gaua G22	Aoba 576	Aoba 505	Aoba 516	Aoba 538	Aoba 491
SiO ₂	54.42	49.15	49.79	47.95	48.90	50.82	52.03	50.20	46.50	49.33	48.22	46.44	47.84	48.29	49.66	48.81	45.31
TiO ₂	1.00	0.90	0.93	0.65	0.80	0.64	0.63	0.46	0.74	0.96	0.91	0.81	0.72	0.68	0.87	0.88	0.46
Al ₂ O ₃	16.82	13.44	13.33	19.47	16.07	13.67	15.70	10.30	11.36	15.21	14.74	11.69	13.19	12.99	16.01	16.21	8.64
Fe ₂ O ₃	2.76	10.29	10.48	4.20	12.04	2.73	4.35	2.43	5.52	6.04	5.65	6.06	4.34	4.41	4.50	4.56	4.49
FeO	5.40			5.52		6.79	5.46	5.90	5.48	6.08	6.28	5.99	7.81	7.94	8.11	8.20	8.08
MnO	0.28	0.16	0.18	0.18	0.20	0.21	0.18	0.17	0.26	0.30	0.29	0.30	0.21	0.20	0.21	0.20	0.21
MgO	5.26	11.04	11.33	5.79	6.30	9.74	7.36	13.71	14.81	6.33	6.22	11.00	10.83	10.21	5.80	5.49	22.09
CaO	8.62	10.30	10.40	11.95	11.13	12.90	11.23	13.69	11.78	10.66	11.59	13.01	11.38	11.95	10.47	10.62	8.33
Na ₂ O	2.82	2.38	2.31	2.75	2.54	1.89	2.07	1.60	2.04	2.90	2.94	2.22	2.29	2.11	2.96	2.93	1.40
K ₂ O	1.03	0.60	0.54	0.37	0.89	0.38	0.43	0.38	0.60	0.79	1.48	0.78	1.15	1.04	1.15	1.79	0.79
P ₂ O ₅	0.27	0.17	0.16	0.08	0.17	0.12	0.08	0.06	0.15	0.22	0.35	0.23	0.23	0.20	0.25	0.32	0.21
L.O.I.	1.02	1.18	0.58	0.74	0.22	0.20	0.16	0.52	1.09	1.19	1.43	1.33					
Cs	0.32					0.15	0.11		0.05	0.1	0.44	0.1					
Pb	6.09					3.27	2.9		2.05	2.02	6.96	5.25	4.6	1.8	4.4	7.6	1.45
Rb	25	6.5	5.6	2.2	20	5.4	6.7	6	8.9	12	28		18.7	17.2	20.2	28.2	13.9
Ba	353	217	194		247	123	162	181	193	237	516	310	360	310	430	510	230
Sr	524	355	332	584	547	240	255	218	502	529	998	687	677	601	538	935	422
La	13.55	6.53	6.56	3.18	9.38	1.86	2.34	2.42	8.33	9.83	17.36	11.21	12.76	10.46	8.85	15.51	8.22
Ce	31.69	15.60	16.30	7.25	21.20	4.92	5.55	4.87	17.00	22.96	39.88	24.28	28.40	24.10	20.70	36.40	16.90
Pr	4.00	2.10	2.35	1.10	2.77	0.81	0.88	0.67	2.45	2.89	4.80	3.46	3.38	2.99	2.75	4.75	2.20
Nd	16.91	10.50	10.80	5.75	13.50	4.36	4.69	3.76	11.30	14.01	21.04	16.95	15.38	13.38	12.82	21.53	10.03
Sm	3.86	2.81	2.71	1.68	2.74	1.48	1.59	1.19	2.37	3.81	4.83	4.06	3.17	2.84	3.16	4.73	2.20
Eu	1.21	1.20	0.90	0.84	0.97	0.51	0.59	0.44	0.79	1.25	1.40	1.27	1.01	0.88	1.04	1.38	0.69
Gd	3.77	3.26	3.39	1.94	3.02	1.80	1.97	1.45	2.42	3.19	3.75	3.63	3.15	2.52	3.49	4.07	2.13
Tb	0.61					0.33	0.36			0.51	0.50	0.53	0.49	0.42	0.60	0.65	0.33
Dy	3.86	3.67	3.99	2.30	3.50	2.08	2.38	1.81	2.45	3.16	3.02	3.16	2.94	2.51	3.63	3.60	1.97
Ho	0.86		2.00			0.48	0.51			0.71	0.63	0.55	0.59	0.56	0.77	0.72	0.39
Er	2.50	2.64	2.74	1.33	2.21	1.41	1.52	1.16	1.57	2.11	1.64	1.36	1.70	1.48	2.23	2.04	1.09
Yb	2.55	2.21	2.37	1.25		1.39	1.70	1.12	1.15	2.19	1.55	1.45	1.68	1.38	2.18	1.96	1.06
Lu																	
Y	25.4	23.0	24.0		19.0	17.8		12.5	13.1	27.4	19.0	13.3	17.9	17.4	26.5	21.3	12.1
Th	1.48					0.17	0.22		0.60	0.86	1.91	1.21	1.73	1.16	1.18	2.51	1.07
U	0.55					0.10	0.16		0.26	0.34	0.68	0.45	0.58	0.36	0.41	0.80	0.30
Zr	108	63.7	66	36	51	47	49	18.3	48	61	63	53	50	43	63	67	33
Hf	2.3					0.87	0.99		1.18	1.74	1.78	1.6	1.79	1.37	1.73	2.22	1.04
Nb	4.84	2.4	2.7			0.61			0.94	1.11	1.9	1.02	1.16	1.35	2.06	1.9	0.84
Sc		34	34		44			52					36	39	35	27	29
V	244	245	306	363	384			262	328	390	381	407	380	350	460	450	230
Cr	101	524	666	23	112	372	179	695	854	41	53	398	590	490	91	29	1650
Ni	37	183	214	20	34	75	47	137	265	29	19	120	165	150	32	35	480

Data sources: Barsdell et al. (1982); Barsdell (1988); Barsdell and Berry (1990); Crawford et al. (1988); Dupuy et al. (1982); Eggins (1993); Gorton (1977); Marcelot et al. (1983);

Appendix A cont'd - Vanuatu basalt geochemistry

Volcano Sample	Aoba 68622	Aoba 68588	Aoba 68638	Aoba 68611	Aoba 68562	Aoba 68567	Aoba-ITi 68574	Aoba-ITi 68569	Aoba-ITi 68578	Aoba-ITi 548	Ambrym 1567	Ambrym 6	Ambrym 26	Ambrym 48	Ambrym 58	Ambrym 61	Ambrym 74
SiO ₂	46.90	49.37	48.79	47.81	48.96	47.18	48.75	47.79	47.74	48.83	48.92	50.82	51.45	50.71	48.58	49.21	48.08
TiO ₂	0.54	0.85	0.65	0.70	0.72	0.58	1.24	1.22	1.07	1.07	0.63	0.88	0.70	0.80	0.72	0.76	0.77
Al ₂ O ₃	9.35	16.46	13.21	12.59	13.90	10.87	16.06	14.27	13.84	16.41	13.40	13.87	14.71	17.51	14.36	14.37	15.12
Fe ₂ O ₃	11.61	11.58	11.06	11.29	11.13	11.14	13.16	11.65	12.10	4.37	1.71	11.50	10.68	9.96	10.22	10.36	11.08
FeO										7.87	8.51						
MnO	0.20	0.20	0.18	0.19	0.20	0.19	0.23	0.21	0.21	0.20	0.20	0.20	0.18	0.17	0.17	0.18	0.18
MgO	19.35	5.39	10.41	12.08	9.95	16.05	5.26	8.56	9.65	6.22	11.50	7.71	9.16	5.12	10.44	10.33	9.77
CaO	9.97	10.83	12.10	11.86	11.50	11.11	10.95	12.58	12.34	10.81	11.96	10.33	10.08	10.09	12.44	12.22	11.64
Na ₂ O	1.27	2.93	2.19	1.85	2.22	1.38	2.91	1.97	2.01	2.78	1.99	2.55	2.55	2.89	2.02	2.17	2.81
K ₂ O	0.84	1.75	1.00	0.89	1.31	1.52	1.29	1.33	0.75	1.16	1.03	1.74	1.09	1.73	0.62	0.78	0.66
P ₂ O ₅	0.17	0.30	0.18	0.18	0.26	0.34	0.31	0.37	0.20	0.28	0.17	0.34	0.21	0.30	0.11	0.16	0.14
L.O.I.		0.22	-0.51	0.15	-0.23	-0.22	-0.02	-0.22	-0.21		0.43	-0.42	-0.41	0.08	-0.36	-0.42	-0.26
Cs																	
Rb	12	28	15	13	22	52	18	27	11	16.7	18.2	37	21	32	9	14	11
Ba	329	597	366	345	445	433	401	431	294	420	240	415	254	395	191	220	187
Sr	490	938	585	583	673	638	676	627	487	620	480	542	436	704	313	352	332
La	8.13	14.30	8.74	9.57	13.40	16.10	14.80	16.80	9.49	14.61	9.49	11.50	7.38	10.10	4.42	4.97	4.12
Ce	19.00	33.90	21.10	22.50	30.20	33.20	36.00	37.40	23.80	32.60		27.00	17.20	23.80	12.30	12.90	11.43
Pr	2.49	4.37	2.83	2.98	3.71	4.44	4.55	4.74	3.14	4.21	2.95	3.31	2.30	2.88	1.70	1.73	1.60
Nd	11.40	19.40	12.90	13.70	17.80	21.50	21.70	22.60	15.20	19.50	13.17	16.60	11.40	14.70	8.95	9.07	8.59
Sm	2.62	4.50	3.05	3.89	4.48	4.54	5.00	5.06	3.88	4.29	2.63	4.68	2.85	3.52	3.01	2.27	2.52
Eu	0.83	1.52	1.08	1.15	1.21	1.47	1.63	1.51	1.29	1.41	0.83	1.30	0.87	1.00	0.90	0.80	0.86
Gd	2.44	4.09	3.04	3.39	3.84	4.16	5.18	5.05	4.15	4.54	2.63	4.03	3.07	3.45	2.89	2.75	3.09
Tb										0.73	0.41						
Dy	2.10	3.26	2.96	3.22	3.53	3.70	5.27	5.02	4.45	4.43	2.44	3.57	3.12	3.34	3.04	2.79	3.21
Hf										0.94	0.48						
Er	1.24	1.73	1.96	1.83	1.94	2.11	3.13	2.82	2.58	2.75	1.32	1.89	1.91	2.05	1.62	1.58	1.97
Yb	0.99	1.48	1.73	1.57	1.67	1.92	2.77	2.60	2.35	2.64	1.26	1.59	1.58	1.66	1.29	1.25	1.56
Lu																	
Y	12.0	21.0	16.0	17.0	17.0	17.0	31.0	30.0	24.0	29.4	15.1	18.0	17.0	18.0	16.0	17.0	16.0
Th		2.90	2.30	1.90		3.00	2.80	3.70		1.74	1.38			1.50			
U										0.50	0.35						
Zr	34	65	41	47	53	60	94	102	70	91	45	71	55	69	36	44	40
Hf										2.59	1.36						
Nb	1	2	1	2	2	2	5	7	4	5.06	1.48	3	2	3	1	2	1
Sc	38	29	44	41	36	39	36	42	44	38		37	35	31	47	44	44
V	257	428	343	385	350	280	454	343	370	490		357	304	339	287	285	280
Cr	1221	20	465	552	351	896	13	241	308	160		279	541	86	464	434	324
Ni	457	40	163	190	143	330	28	78	101	63		88	174	47	109	115	97

Data sources: Barsdell et al. (1982); Barsdell (1988); Barsdell and Berry (1990); Crawford et al. (1988); Dupuy et al. (1982); Eggins (1993); Gorton (1977); Marcelot et al. (1983); Roca (1978); Barsdell and Eggins (unpublished data)

Appendix A cont'd - Vanuatu basalt geochemistry

Volcano Sample	Ambrym 96	WestEpi 666	WestEpi EPI24	WestEpi EP23	WestEpi 71047	WestEpi 71065	WestEpi 71046	WestEpi 71071	EastEpi 670	EastEpi EPI26	EastEpi EPI10	Mataso MTA4	Mataso MTA14	Ririna R13	Emae EM4	Tongoa 698	Tongoa 697
SiO ₂	48.75	55.25	48.17	50.07	47.80	48.00	48.20	50.90	47.79	47.70	48.39	46.83	46.72	50.21	46.61	51.14	49.42
TiO ₂	0.66	0.67	0.52	0.76	0.54	0.45	0.39	0.64	0.54	0.57	0.59	0.84	0.83	0.83	0.70	0.71	0.60
Al ₂ O ₃	10.28	15.94	16.40	17.18	18.40	13.90	11.50	16.00	16.49	16.98	12.99	17.13	16.43	16.13	14.61	14.03	13.14
Fe ₂ O ₃	11.19	1.43	1.50	1.50	11.50	10.50	9.90	10.80	1.76	1.50	1.50	12.94	11.87	12.06	11.94	1.70	1.83
FeO		7.15	8.45	8.90					8.80	9.23	8.30					8.51	9.16
MnO	0.18	0.16	0.19	0.19	0.19	0.18	0.16	0.19	0.20	0.20	0.18	0.22	0.20	0.20	0.20	0.20	0.20
MgO	13.28	5.49	8.59	5.73	6.80	11.20	13.50	6.73	8.94	7.46	12.35	6.77	7.11	5.85	8.47	8.54	9.37
CaO	12.10	9.18	13.43	10.75	12.50	13.50	14.40	11.70	13.24	13.03	11.63	12.93	12.45	11.08	13.07	12.06	12.77
Na ₂ O	1.86	2.49	1.86	2.55	1.80	1.55	1.05	2.31	1.78	1.98	2.09	2.00	2.25	2.47	2.32	2.05	1.76
K ₂ O	1.13	2.00	0.30	1.38	0.45	0.35	0.31	0.77	0.38	0.50	0.82	0.52	1.39	1.03	0.86	0.87	1.45
P ₂ O ₅	0.22	0.23	0.12	0.33	0.08	0.05	0.07	0.13	0.09	0.14	0.19	0.16	0.49	0.23	0.20	0.20	0.30
L.O.I.	-0.30	1.52	0.07	0.07	0.07	0.01	0.10	-0.08	0.59	0.17	0.09	-0.16	-0.08	0.08	0.16	0.57	0.61
Cs																	
Pb	4.1	7.4			1.9	2.1	2.2	5.3	2.5							4.5	4
Rb	23	44.7	2.5	46.7	8	5.7	6	12.3	6.2	5.1	12.5	11	44	16.2	10.7	13.8	35.5
Ba	289	600	122	266	173	161	137	266	120	138	195	215	213	180	209	140	160
Sr	395	496	374	587	461	322	246	444	378	445	530	833	980	560	623	400	539
La	6.58	17.20	2.40	6.70	4.70	3.03	3.05	5.30	2.78	3.20	5.30	6.00	15.60	7.10	6.40	6.37	8.71
Ce	15.80	38.00	5.60	15.20	10.10	7.69	7.26	13.20	7.03	6.70	12.00	14.80	37.50	15.80	13.50	15.63	20.70
Pr	2.25	4.22			1.42	0.95	1.01	1.80	0.94			2.24	5.10			2.06	2.71
Nd	10.50	17.87			7.05	5.75	5.04	9.20	4.85			10.90	24.90			10.00	12.29
Sm	2.76	3.80	1.40	2.30	1.68	1.40	1.54	2.40	1.31	1.50	1.90	2.89	5.70	3.00	2.40	2.41	2.65
Eu	0.95	1.10	0.54	0.87	0.67	0.47	0.57	0.90	0.52	0.57	0.66	1.09	2.10	0.96	0.80	0.80	0.84
Gd	2.78	3.75			2.21	1.76	1.83	2.80	1.65			2.98	5.46				
Tb		0.58	0.30	0.49					0.28	0.30	0.30			0.56	0.47	0.43	0.42
Dy	2.66	3.43			2.47	2.10	1.91	3.20	1.88			3.10	3.95			2.62	2.26
Ho		0.72							0.39							0.59	0.46
Er	1.54	2.12			1.50	1.14	1.06	2.20	1.21			1.79	1.96			1.76	1.21
Yb	1.30	2.10	1.30	1.60	1.43	1.07	0.98	1.80	1.07	1.01	1.03	1.41	1.40	1.80	1.21	1.62	1.07
Lu			0.22	0.28						0.16	0.18			0.28	0.19		
Y	14.0	23.5	13.4	19.4	13.7	12.4	8.7	18.3	14.4	14.4	14.2	17.0	18.0	20.9	18.2	17.5	17.1
Th		3.28	0.26	0.97					0.26	0.41	0.82			0.90	0.86	1.12	1.67
U		1.05							0.11							0.38	0.60
Zr	46	101	28	77	20.8	18	13.5	36	19	32	39	28	64	57	33	46	57
Hf		2.35	0.65						0.44		1.12				1	1.44	1.2
Nb	2	3.54	1	3.9					0.46	1.1	1.3			1.9	1.4	1.12	1.15
Sc	52		48		45	57	66	49		39	34	43	37	38	34	28	31
V	281		279	323	371	321	295	335		335	270	491	444	323	309	240	250
Cr	876		198	87	39.5	533	820	156		86	670	55	92	46	227	200	260
Ni	220		58	30	37	124	172	38		38	200	32	60	33	75	58	46

Data sources: Barsdell et al. (1982); Barsdell (1988); Barsdell and Berry (1990); Crawford et al. (1988); Dupuy et al. (1982); Eggins (1993); Gorton (1977); Marcelot et al. (1983); Roca (1978); Barsdell and Eggins (unpublished data)

Appendix A cont'd - Vanuatu basalt geochemistry

Volcano Sample	Efate V36	Efate V20	E'mango E11	E'mango E46	Tanna T93	Tanna TA72	Tanna T24	Tanna TAC76	Tanna TAC84	Tanna TAC90	Tanna T108	Tanna T129B	Anatom AY4	Anatom AYC55	Anatom AYC62	Anatom Aymac36	Anatom Aymac68
SiO ₂	46.32	47.28	46.97	49.46	47.70	47.33	48.21	51.74	53.14	46.11	46.24	49.50	48.84	49.30	48.10	49.60	46.50
TiO ₂	0.78	1.11	0.73	0.61	0.72	0.82	0.61	0.65	0.78	0.84	0.85	0.31	0.85	0.57	0.79	0.62	0.59
Al ₂ O ₃	18.50	17.55	17.76	17.40	16.14	18.60	13.41	16.44	14.72	17.79	16.43	7.59	15.54	12.77	17.25	18.10	13.20
Fe ₂ O ₃	4.61	5.97	3.34	3.48	3.41	4.38	12.07	10.85	10.91	13.70	13.27	8.82	4.82	10.84	11.43	10.80	10.80
FeO	5.50	6.40	8.02	7.04	8.28	6.78							5.98				
MnO	0.17	0.22	0.22	0.19	0.22	0.22	0.22	0.18	0.18	0.21	0.19	0.15	0.20	0.18	0.19	0.19	0.15
MgO	7.45	5.26	6.84	6.92	7.80	6.02	9.58	6.50	5.81	7.19	6.89	16.79	7.16	10.25	6.52	6.00	12.90
CaO	12.59	11.18	11.24	12.13	12.51	11.76	13.45	10.63	8.21	12.16	11.65	15.31	11.90	12.53	11.22	11.30	12.60
Na ₂ O	2.24	2.84	1.85	2.02	1.84	2.35	1.78	2.32	3.05	1.43	1.47	0.69	2.30	1.62	1.86	1.89	1.39
K ₂ O	0.53	0.63	0.41	0.62	0.59	0.60	0.56	0.41	2.08	0.49	1.29	0.31	0.67	0.80	1.64	0.85	0.40
P ₂ O ₅	0.26	0.39	0.15	0.14	0.16	0.18	0.08	0.12	0.34	0.22	0.31	0.06	0.17	0.16	0.37	0.17	0.08
L.O.I.	0.06	0.16	0.42	0.03	0.26	0.20	0.40	-0.05	0.21	0.07	1.03	-0.08	0.36	1.15	0.12	0.39	0.94
Cs																	
Rb	6.6	6.5	7.1	6.9	8.3	6.4	7	11	31	3	19	3.2	4.7	9	25	12	5
Ba			133	151	101	159	155	254	447	142	152	86	120	121	207	131	91
Sr	987	972	441	301	430	955	387	742	516	523	546	220	450	389	806	554	269
La	4.90	6.70	3.00	3.10	3.30	5.70	2.95	4.58	10.30	3.25	4.67	2.16	4.00	6.12	12.60	6.88	2.46
Ce	11.00	14.80	8.00	7.10	7.30	11.80	7.56	12.10	24.80	9.27	12.10	4.85	9.20	13.80	28.90	15.40	5.60
Pr							1.13	1.65	3.69	1.36	1.73	0.82		2.08	3.87	2.14	0.91
Nd							5.84	8.19	16.30	7.35	9.19	3.93		10.20	18.90	9.68	4.74
Sm	2.10	2.90	1.90	2.00	1.60	2.60	1.86	2.34	4.13	2.46	2.78	1.16	2.20	2.73	4.79	2.58	1.51
Eu	0.71	1.00	0.64	0.65	0.59	0.84	0.79	0.72	1.02	0.91	0.93	0.43	0.67	1.07	1.64	0.87	0.57
Gd							1.96	2.43	3.91	2.69	2.79	1.22		3.02	5.05	2.82	2.00
Tb	0.33	0.46	0.36	0.37	0.35	0.38							0.42				
Dy							2.20	2.51	4.00	2.89	2.62	1.40		2.78	4.03	2.64	2.20
Ho																	
Er							1.37	1.56	2.49	1.60	1.77	0.96		1.75	2.23	2.03	1.42
Yb	0.98	1.42	1.45	1.70	1.24	1.41	1.16	1.72	2.42	1.45	1.51	0.92	1.62	1.41	1.86	1.68	1.11
Lu	0.16	0.23	0.28	0.32	0.18	0.19							0.29				
Y	14.0	23.1	15.3	15.7	23.5	22.8	12.3	15.0	24.0	15.3	14.6	7.0	21.2	17.0	23.0	15.3	12.0
Th	0.42	0.78	0.24	0.26	0.29	0.61							0.44				
U																	
Zr	29	37	27	29	38	38	18.8	28.4	81	24	31.6	11	40	38	61	34	21.3
Hf				0.83	0.8	1.29							1.24				
Nb	2	2.1	1.2	1.4	1.4	2.2											
Sc	26	28	39	48	26	24	64	43	33	58	52	67	34	56	46	39	54
V	347	474	379	314	349	312	377	333	309	416	441	234	324	310	386	302	358
Cr	204	31	67	67	81	28	388	184	171	95	115	1404	144	456	115	98.8	860
Ni	88	17	34	30	29	29	84	36	64	37	44	237	39	93.3	50	33.1	244

Data sources: Barsdell et al. (1982); Barsdell (1988); Barsdell and Berry (1990); Crawford et al. (1988); Dupuy et al. (1982); Eggins (1993); Gorton (1977); Marcelot et al. (1983); Roca (1978); Barsdell and Eggins (unpublished data)